HGS™

Theory Manual

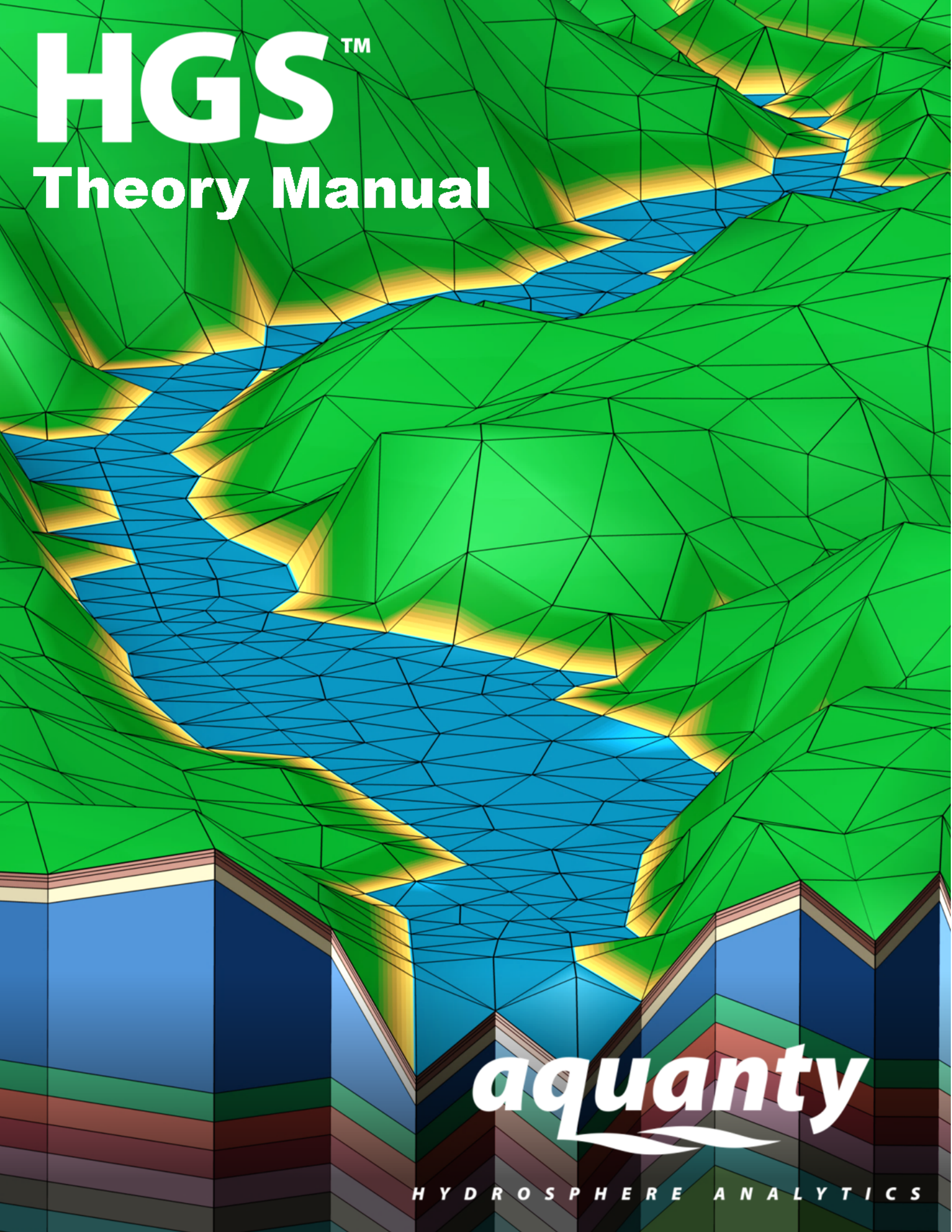

aquanty

HYDROSPHERE ANALYTICS

HGS Simulations is a product of Aquanty Inc.
600 Weber Street North, Unit B
Waterloo, Ontario N2V 1K4

This manual documents HydroGeoSphere (HGS) version 3010.
Released: September 3, 2026.

Copyright © 2012–2026, Aquanty Inc. All rights reserved.

This publication is a product of Aquanty Inc. and may not be reproduced either commercially or non-commercially by any means including but not limited to electronic replication, photocopy, or mechanical replication without direct written permission from Aquanty Inc.

Permissions may be sought directly from Aquanty Inc:
Phone: 1-855-aquanty
Email: info@aquanty.com

Preface

Effective management of watersheds and ecosystems requires a comprehensive knowledge of hydrologic processes, and impacts of point-source and non-point source pollution on water quality. Simulation models are being used increasingly to provide predictive capability in support of environmental and water resource assessment and restoration projects. However, the models used are often based on simplifications to complex hydrologic and transport processes. Such models incorporate restrictive assumptions pertaining to spatial variability, dimensionality and the interactions between various components of the flow and transport processes. Realizing the limitations of current models for complex, real-world applications, **HydroGeoSphere**, a 3-D fully-integrated surface and subsurface flow simulator, was developed. The **HydroGeoSphere** model is an outcome of more than two decades of research and development under the leadership of Dr. Edward Sudicky and Dr. Peter Forsyth at the University of Waterloo and Dr. Rene Therrien at Laval University. The **HydroGeoSphere** code provides a rigorous simulation capability that combines fully-integrated hydrologic/water quality/subsurface flow and transport capabilities with a well-tested set of user-programmable interface tools.

A unique feature in **HydroGeoSphere** is that when the flow of water is simulated in a fully-integrated mode, water derived from rainfall inputs is allowed to partition into components such as overland and stream flow, evaporation, infiltration, recharge and subsurface discharge into surface water features such as lakes, streams and wetlands in a natural, physically-based fashion. That is, the fully-coupled numerical solution approach allows the *simultaneous* solution of both the surface and variably-saturate subsurface flow regimes at each time step. This approach also permits dissolved solutes and thermal energy to be naturally exchanged between the surface and subsurface flow domains. The solute and thermal energy transport equations are also solved *simultaneously* at each timestep in both regimes. This makes **HydroGeoSphere** a unique and ideal tool to simulate the movement of water, energy and solutes within watersheds in a realistic, physically-based manner.

HydroGeoSphere uses the control volume finite element approach to simulate coupled surface and subsurface flow and transport. Fully 3-D simulations of variably-saturated fractured or granular aquifers may be performed. **HydroGeoSphere** provides several discretization options ranging from simple rectangular domains to irregular domains with complex geometry and layering. Mixed element types provide an efficient mechanism for simulating flow and transport processes in discrete features such as fractures (2-D rectangular or triangular elements), pumping/injection wells, streams or tile drains (1-D line elements). External flow stresses can include specified rainfall rates, evapotranspiration, snow melt and aquifer pumping or injection. External transport fluxes can include specified concentrations and mass fluxes, ambient air temperatures and incoming short and long-wave solar radiation. The **HydroGeoSphere** model also includes the capability to handle the dissolution of light and dense nonaqueous phase liquids from contaminant releases into the subsurface, as well as the degradation and fate of multiple contaminant species emitted from source zones. **HydroGeoSphere** includes options for adaptive-time stepping and output control procedures and an ILU-preconditioned Krylov subspace sparse iterative

matrix solution package. A Newton–Raphson linearization package provides improved robustness. **HydroGeoSphere** is written in Fortran and is compiled by the Intel Visual Fortran® compiler. It will run without modification on any Microsoft Windows® or Linux based platforms with sufficient RAM. **HydroGeoSphere** has also been parallelized using OpenMP for execution on widely-available shared-memory architectures.

This manual describes the physical and mathematical concepts underlying **HydroGeoSphere** and the implementation of these concepts in the numerical model.

Contents

List of Figures viii

List of Tables x

1 Introduction 1

1.1 General . . . 1

1.2 Integrated Hydrologic Model Conceptualization . . . 2

1.3 **HydroGeoSphere** Formulation . . . 4

1.4 Attributes of **HydroGeoSphere** . . . 6

1.5 Operation and Input Options . . . 8

1.6 Document Organization and Usage Guide . . . 8

2 Theory 10

2.1 Subsurface Flow . . . 10

2.1.1 General . . . 10

2.1.2 Governing Equations . . . 10

2.1.2.1 Porous Medium . . . 10

2.1.2.2 Discrete Fractures . . . 13

2.1.2.3 Dual Continuum . . . 14

2.1.2.4 1D Hydromechanical coupling . . . 15

2.2 Surface Flow . . . 17

2.2.1 General . . . 17

2.2.2 Governing Equations . . . 18

2.2.2.1 Surface Runoff . . . 18
2.2.2.2 Treatment of Rill Storage and Storage Exclusion for Rural and Urban Environments . . . 19
2.3 One-Dimensional Hydraulic Features . . . 23
2.3.1 General . . . 23
2.3.2 Governing Equations . . . 23
2.3.2.1 General One-Dimensional Flow . . . 23
2.3.2.2 Flow Through Subsurface Wells . . . 24
2.3.2.3 Flow Through Subsurface Pipe Systems . . . 25
2.3.2.4 Open Channel Flow . . . 26
2.4 Flow Coupling . . . 27
2.4.1 Dual Continuum Subsurface Coupling . . . 27
2.4.2 Surface - Subsurface Coupling . . . 28
2.5 Flow Boundary Conditions . . . 29
2.5.1 Subsurface flow . . . 29
2.5.2 Surface Flow . . . 29
2.5.3 Interception and Evapotranspiration . . . 29
2.5.3.1 Interception and Canopy Evaporation . . . 29
2.5.3.2 Evapotranspiration . . . 30
2.5.3.3 Actual Evapotranspiration . . . 32
2.6 Winter Hydrological Processes . . . 33
2.6.1 Surface Water Flow with Snowmelt . . . 33
2.6.2 Groundwater Flow with Freezing and Thawing of Pore Water . . . 33
2.6.3 Dual Continuum Freezing and Thawing of Pore Water . . . 35
2.7 Solute Transport . . . 35
2.7.1 Governing Equations . . . 35
2.7.1.1 Porous Medium . . . 36
2.7.1.2 Discrete Fractures . . . 37
2.7.1.3 Double Porosity . . . 37
2.7.1.4 Isotopic Fractionation . . . 38

2.7.1.5 Dual Continuum . . . 38
2.7.1.6 Wells . . . 39
2.7.1.7 Tile Drains . . . 39
2.7.1.8 Surface Domain . . . 40
2.7.1.9 Channels . . . 40
2.8 Solute Transport Coupling . . . 41
2.8.1 Mobile - Immobile Region Coupling . . . 42
2.8.2 Isotopic Fractionation Coupling . . . 42
2.8.3 Dual Continuum Subsurface Coupling . . . 42
2.8.4 Surface Subsurface Coupling . . . 43
2.9 Solute Transport Boundary Conditions . . . 43
2.9.1 Subsurface . . . 43
2.9.2 Surface . . . 44
2.10 Colloid Transport . . . 44
2.10.1 Subsurface - Porous Medium and Dual Continuum . . . 44
2.11 Thermal Energy Transport . . . 45
2.11.1 Porous Medium . . . 45
2.11.2 Discrete Fractures . . . 47
2.11.3 Dual Continuum . . . 47
2.11.4 Wells . . . 48
2.11.5 Tile Drain . . . 48
2.11.6 Channel . . . 48
2.11.7 Surface Water . . . 48
2.11.7.1 Atmospheric Inputs . . . 49
2.11.8 Thermal Energy Transport Boundary Conditions . . . 51
2.11.9 Thermal Energy Coupling . . . 52
2.12 Travel Time Probability . . . 53
2.12.1 Definitions . . . 53
2.12.2 Basic equations . . . 53

2.12.2.1 Forward model . . . 53
2.12.2.2 Backward model . . . 54
2.12.2.3 Total transit time . . . 55
2.12.2.4 Outlet/Inlet Transit Time PDF . . . 56
2.12.2.5 Travel Time Probabilities . . . 56
2.12.2.6 Age, Life Expectancy and Travel Time Statistics . . . 57
2.12.2.7 Mean Age and Mean Life Expectancy Direct Solutions . . . 57
2.12.2.8 Evaluating the travel time PDF from the travel time CDF 59
2.12.2.9 Capture zone probability . . . 60

3 Numerical Implementation 61

3.1 General . . . 61
3.2 Control Volume Finite Element Method . . . 62
3.3 Finite Difference Formulation . . . 65
3.4 Discretized Subsurface Flow Equations . . . 66
3.4.1 Porous Medium . . . 66
3.4.2 Discrete Fractures . . . 67
3.4.3 Dual Continuum . . . 68
3.5 Discretized Surface Flow Equation . . . 68
3.6 One-Dimensional Hydraulic Features . . . 69
3.7 Flow Coupling . . . 71
3.7.1 Dual-Continuum Subsurface Coupling . . . 72
3.7.2 Surface - Subsurface Coupling . . . 72
3.8 Flow Boundary Conditions . . . 74
3.8.1 Subsurface Flow . . . 74
3.8.2 Surface Flow . . . 75
3.8.3 Interception and Evapotranspiration . . . 76
3.8.3.1 Interception and Canopy Evaporation . . . 76
3.8.3.2 Surface and Subsurface Evapotranspiration . . . 77
3.9 Elemental Velocities . . . 77

3.10 Discretized Solute Transport Equations 78
3.10.1 Porous Medium 78
3.10.2 Discrete Fractures 79
3.10.3 Double Porosity 80
3.10.4 Isotopic Fractionation 80
3.10.5 Dual Continuum 80
3.10.6 Wells 80
3.10.7 Tile Drains 81
3.10.8 Surface runoff 81
3.10.9 Channels 81
3.10.10 Thermal Energy 82
3.11 Travel Time Probability 82
3.12 Solute Transport Coupling 85
3.13 Solute Transport Boundary Conditions 85
3.13.1 Subsurface Transport 85
3.14 Numerical Techniques 86
3.14.1 Matrix Solution 86
3.14.2 Newton-Raphson Method 87
3.14.3 Primary Variable Substitution 89
3.14.4 Time Stepping 89
3.14.5 Mass Balance 90
3.14.6 Solution Procedures 90

References **91**

Mathematical Notation **97**

Index **104**

List of Figures

1.1 Regional Hydrologic Cycle (adapted from Viessman Jr. and Lewis (1996)). 3

1.2 Integrated Numerical Simulation of a Hydrologic System. 5

2.1 Treatment of Storage Terms for Various Settings (adapted from Panday and Huyakorn (2004, Figure 2)). 21

2.2 Conceptual Model for Depression Storage and Obstruction Storage Exclusion (adapted from Panday and Huyakorn (2004, Figure 3)). 22

2.3 Rectangular 1-D channel cross section showing the stream bank height Z_{bank}, incision depth i_c, streambed thickness $l_{exch(pm,c)}$, overland head h_o, and channel head h_c. 26

2.4 Schematic illustration of a groundwater reservoir Ω, with inlet (Γ_-) and outlet (Γ_+) boundaries: (a) Age problem with normal flow field; (b) Life expectancy problem with reversed flow field. The cross stands for a small water sample, to illustrate the random variable total transit time (T) as the sum of the two random variables age (A) and life expectancy (E). 55

2.5 Descriptive statistics on the travel time PDF. 58

3.1 Nodal control volumes on the surface of a uniform triangular mesh with nine nodes (black disks) and eight elements. Black lines define element edges and red lines define nodal control volume edges, which intersect at the centroid (hollow disks) of each element. 62

3.2 Spatial Discretization of the Surface Flow System and its Connection to the Subsurface (adapted from Panday and Huyakorn (2004, Figure 5)). 73

3.3 Procedure for the evaluation of the travel time PDF at the element centroid, for the case of a brick element. 84

3.4 Schematic illustration of SCPR method. Left: Four quadrangles defining a patch of elements used to evaluate the velocity at a node (red circle), with indicated sample points (+); Right: Example of a patch made of 8 brick elements. 84

List of Tables

2.1 Types of Coupling and Dimensionality for Fluid Flow. 28
2.2 Types of Coupling and Dimensionality Solute Transport. 41

Chapter 1

Introduction

1.1 General

A diverse group of problems exists that requires quantification of the entire hydrologic cycle by integrated simulation of water flow, contaminant and thermal energy migration in the surface and subsurface regimes. Increased demand on limited resources for potable water and other purposes has driven the development of innovative management practices including water recycling, drainage water reuse for salt-tolerant crops, conjunctive use of surface and subsurface water resources, maintenance of ecosystems and artificial recharge of subsurface aquifers during wet periods. A quantification of available water within the hydrologic system and the impacts of withdrawals is essential for addressing these complex water management issues. The complex cycle of irrigation, evaporation, infiltration, discharge to nearby lakes, rivers, and streams, and aquifer pumping, needs to be quantified to resolve supply and demand issues. Concerns over drying and restoration of wetlands or the effects of subsurface water withdrawals on surface water features also require an integrated, fully-coupled analysis of the various flow regimes. Ecosystems of lakes, rivers, and wetlands depend on certain minimum flows as do hydropower generation, recreational use, and downstream water users. Regulating water use in hydraulically-connected surface water bodies and surficial aquifer systems necessitates an understanding of surface/subsurface water interactions and overall seasonal hydrologic cycle behavior.

Since the early 1970s, there has been an evolution of hydrologic models for single-event and continuous simulations of rainfall-runoff processes. Earlier models quantify various hydrologic components using simplified procedures (including a unit hydrograph method, empirical formulas, system lumping, and analytical equations) that are incapable of describing flow physics and contaminant and thermal energy transport in any detail. In the past, numerical models based on complex multi-dimensional governing equations have not received much attention because of their computational, distributed input and parameter estimation requirements. Today, with the availability of powerful personal computers and multi-processor workstations, efficient computational methods, and sophisticated GIS, remote sensing and advanced visualization tools, the hydrologic community is realizing the tremendous potential

and utility of physically-based numerical simulators. As pointed out by Woolhiser (1996, p. 126), "there seems to be little disagreement regarding the usefulness of physically-based models for understanding hydrologic systems." Models of this type are widely held to offer the greatest opportunity to examine hydrologic impact of land use change (Refsgaard, 1997; Senarath et al., 2000). Distributed hydrologic models also have immense potential and utility for "forecasting the movement of pollutants and sediments" (Beven, 1985).

The resulting model, which we call **HydroGeoSphere**, is documented herein. Provided in the following chapters are detailed descriptions and formulations of the various components of the model.

HydroGeoSphere is supported by a flexible, user-friendly programmable interface that may be used to seamlessly prepare input data sets, or visualize and interpret simulation results.

1.2 Integrated Hydrologic Model Conceptualization

HydroGeoSphere is based on a rigorous conceptualization of the hydrologic system comprising surface and subsurface flow regimes with interactions. The model is designed to take into account all key components of the hydrologic cycle (Figure 1.1). For each time step, the model solves surface and subsurface flow, mass and energy transport equations simultaneously and provides complete water balance and solute budgets. Referring to Figure 1.1, the surface water budget can be written as:

$$P = (Q_{S2} - Q_{S1}) - Q_{GS} + ET_S + Q_S^W + \Delta S_S/\Delta t \tag{1.1}$$

and the subsurface water budget as:

$$I = (Q_{G2} - Q_{G1}) + Q_{GS} + ET_G + Q_G^W + \Delta S_G/\Delta t \tag{1.2}$$

giving the total hydrologic budget as the sum of Equations 1.1 and 1.2:

$$P = (Q_{S2} - Q_{S1}) + (Q_{G2} - Q_{G1}) + (ET_S + ET_G) + (Q_S^W + Q_G^W) + (\Delta S_S + \Delta S_G)/\Delta t \tag{1.3}$$

where P is the net precipitation (actual precipitation - interception), Q_{S1} and Q_{S2} are the surface water inflow and outflow, Q_{GS} is the surface/subsurface water interactive flow, ET_S is the evapotranspiration from the surface flow system, Q_S^W is the overland water withdrawal, ΔS_S is the surface water storage over time step Δt, Q_{G1} and Q_{G2} are the subsurface water inflow and outflow, ET_G is the evapotranspiration from the subsurface flow system, Q_G^W is the subsurface water withdrawal and ΔS_G is the subsurface water storage over time step Δt.

In order to accomplish the integrated analysis, **HydroGeoSphere** utilizes a rigorous, mass conservative modeling approach that fully couples the surface flow and transport equations with the 3-D, variably-saturated subsurface flow and transport equations. This approach is significantly more robust than previous conjunctive approaches that rely on linkage of separate surface and subsurface modeling codes.

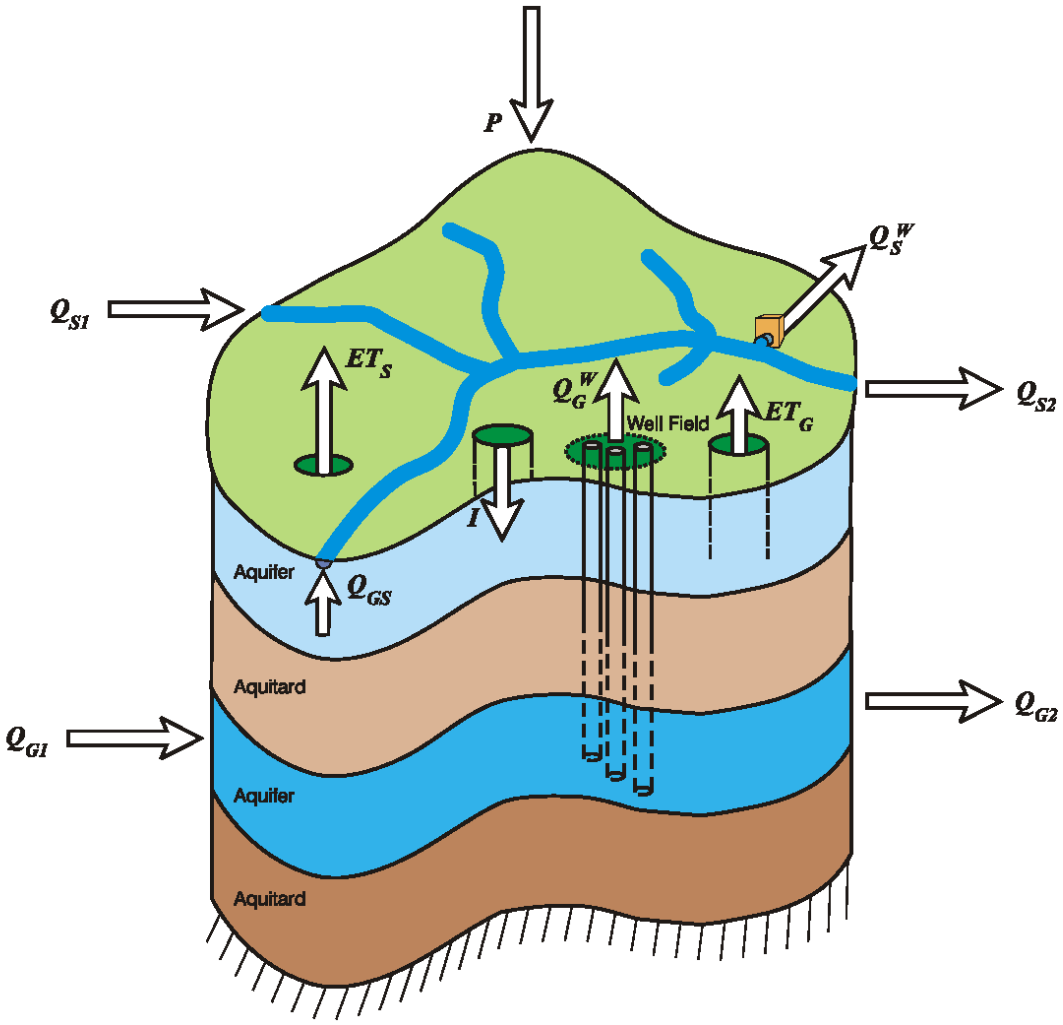

Figure 1.1: Regional Hydrologic Cycle (adapted from Viessman Jr. and Lewis (1996)).

1.3 HydroGeoSphere Formulation

HydroGeoSphere uses the two-dimensional, depth-integrated diffusion-wave approximation of the Saint Venant equation for surface water flow (Viessman Jr. and Lewis, 1996), thereby neglecting the inertial terms of the momentum equation. An integrated hydrologic analysis is accomplished by the coupled solution of the diffusion-wave equation governing 2-D (areal) surface water flow and the Richards' equation governing 3-D unsaturated/saturated subsurface flow. For problems that also involve solute or thermal energy transport, the classical advection-dispersion equation is used in all domains.

The surface and subsurface flow and transport domains are discretized simultaneously as shown in Figure 1.2. The gridding options for 2-D surface flow and transport include the depicted rectangular grid that allows variable grid spacing, as well as a triangular grid option for geometric flexibility. The coupled surface and subsurface domains consist of: (1) a single layer of surface nodes, shown by triangles in Figure 1.2, situated on the land surface, (2) layers of subsurface soil and aquifer nodes, shown by circles, representing the vadose zone, subsurface aquifers and aquitards, and (3) a set of one-dimensional line elements, shown by squares, representing surficial channels, wells, tile drains, storm and sanitary drains, water mains or other linear features. The 2-D surface flow grid is draped over the subsurface 3-D mesh to maintain the areal topography of the land surface and to ensure that the nodes in the surface grid are coincident with those at the top of the subsurface mesh.

The 3-D saturated-unsaturated flow and transport equations for the vadose and saturated zones are solved using the control volume finite element method. The top layer of surface nodes discretizes the 2-D surface flow regime, which is assembled into the matrix equations in a fully-implicit manner using a diffusion-wave approximation to the Saint Venant equations. Two methods are used to couple the two flow and transport domains. The first uses a numerical superposition principle whereby the top layer of nodes represents both surface and subsurface domains. The second method uses Darcy flux (for flow) and Fickian (for transport) relations to transfer water from the surface nodes to the first layer of subsurface nodes (or vice versa), with the assumption that they are separated by a (possibly) thin boundary layer across which the leakance occurs. A single system of matrix equations arising from both discretized flow and transport regimes is then assembled for the entire hydrologic setting with appropriate boundary conditions being applied to the combined system. The fully-integrated set of nonlinear discrete equations is linearized using Newton-Raphson schemes, and is solved simultaneously in an iterative fashion at every time step.

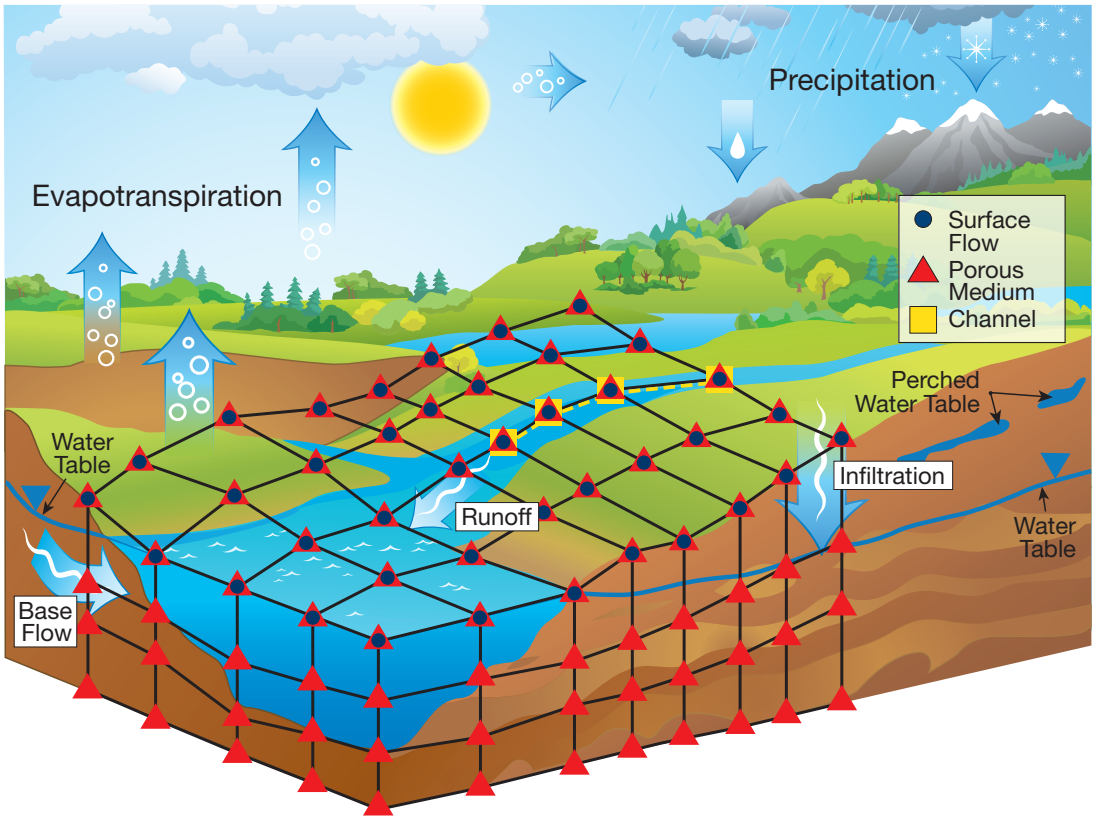

Figure 1.2: Integrated Numerical Simulation of a Hydrologic System.

1.4 Attributes of HydroGeoSphere

HydroGeoSphere is a powerful numerical simulator specifically developed for supporting water resource and engineering projects pertaining to hydrologic systems with surface and subsurface flow and transport components.

In terms of simulation capability and computational aspects, the **HydroGeoSphere** code has the following attributes:

Fluid flow

- Complete hydrologic cycle modeling using detailed physics of surface and subsurface flow in one integrated code. The surface regime can be represented as 2-D areal flow for the entire surface or as 2-D runoff into 1-D channels. The subsurface regime consists of 3-D unsaturated/saturated flow. Both regimes naturally interact with each other through considerations of the physics of flow between them.
- Physically-based accounting of all components of the hydrologic cycle water budget.
- Accurate delineation and tracking of the water table position, taking into account flow in the unsaturated zone, delayed yield and vertical flow components.
- Handling of non-ponding or prescribed ponding recharge conditions.
- Automatic handling of seepage face conditions at the land-atmosphere interface.
- Automatic and correct apportioning of the total flow rate of a multi-layer well to the well nodes, including the simulation of water flow and solute/temperature mixing within the water column in the well.
- Accommodation of wellbore storage.
- Arbitrary combinations of porous, discretely-fractured, dual-porosity and dual-permeability media for the subsurface.

Mass and thermal energy transport

- Capability of modeling non-reactive and reactive chemical species transport in the associated surface and subsurface flow fields, including solute interactions between the surface and subsurface flow regimes.
- Calculation of temperatures in the surface and subsurface flow regimes as driven by air temperature and incoming solar radiation, accounting for land surface-atmospheric thermal interactions.
- Accurate handling of fluid and mass/thermal energy exchanges between fractures and matrix including matrix diffusion effects and solute/thermal energy advection in the matrix.

- Straight or branching decay chains representing degradation reactions.

Numerical methods

- The fully-implicit coupling approach used by the code provides for a robust mass conserved solution scheme, which is essential for systems with strong interactions between regimes.
- Parallelization employing OpenMP.
- Advanced computational algorithms and a flexible, user-programmable interface allow the code to perform unprecedented, fully-integrated, 3-D simulation/animation on a personal computer.
- Fluid, solute and energy balance tracking.
- Unstructured finite-element grids.
- Axi-symmetric grid option.
- 7-point finite-difference option.
- 8-node block or 6-node prism elements, 3- and 4-node plate elements for fractures and surface water, and 2-node line elements for wells, storm and sanitary sewers, water supply mains and tile drains or other types of linear infrastructure features.
- Adaptive time-stepping schemes with automatic generation and control of time steps, sub-timing option at select nodes where flow and transport is rapid.
- Straightforward organization and control of simulation output.
- Robust and efficient ILU-preconditioned iterative sparse-matrix solver.
- Robust and efficient Newton-Raphson linearization option.
- Flexible pre- and post-processing capabilities.

For field applications and research investigations, **HydroGeoSphere** can be used to perform event-based and continuous simulations on widely varying spatial scales ranging from single soil column profiles to large-scale basins, which may include several catchments. Examples of field applications of **HydroGeoSphere** include:

- Integrated water resource assessment.
- Watershed hydrologic analysis, including impacts of land-use or climate-change impacts on both surface and subsurface water.
- Floodplain hydrologic analysis.
- Fluvial hydraulic analysis.
- Contaminant migration and fate in both surface and subsurface water.

1.5 Operation and Input Options

The **HydroGeoSphere** conjunctive surface-subsurface flow simulator enjoys the benefit of having already available and affordable GUI tools for grid generation and subsurface flow model input as well as Tecplot for 3-D visualization and animation. In order to handle spatial data analysis and visualization of surface water domain, GIS tools such as ArcView and ArcInfo may be used.

The modular code features and input/output structures of **HydroGeoSphere** result in four steps to solve a given problem.

1. Build the necessary data files for the pre-processor **grok** (as discussed in the reference manual `hydrosphere_ref.pdf`).
2. Run **grok** to generate the input data files for **HydroGeoSphere**.
3. Run **HydroGeoSphere** to solve the problem and generate output data files.
4. Postprocess the output files to visualize and analyze the results and produce reports.

At a minimum, Step 1 involves creating data files that contain information for discretizing the problem domain, defining material properties for each element and specifying flow boundary conditions.

Simulation output pertaining to surface flow regime calculations is reported to the main **HydroGeoSphere** output file in a similar manner to that for the subsurface flow calculations. Binary files are created individually for further investigation or post processing.

1.6 Document Organization and Usage Guide

This document is organized into two chapters. These chapters and their purposes are outlined below.

Chapter 2 presents the mathematical theory that describes the various physical processes that are presented in the model.

Chapter 3 shows how the mathematical theory is implemented in the **HydroGeoSphere** code, with an emphasis on the numerical techniques used to address non-linearities that arise when dealing with, for example, variably-saturated flow.

A complete list of references cited in each chapter can be found in the References section. A summary of mathematical notation and a comprehensive index are provided at the end of this document.

In addition to this document, the reference manual (`hydrosphere_ref.pdf`) introduces the user to the basic operations of the pre-processor and describes the input instructions used to determine:

- Problem description.
- Simulation control.
- Grid generation.
- Selection of grid components (nodes, elements, etc.)

as well as for the saturated-unsaturated subsurface flow, surface flow, and solute and energy transport problems.

The verification manual (`hydrosphere_verif.pdf`) contains descriptions of several verification problems that were designed to test and demonstrate the capabilities of **HydroGeoSphere** in solving a variety of flow and transport phenomena. It compliments the set of verification tests that are installed alongside **HydroGeoSphere**.

Chapter 2

Theory

2.1 Subsurface Flow

2.1.1 General

The current implementation of **HydroGeoSphere** assumes that the subsurface flow equation in a porous medium is always solved during a simulation, either for fully-saturated or variably-saturated flow conditions. We therefore first present the basic subsurface flow equation solved by **HydroGeoSphere**. This basic equation can be expanded to incorporate, among other features, discrete fractures, a second interacting porous continuum (e.g. fractures or macropores), wells, tile drains and surface flow. The following assumptions are made for subsurface flow:

- The fluid is essentially incompressible.
- The porous medium and fractures (or macropores), if present, are non-deformable.
- The system is under isothermal conditions.
- The air phase is infinitely mobile.

2.1.2 Governing Equations

2.1.2.1 Porous Medium

The following modified form of Richards' equation is used to describe three-dimensional transient subsurface flow in a variably-saturated porous medium:

$$-\nabla \cdot (w_m \mathbf{q}) + \sum \Gamma_{\mathrm{ex}} + Q = w_m \frac{\partial}{\partial t}(\theta_s S_w) \tag{2.1}$$

where w_m [dimensionless] is the volumetric fraction of the total porosity occupied by the porous medium (or primary continuum). This volumetric fraction is always equal to 1.0 except when a second porous continuum is considered for a simulation, which is the case when the dual continuum option is used to represent existing fractures or macropores. The fluid flux $\mathbf{q}$ [L T^{-1}] is given by:

$$\mathbf{q} = -\mathbf{K} \cdot k_r \nabla(\psi + z) \tag{2.2}$$

where $k_r = k_r(S_w)$ represents the relative permeability of the medium [dimensionless] with respect to the degree of water saturation S_w [dimensionless], ψ is the pressure head [L], z is the elevation head [L] and θ_s is the saturated water content [dimensionless], which is assumed equal to the porosity. Fluid exchange with the outside of the simulation domain, as specified from boundary conditions, is represented by Q [L^3 L^{-3} T^{-1}], which is a volumetric fluid flux per unit volume representing a source (positive) or a sink (negative) to the porous medium system.

The hydraulic conductivity tensor, $\mathbf{K}$ [L T^{-1}], is given by:

$$\mathbf{K} = \frac{\rho g}{\mu}\mathbf{k} \tag{2.3}$$

where g is the gravitational acceleration [L T^{-2}], μ is the viscosity of water [M L^{-1} T^{-1}], $\mathbf{k}$ is the permeability tensor of the porous medium [L^2] and ρ is the density of water [M L^{-3}], which can be a function of the concentration C [M L^{-3}] of any given solute such that $\rho = \rho(C)$.

Water saturation is related to the water content θ [dimensionless] according to:

$$S_w = \frac{\theta}{\theta_s} \tag{2.4}$$

In Equation 2.1, Γ_{ex} represents the volumetric fluid exchange rate [L^3 L^{-3} T^{-1}] between the subsurface domain and all other types of domains supported by the model and it is expressed per unit volume of the other domain types. Currently, these additional domains are surface, wells, tile drains, discrete fractures and dual continuum. The definition of Γ_{ex} (positive for flow into the porous medium) depends on the conceptualization of fluid exchange between the domains and will be defined in later sections that discuss these respective flow domains. In the equations shown for the other domains, we will use the notation ex=*f*, ex=*d*, ex=*w*, ex=*t*, ex=*o*, ex=*c*, for the fracture, dual continuum, well, tile drain, surface and channel domains, respectively.

The primary variable of solution for the nonlinear flow Equation 2.1 is the pressure head, and constitutive relations must be established that relate the primary unknown ψ to the secondary variables S_w and k_r. The relative permeability may be expressed in terms of either the pressure head or the water saturation. Commonly used functions incorporated in the model are those presented by van Genuchten (1980) and Brooks and Corey (1964).

Using the Brooks and Corey functions, the saturation is given by:

$$\begin{aligned} S_w &= S_{wr} + (1 - S_{wr}) \mid \alpha\psi \mid^{-\beta} \quad \text{for} \quad \psi < -1/\alpha \\ S_w &= 1 \quad \text{for} \quad \psi \geq -1/\alpha \end{aligned} \tag{2.5}$$

and the relative permeability is obtained from:

$$k_r = S_e^{(2/\beta + l_p + 2)} \tag{2.6}$$

where α [L^{-1}] is the inverse of the air-entry pressure head, β [-] is the pore-size distribution index, l_p is the pore-connectivity parameter assumed equal to 2.0 in Brooks and Corey (1964), and S_e is often called an effective saturation, given by $S_e = (S_w - S_{wr})/(1 - S_{wr})$, with S_{wr} being the residual water saturation [-].

Based on earlier work by Mualem (1976), van Genuchten (1980) later proposed the following saturation-pressure relation:

$$\begin{aligned} S_w &= S_{wr} + (1 - S_{wr}) \left[1 + \mid \alpha\psi \mid^{\beta}\right]^{-\nu} \quad \text{for} \quad \psi < 0 \\ S_w &= 1 \qquad\qquad\qquad\qquad\qquad\qquad\quad \text{for} \quad \psi \geq 0 \end{aligned} \tag{2.7}$$

with the relative permeability given by:

$$k_r = S_e^{(l_p)} \left[1 - \left(1 - S_e^{1/\nu}\right)^{\nu}\right]^2 \tag{2.8}$$

where

$$\left(\nu = 1 - \frac{1}{\beta}\right), \qquad \beta > 1 \tag{2.9}$$

and where α and β are usually obtained from a fit of Equations 2.7 and 2.8 to experimental results. For his relative permeability model, Mualem (1976) has estimated that the pore-connectivity parameter l_p is equal to 0.5 for most soils.

Although other fundamental relations exist, any arbitrary, but physically realistic, function for $S_w(\psi)$ and $k_r(S_e)$ can also be handled through the use of tabular data input for these parameters, which is also made available in the model. Furthermore, hysteresis is not considered here, but may be included in a future version of **HydroGeoSphere**.

To describe subsurface flow in the saturated zone, the storage term forming the right-hand side of Equation 2.1 is expanded in a way similar to that presented by Cooley (1971) and Neuman (1973). They relate a change in storage in the saturated zone to a change in fluid pressure through compressibility terms as is conventionally done in hydrogeological applications. They also assume that the bulk compressibility of the medium is constant for saturated and nearly-saturated conditions. For unsaturated conditions, it is assumed that the compressibility effects on storage of water are negligible compared to the effect of changes in saturation. The following expression is obtained for the storage term in Equation 2.1 (Cooley, 1971; Neuman, 1973):

$$\frac{\partial}{\partial t}\left(\theta_s S_w\right) \approx S_w S_s \frac{\partial \psi}{\partial t} + \theta_s \frac{\partial S_w}{\partial t} \tag{2.10}$$

where S_s is the specific storage coefficient of the porous medium [L^{-1}].

2.1.2.2 Discrete Fractures

A fracture is idealized here as the space between two-dimensional parallel surfaces, with the tacit assumptions that the total head is uniform across the fracture width. The equation for variably-saturated flow in a fracture of width w_f [L] can be written by extending the saturated fracture flow equations Berkowitz et al. (1988); Sudicky and McLaren (1992) and using the analogy of Richards Equation (Equation 2.1) for the porous matrix. With this extension, the governing two-dimensional flow equation in a fracture has the form:

$$-\overline{\overline{\nabla}} \cdot (w_f \mathbf{q_f}) - w_f \Gamma_f = w_f \frac{\partial S_{wf}}{\partial t} \tag{2.11}$$

where the fluid flux $\mathbf{q_f}$ [L T^{-1}] is given by:

$$\mathbf{q_f} = -\mathbf{K_f} \cdot k_{rf} \overline{\overline{\nabla}} (\psi_f + z_f) \tag{2.12}$$

where $\overline{\overline{\nabla}}$ is the two-dimensional gradient operator defined in the fracture plane, k_{rf} is the relative permeability of the fracture [-], ψ_f and z_f are the pressure and the elevation heads within the fracture [L], and S_{wf} is the water saturation for the fracture [-]. The saturated hydraulic conductivity of a fracture $\mathbf{K_f}$ [L T^{-1}], having a uniform aperture w_f is given by (Bear, 1972):

$$\mathbf{K_f} = \frac{\rho g \, w_f^2}{12 \mu} \tag{2.13}$$

where the fluid density can be a function of the concentration C_f of any given solute in the fracture [M L^{-3}], such that $\rho = \rho(C_f)$.

Constitutive relations are also required to describe variably-saturated flow in the fractures. There is a very limited number of studies where these relationships have been derived experimentally (see e.g., Reitsma and Kueper (1994)). Several theoretical studies have, nevertheless, been performed in order to characterize the nature of the relationships. Wang and Narasimhan (1985) and Rasmussen and Evans (1989) generated synthetic relations between pressure, saturation and relative permeability for a single fracture surface containing a distribution of apertures. Their results were based on capillary theory and they used the well-known cubic law to represent flow in the fracture. Pruess and Tsang (1990) considered the problem of two-phase flow in a rough-walled fracture surface. They subdivided the fracture surface into sub-elements and assigned a spatially-correlated aperture to each. The occupancy of each element by either the wetting or the non-wetting phase fluid was based on a prescribed entry pressure relationship. Once the fluid occupancy was assigned to each element, the relative permeabilities were obtained by performing two single-phase flow simulations: one for the region occupied by the wetting phase and the other for the non-wetting phase.

In **HydroGeoSphere**, relative permeability and saturation-pressure head relationships for the fractures are given by either the Brooks-Corey model (Equations 2.5 and 2.6), the Van Genuchten model (Equations 2.7 and 2.8) or they can be given in tabular forms, which gives flexibility to the user and does not restrict data entry to fixed functions.

Another process that could be considered when describing flow in variably-saturated fractured porous media is the reduction of the area available for flow across a fracture-matrix interface. Some portions of a fracture, as it desaturates, cannot transmit any water and thus reduce the area available for matrix flow across the fracture. We use the approach of Wang and Narasimhan (1985) who represented this phenomenon with a function describing the change in effective fracture-matrix area as a function of pressure. This effective area is only applied to those matrix nodes that are also fracture nodes.

Using arguments similar to those invoked for the porous medium equation, the storage term in Equation 2.11 describing variably-saturated flow in the fractures becomes:

$$\frac{\partial}{\partial t} S_{wf} \approx S_{wf} S_{sf} \frac{\partial \psi_f}{\partial t} + \frac{\partial S_{wf}}{\partial t} \tag{2.14}$$

where S_{sf} is the specific storage coefficient for the fractures [L^{-1}]. Because it is assumed here that the fractures are non-deformable and fluid-filled, there is no contribution to the storage term from fracture compressibility. Thus, the specific storage coefficient for a fracture under saturated conditions is related to the water compressibility, α_w [L T^2 M^{-1}], according to:

$$S_{sf} = \rho g \alpha_w \tag{2.15}$$

The validity of assuming non-deformable fractures is likely to be reasonable if the fractures have a high normal stiffness or if changes in the effective stress field within the system due to pumping, for example, are small.

2.1.2.3 Dual Continuum

The **HydroGeoSphere** model can simulate variably-saturated fluid flow in a dual continuum based on the formulation presented by Gerke and van Genuchten (1993). The dual continuum formulation in **HydroGeoSphere** involves two separate continua, with the first continuum represented by the porous medium. We present here the formulation for the second continuum, which is linked to the porous medium continuum by a fluid exchange term. This second continuum could represent, for example, fractures or macropores that are present in a porous matrix.

Similarly to flow in the porous medium, three-dimensional variably-saturated flow in the second continuum is described by a modified form of Richards' equation:

$$-\nabla \cdot (w_d \mathbf{q_d}) - \Gamma_d \pm Q_d = w_d \frac{\partial}{\partial t} (\theta_{sd} S_{wd}) \tag{2.16}$$

where the fluid flux $\mathbf{q_d}$ [L T^{-1}] is given by:

$$\mathbf{q_d} = -\mathbf{K_d} \cdot k_{rd} \nabla (\psi_d + z_d) \tag{2.17}$$

where k_{rd} is the relative permeability of the medium [-] with respect to the degree of water saturation S_{wd} [-], ψ_d is the pressure head [L], z_d is the elevation head [L] and θ_{sd} is the saturated water content [-], which is equal to the porosity of the dual continuum. Fluid

exchange with the outside of the simulation domain is represented by a volumetric fluid flux per unit volume Q_d [L^3 L^{-3} T^{-1}]. The volumetric fraction of the total porosity occupied by the dual continuum is given by w_d [-]. We assume here that the sum of volumetric fraction of the dual continuum w_d and that of the porous medium w_m is equal to 1.0.

The hydraulic conductivity tensor of the dual continuum, $\mathbf{K_d}$ [L T^{-1}], is given by:

$$\mathbf{K_d} = \frac{\rho g}{\mu}\mathbf{k_d} \tag{2.18}$$

where $\mathbf{k_d}$ is the permeability tensor of the dual continuum [L^2] and where the density of water can be a function of the concentration C_d [M L^{-3}] of any given solute in the dual continuum such that $\rho = \rho(C_d)$.

Similarly to the porous medium, the functional relationships relating pressure head to saturation and relative permeability to saturation are described by either the Van Genuchten or the Brooks-Corey functions, or are given in tabular form.

For cases where the dual continuum represents fractures, some expressions can be derived to relate the permeability of the fractures to a representative fracture aperture and spacing (for example, Bear (1972)). For example, for a set of parallel fractures of uniform aperture w_f with a uniform spacing equal to f_s [L], and assuming one-dimensional flow in a direction parallel to the fracture, the equivalent permeability of the set of fractures is given by:

$$\mathbf{k_d} = \frac{w_f^2}{12} \quad \text{with} \quad \mathbf{w_d} = \frac{w_f}{f_s} \tag{2.19}$$

For the second continuum the storage term in Equation 2.16 is expanded in a manner similar to Equation 2.10 for the porous medium, using the specific storage S_{sd} [L^{-1}] for the second continuum.

2.1.2.4 1D Hydromechanical coupling

The **HydroGeoSphere** code can be used to simulate transient flow affected by surface loading conditions. Examples of surface loading conditions include: advent or retreat of glaciation, erosion, and deposition.

Under hydromechanical equilibrium conditions, the governing equations are (Neuzil, 2003):

$$\frac{\partial \sigma_{ij}}{\partial x_j} = 0 \tag{2.20a}$$

$$\sigma_{ij} = 2G\varepsilon_{ij} + 2G\frac{\nu}{1-2\nu}\varepsilon_{kk}\delta_{ij} + \alpha p \delta_{ij} \tag{2.20b}$$

$$\frac{\partial}{\partial x_i}\left(K_{ij}\frac{\partial h}{\partial x_j}\right) = S_{s3}\frac{\partial h}{\partial t} - \beta S_{s3}\frac{1}{\rho g}\frac{\partial \sigma_t}{\partial t} \pm Q \tag{2.21}$$

where σ_{ij} is the total stress [M T^{-2} L^{-1}] defined by Equation 2.20b, ε_{ij} is the mechanical strain [-], G is the shear modulus [M T^{-2} L^{-1}], ν is Poisson's ratio [-], α is the effective-stress hydroelastic constant [-], p is fluid pressure [M T^{-2} L^{-1}], S_{s3} is the three-dimensional specific storage coefficient [L^{-1}] of the porous medium originally defined in Equation 2.10, β is the three-dimensional loading efficiency [-], and σ_t is the mean normal total stress [M T^{-2} L^{-1}]. The loading efficiency is the fraction of stress that is transferred to fluid pressure. The ratio $\sigma_t/\rho g$ may be interpreted as equivalent fresh water height of the mean normal total stress at a given point. The three-dimensional loading efficiency, α, shear modulus, mean normal total stress, and specific storage are defined below:

$$\beta = \frac{\left(\frac{1}{K} - \frac{1}{K_s}\right)}{\left(\frac{1}{K} - \frac{1}{K_s}\right) + \left(\frac{\theta_s}{K_f} - \frac{\theta_s}{K_s}\right)} \tag{2.22}$$

$$\alpha = \left(1 - \frac{K}{K_s}\right) \tag{2.23}$$

$$G = \frac{E}{2\,(1+\nu)} \tag{2.24}$$

$$\sigma_t = \frac{\sigma_{kk}}{3} \tag{2.25}$$

$$S_{s3} = \left(\frac{1}{K} - \frac{1}{K_s}\right) + \rho g \left(\frac{\theta_s}{K_f} - \frac{\theta_s}{K_s}\right) \tag{2.26}$$

where K is the bulk modulus of porous media [M T^{-2} L^{-1}], K_s is the solid bulk modulus [M T^{-2} L^{-1}], K_f is the fluid bulk modulus [M T^{-2} L^{-1}], and E is Young's elastic modulus [M T^{-2} L^{-1}]. The three-dimensional loading efficiency is the ratio of change in fluid pressure to change in mean total stress under undrained conditions. For highly compressible media, β approaches unity while in stiff media it can be zero (Neuzil, 2003). As porosity approaches zero, K approaches K_s and the effects of water pressure on total stress (Equation 2.20b) and the effects of change of total stress on water storage (Equations 2.22 and 2.26) also vanish.

However, the current version of **HydroGeoSphere** does not have a mechanical or an equilibrium module that is coupled with the flow module. The mean normal total stress, which may be spatially distributed and vary with time, must be estimated externally to **HydroGeoSphere**. However, under the condition of purely vertical strain, the flow component can be decoupled or partially decoupled from the mechanical component.

Mechanical and hydraulic behaviour can also be partially coupled under the conditions of relatively homogeneous and areally extensive vertical loading. Under these conditions, Equation 2.21 is written as

$$\frac{\partial}{\partial x_i}\left(K_{ij}\frac{\partial h}{\partial x_j}\right) = S_{s1}\frac{\partial h}{\partial t} - \zeta S_{s1}\frac{1}{\rho g}\frac{\partial \sigma_{zz}}{\partial t} \pm Q \tag{2.27}$$

where σ_{zz} is the vertical total stress [M T^{-2} L^{-1}], S_{s1} is the modified one-dimensional specific storage [L^{-1}] (Neuzil, 2003) and ζ is the one-dimensional loading efficiency [-]. S_{s1} and ζ are defined below:

$$S_{s1} = \left(\frac{1}{K} - \frac{1}{K_s}\right)\left(1 - 2\alpha\frac{1-2\nu}{3(1-\nu)}\right) + \rho g\left(\frac{\theta_s}{K_f} - \frac{\theta_s}{K_s}\right) \tag{2.28a}$$

$$\zeta = \frac{\beta(1+\nu)}{3(1-\nu) - 2\alpha\beta(1-2\nu)} \tag{2.28b}$$

It can be seen that Equation 2.27 is a subset of Equation 2.21 which is more general.

Equations 2.20 to 2.26 are developed for isotropic materials, for transversely anisotropic materials (isotropic along horizontal planes and anisotropic in the vertical direction), β , σ_t, and S_{s3} in Equation 2.21 must be replaced by:

$$\beta' = \frac{\frac{1}{K_H} - \frac{1}{K_s}}{\left(\frac{2}{3K_H} - \frac{1}{3K_V} - \frac{1}{K_s}\right) + \left(\frac{\theta_s}{K_f} - \frac{\theta_s}{K_s}\right)} \tag{2.29}$$

$$\sigma'_t = \frac{\sigma_{xx}}{3} + \frac{\sigma_{yy}}{3} + \frac{\sigma_{zz}}{3}\left(\frac{\frac{1}{K_V} - \frac{1}{K_s}}{\frac{1}{K_H} - \frac{1}{K_s}}\right) \tag{2.30}$$

$$S'_{s3} = \left(\frac{2}{3K_H} + \frac{1}{3K_V} - \frac{1}{K_s}\right) + \left(\frac{\theta_s}{K_f} - \frac{\theta_s}{K_s}\right) \tag{2.31}$$

where σ_{xx}, and σ_{yy} are total stresses [M T^{-2} L^{-1}] in the horizontal x and y directions, respectively, σ_{zz} is the total stress [M T^{-2} L^{-1}] in the vertical direction, K_H and K_V are bulk moduli in the horizontal and vertical directions, respectively. It is implicitly assumed that solid grain compressibility is isotropic. A general formulation for anisotropic materials is given by Guvanasen and Chan (2000).

2.2 Surface Flow

2.2.1 General

This section describes the mathematical theory of the surface water flow package of the **HydroGeoSphere** simulator. Surface flow on catchment basins is an important component of the hydrologic cycle, governing flow to and from the subsurface, channel networks, rivers, lakes and reservoirs. Lake and reservoir flow dynamics and hydrologic conditions of wetlands are also areal surface flow processes.

Areal surface flow is represented in **HydroGeoSphere** by a two-dimensional depth-averaged flow equation, which is the diffusion-wave approximation of the Saint Venant equation for surface water flow. Before presenting the diffusion-wave equation solved by **HydroGeoSphere** we present the simplifications needed to obtain this equation from the full two-dimensional Saint Venant equations.

2.2.2 Governing Equations

2.2.2.1 Surface Runoff

The two-dimensional Saint Venant equations for unsteady shallow water flow consist of three equations, which are given by the following mass balance equation:

$$\frac{\partial \phi_o h_o}{\partial t} + \frac{\partial(\overline{v}_{xo} d_o)}{\partial x} + \frac{\partial(\overline{v}_{yo} d_o)}{\partial y} + d_o \Gamma_o \pm Q_o = 0 \tag{2.32}$$

coupled with the momentum equation for the x-direction:

$$\frac{\partial}{\partial t}(\overline{v}_{xo} d_o) + \frac{\partial}{\partial x}(\overline{v}_{xo}^2 d_o) + \frac{\partial}{\partial y}(\overline{v}_{xo}\overline{v}_{yo} d_o) + g d_o \frac{\partial d_o}{\partial x} = g d_o (S_{ox} - S_{fx}) \tag{2.33}$$

and the momentum equation for the y-direction:

$$\frac{\partial}{\partial t}(\overline{v}_{yo} d_o) + \frac{\partial}{\partial y}(\overline{v}_{yo}^2 d_o) + \frac{\partial}{\partial x}(\overline{v}_{xo}\overline{v}_{yo} d_o) + g d_o \frac{\partial d_o}{\partial y} = g d_o (S_{oy} - S_{fy}) \tag{2.34}$$

where d_o is the depth of flow [L], z_o is the bed (land surface) elevation [L], h_o is the water surface elevation [L] ($h_o = z_o + d_o$), $\overline{v}_{xo}$ and $\overline{v}_{yo}$ are the vertically averaged flow velocities in the x- and y-directions [L T^{-1}], Q_o is a volumetric flow rate per unit area representing external source and sinks [L T^{-1}], $d_o \Gamma_o$ [L T^{-1}] is a volumetric flow rate per unit area representing flow between the surface and subsurface domains, and ϕ_o is a surface flow domain porosity which is unity for flow over a flat plane, and varies between zero at the land surface and unity at the top of all rills and obstructions, for flow over an uneven surface. This conceptualization is discussed further in Section 2.2.2.2.

The variables S_{ox}, S_{oy}, S_{fx}, and S_{fy} are dimensionless bed and friction slopes in the x- and y-directions, respectively. Using Manning's equation, the friction slopes are approximated by

$$S_{fx} = \frac{\overline{v}_{xo}\overline{v}_{so} n_x^2}{d_o^{4/3}} \tag{2.35}$$

$$S_{fy} = \frac{\overline{v}_{yo}\overline{v}_{so} n_y^2}{d_o^{4/3}} \tag{2.36}$$

where $\overline{v}_{so}$ is the vertically averaged velocity [L T^{-1}] along the direction of maximum slope s ($\overline{v}_{so} = \sqrt{v_{xo}^2 + v_{yo}^2}$), n_x and n_y are the Manning roughness coefficients [L$^{-1/3}$ T] in the x- and y-directions.

Momentum Equations 2.33 and 2.34 can be simplified by neglecting the first three terms on the left hand side, representing inertia (Gottardi and Venutelli, 1993) and using the approximation of the friction slopes (Equations 2.35 and 2.36) to give

$$\overline{v}_{ox} = -K_{ox} \frac{\partial h_o}{\partial x} \tag{2.37}$$

$$\overline{v}_{oy} = -K_{oy} \frac{\partial h_o}{\partial y} \tag{2.38}$$

where K_{ox} and K_{oy} are surface conductances [L T^{-1}] given by

$$K_{ox} = \frac{d_o^{2/3}}{n_x} \frac{1}{[\partial h_o / \partial s]^{1/2}} \tag{2.39}$$

$$K_{oy} = \frac{d_o^{2/3}}{n_y} \frac{1}{[\partial h_o / \partial s]^{1/2}} \tag{2.40}$$

and s is taken in the direction of maximum slope.

The surface flow equation solved by **HydroGeoSphere** is finally obtained by substituting Equations 2.37 and 2.38 into continuity Equation 2.32, which gives the following diffusion wave approximation for surface flow:

$$\frac{\partial \phi_o h_o}{\partial t} - \frac{\partial}{\partial x}\left(d_o K_{ox} \frac{\partial h_o}{\partial x}\right) - \frac{\partial}{\partial y}\left(d_o K_{oy} \frac{\partial h_o}{\partial y}\right) + d_o \Gamma_o \pm Q_o = 0 \tag{2.41}$$

with Equations 2.39 and 2.40 providing expressions for conductances K_{ox} and K_{oy}.

In addition to neglecting the inertial terms, the assumptions associated with the diffusion-wave equation are those of the Saint Venant equations, which are depth-averaged flow velocities, hydrostatic pressure distribution vertically, mild slope, and dominant bottom shear stresses. Furthermore, it is assumed that Manning's formula is valid to calculate frictional resistance forces for unsteady flow.

To simplify the presentation of the discretized surface flow equation in the next chapter, Equation 2.41 is rewritten in vectorial notation:

$$-\nabla \cdot (d_o \mathbf{q_o}) - d_o \Gamma_o \pm Q_o = \frac{\partial \phi_o h_o}{\partial t} \tag{2.42}$$

where the fluid flux $\mathbf{q_o}$ [L T^{-1}] is given by:

$$\mathbf{q_o} = -\mathbf{K_o} \cdot k_{ro} \nabla (d_o + z_o) \tag{2.43}$$

where k_{ro} is a dimensionless factor that accounts for the reduction in horizontal conductance from obstruction storage exclusion, which is discussed in Section 2.2.2.2.

2.2.2.2 Treatment of Rill Storage and Storage Exclusion for Rural and Urban Environments

For investigations of urban runoff or agricultural settings, the storage and flow terms of Equation 2.41 have been further enhanced to include rill storage, also known as depression storage, and exclusion effects from obstruction storage. Figure 2.1 shows various physical settings that can be simulated by the model, given an appropriate formulation of the storage and flow terms.

It can be assumed that flow occurs over a flat plane, as shown in Figure 2.1a, without any rill storage or obstruction storage effects. In that case, the surface flow domain porosity

ϕ_o is always unity. For flood calculations in urban environments, the setting may be much different as shown in Figure 2.1b, with flow occurring between the grid of buildings in an averaged sense over the grid area. If the flood is high enough to cover the buildings, only then is the full area available for flow and storage of water, otherwise, if not accounted for, lower flood-depths and incorrect discharge would be predicted for an urban flood event. The storage capacity that is reduced by the presence of the urban features is called obstruction storage exclusion. Obstruction storage exclusion may also result from vegetation in rural or agricultural settings. In addition, these features may also affect the conductance of the horizontal flow term due to additional frictional resistance and small scale energy dissipation over the obstruction heights. Rill storage can be an important factor in several urban as well as rural settings as shown in Figure 2.1c. It represents the amount of storage that must be filled before any lateral surface flow can occur. Microtopographic relief, relative to the scale of the finite elements in the grid, is included in rill storage and can have a substantial impact on hydrograph shape (Woolhiser et al., 1997). Finally, for agricultural plots or grass lands (shown in Figure 2.1d), the storage effects of rills as well as storage exclusion of the crop must be taken into account and both rill and obstruction storage need to be included in the model. In addition, horizontal flow term conductances may also be affected over the obstruction heights.

Rill storage and obstruction storage exclusion are both modeled by assuming that the combined depressions and exclusions have a maximum elevation and that the area covered by surface water varies between zero and full area, from land surface up to this maximum elevation as shown in Figure 2.2. The variation of area covered by surface water with depth (H_s) is expressed as a volumetric height which is assumed to be parabolic. The slope of this curve is a porosity or void ratio which varies between zero at land surface up to unity at height H_s. Linear or other functions may have been used, however, a parabolic variation provides for continuous derivatives at land surface and at the maximum height H_s, thus assisting during numerical solution by Newton-Raphson or modified-Picard linearization methods. The heights of depression storage H_d and of storage within the obstructions, H_o, may be estimated such that they geometrically represent the mean spacing (equivalent void space) within the respective storage elements. The depression storage height above land surface ($LS + H_d$), is also used to indicate the elevation below which flow depth is zero in the advection terms of Equation 2.41, when depression storage is modeled for a system. Thus, surface flow occurs laterally only above elevations of $LS + H_d$, i.e., when water levels are above the depression storage elevations. In addition, conductance terms K_{ox} and K_{oy} may be further reduced by a factor k_{ro} above this elevation, up to the obstruction height of storage exclusion to account for the additional resistance losses. The factor k_{ro} varies from zero to unity as the obstruction heights vary from 0 to H_o.

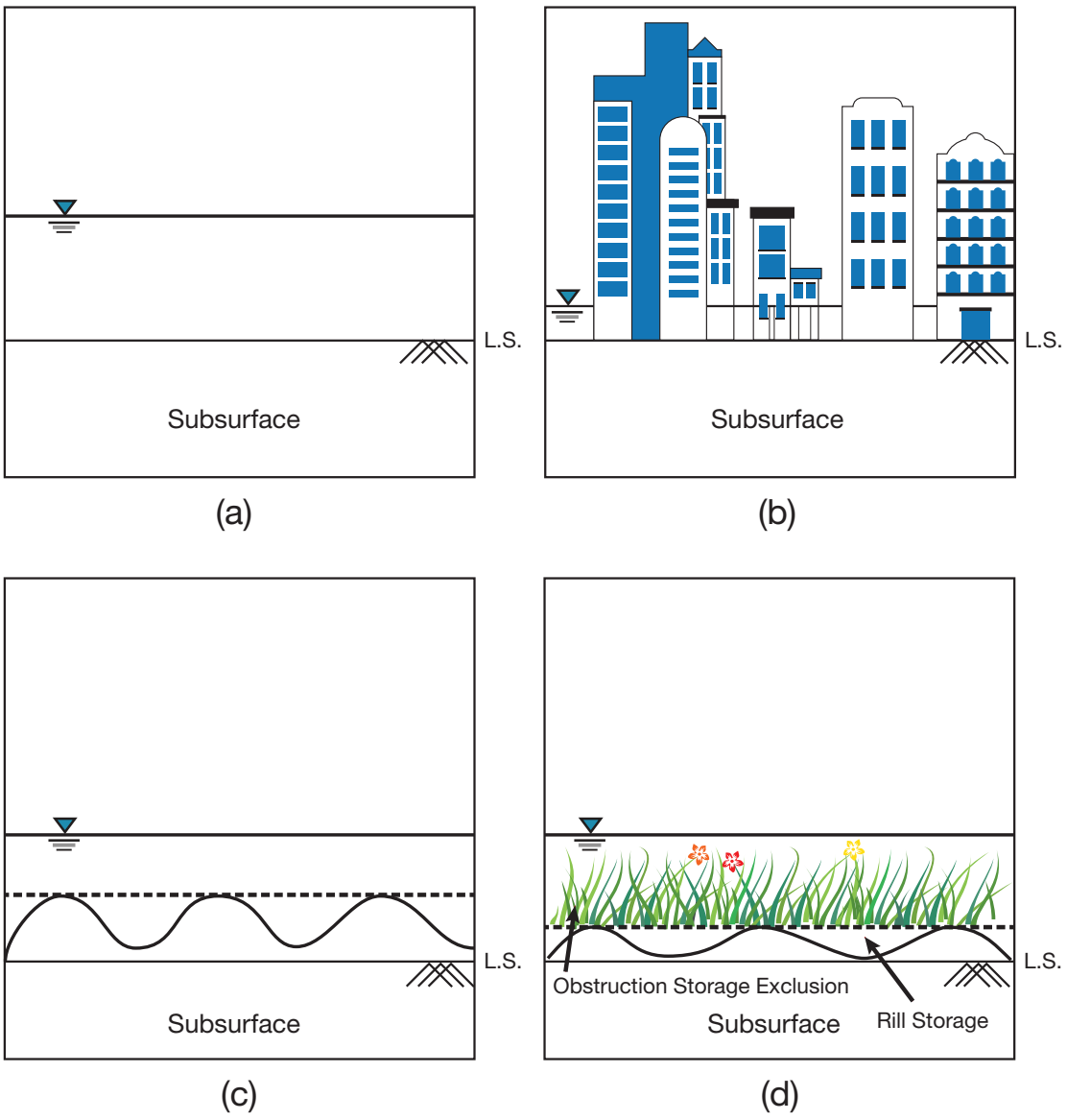

Note that Rill storage, obstruction storage exclusion as well as friction coefficients may be varied on a stress period basis to account for crop growth or changes in land use.

Figure 2.1: Treatment of Storage Terms for Various Settings (adapted from Panday and Huyakorn (2004, Figure 2)).

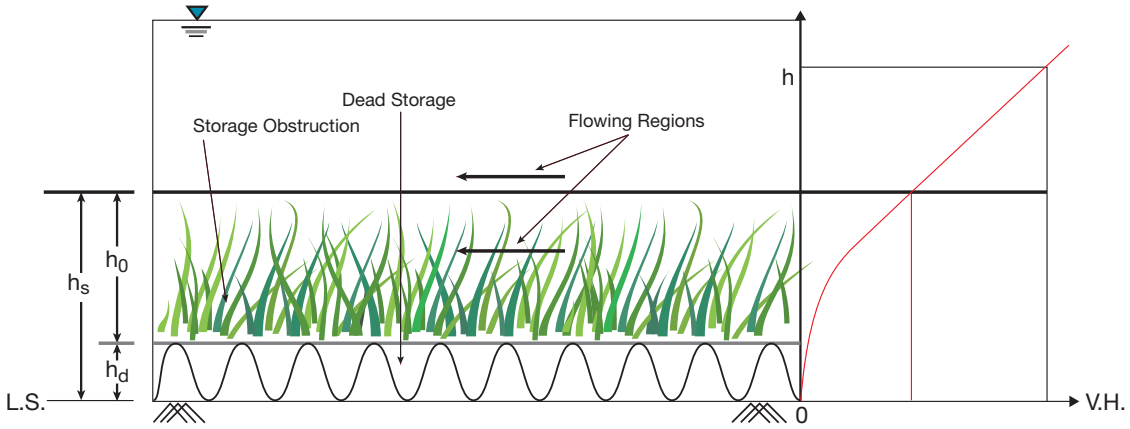

L.S. = Land surface = elevation of top of underlying subsurface node.

h_d = height of depression storage = height at which overland flow starts to occur.

h_o = height of storage within obstructions

h_s = $h_d + h_0$ = maximum height over which area covered by surface water goes from zero to unity.

V.H. = 'volume height' defined as the height from L.S., of an equivalent volume of water without rills or obstructions.

Figure 2.2: Conceptual Model for Depression Storage and Obstruction Storage Exclusion (adapted from Panday and Huyakorn (2004, Figure 3)).

2.3 One-Dimensional Hydraulic Features

2.3.1 General

One-dimensional hydraulic features like streams, rivers, subsurface wells, water supply lines, and drain pipes are simulated by a general one-dimensional equation to describe fluid flow in terms of the Hagen-Poiseuille analytic, Manning's or Hazen-Williams empirical formula. Common node or dual node approaches can be used to simulate the interaction between the 1D flow domain and 2D overland or 3D subsurface domains. The 1-D features in **HydroGeoSphere** can be applied to design urban infrastructures and regional-scale drainage networks.

2.3.2 Governing Equations

2.3.2.1 General One-Dimensional Flow

Water flow along the axis, s, of a one-dimensional features can be described by the following generalized form of the continuity equation integrated over the flow area perpendicular to the principal axis, A_f:

$$-\frac{\partial}{\partial s}(Q_{1D}) + Q_w \delta(s - s_p) = \frac{\partial}{\partial t}[A_f] \tag{2.44}$$

and:

$$Q_{1D} = A_f \cdot q_{1D} \tag{2.45}$$

where Q_{1D} is the fluid flux along the one-dimensional medium, q_{1D} is the linear averaged velocity over the cross sectional flow area A_f and Q_w is the rate of addition or extraction of water at $s = s_p$. In pipe flow, the area of flow is defined as a function of saturation such that:

$$A_f = A_{1D} S_{1D} \tag{2.46}$$

where A_{1D} is the saturated pipe area and S_{1D} is the pipe saturation ranging between 0 and 1 for empty and fully filled pipes.

Various analytical and empirical relationships have been suggested to solve one-dimensional fluid flux for different types of media. Hagen-Poiseuille analytic formula has been used to describe flow along the inside of wells while Manning's equation is widely used for open channel flow for both streams and rivers. Furthermore, the Hazen-Williams equation has been typically recommended for pipe flow in water supply systems. A generalized form to describe the flow along each of the one dimensional hydraulic features is shown in the following form:

$$Q_{1D} = -C \cdot A_f \cdot (R_H)^p \cdot \left[\frac{\partial h_w}{\partial s}\right]^q \tag{2.47}$$

where C is a proportionality constant, p and q are fitting exponents, and R_H is the hydraulic radius.

2.3.2.2 Flow Through Subsurface Wells

Groundwater wells are typically installed at the ground surface and can be used to extract groundwater, monitor subsurface environments, or inject hazardous waste fluids for long-term storage. Generally, the length of the subsurface wells can be assumed to be much larger than the cross-sectional area of the well casing. With this assumption, well hydraulic properties and fluid flow can be simplified, integrated, and averaged over the well cross section into a one-dimensional approximation.

Saturated groundwater flow along the axis of a well, assuming laminar conditions, has been described using Hagen-Poiseuille analytic formula in groundwater hydrology Therrien and Sudicky (2000):

$$Q_{1D} = -\left(\pi r_w^2\right)\left(\frac{r_w^2 \rho g}{8\mu}\right)\frac{\partial h_w}{\partial s} \tag{2.48}$$

and:

$$\frac{\partial}{\partial s}\left(\pi r_w^4 \frac{\rho g}{8\mu}\frac{\partial h_w}{\partial s}\right) + Q_w \delta(s - s_p) + \Gamma_{pm\to w} = \pi r_w^2 S_{sw}\frac{\partial h_w}{\partial t} \tag{2.49}$$

where r_w is the radius of a well, $h_w = h_w(s)$ is the hydraulic head in the well, $S_{sw} = \rho g \beta$ is the specific storage coefficient of a fluid-filled borehole where ρ and β are the density and compressibility of water, g is the gravitational acceleration, and μ is the viscosity of the fluid. For partially saturated wells, Equations 2.48 and 2.49 are modified to include a reduction of flow area, permeability, and water volume due to the decrease in water saturation as described as:

$$Q_{1D} = -k_{rw}\left(S_{ww} \cdot \pi r_w^2\right)\left(r_w^2 \frac{\rho g}{8\mu}\right)\frac{\partial h_w}{\partial s} \tag{2.50}$$

and:

$$\frac{\partial}{\partial s}\left(k_{rw} S_{ww} \pi r_w^4 \frac{\rho g}{8\mu}\frac{\partial h_w}{\partial s}\right) + Q_w \delta(s - s_p) = \pi r_w^2 S_{ww} S_{sw}\frac{\partial h_w}{\partial t} + \pi r_w^2 \frac{\partial S_{ww}}{\partial t} \tag{2.51}$$

where S_{ww} is the degree of saturation and the relative permeability of the well and k_{rw} ranges between 0 (when it is completely dry) and 1 (when it is fully-saturated).

Therrien and Sudicky (2000) accounted for the interaction between the well and the surrounding porous medium by assuming and the flux continuity can also be assumed such that

$$\Gamma_{pm\to w} = -2\pi r_w (k_r)_{exch(pm,w)} K_{exch(pm,w)} \frac{h_w - h}{l_{exch(pm,w)}} \tag{2.52}$$

and:

$$\frac{\partial}{\partial s}\left(k_{rw}S_{ww}\pi r_w^4\frac{\rho g}{8\mu}\frac{\partial h_w}{\partial s}\right)+Q_w\delta(s-s_p)+\Gamma_{pm\to w}=\pi r_w^2 S_{ww}S_{sw}\frac{\partial h_w}{\partial t}+\pi r_w^2\frac{\partial S_{ww}}{\partial t} \quad (2.53)$$

where $\Gamma_{pm\to w}$ is the fluid exchange through the interface between the porous media and well with an exchange the thickness of $l_{exch(pm,w)}$ and a hydraulic conductivity of $K_{exch(pm,w)}$. The upstream relative permeability $(k_r)_{exch(pm,w)}$ is determined between the two domains by:

$$(k_r)_{exch(pm,w)}=\begin{cases}(k_r)_{pm}, & \text{if } h\geq h_w\\ (k_r)_w, & \text{if } h<h_w\end{cases} \quad (2.54)$$

2.3.2.3 Flow Through Subsurface Pipe Systems

For the design of water supply system, pressure driven flow is often described by the Hazen-Williams empirical equation (HWE). The HWE relates the flow of water and hydraulic properties inside of the pipe to the rate of total head loss caused by friction such that

$$Q_{1D}=-k\cdot C_{HW}\cdot A_f\cdot(R_H)^{0.63}\cdot\left[\frac{\partial h_p}{\partial s}\right]^{0.54} \quad (2.55)$$

$$\frac{\partial}{\partial s}\left(k\cdot C_{HW}\cdot A_f\cdot(R_H)^{0.63}\cdot\left[\frac{\partial h_p}{\partial s}\right]^{0.54}\right)+Q_p\delta(s-s_c)=\pi r_p^2 S_{sp}\frac{\partial h_p}{\partial t} \quad (2.56)$$

where $h_p=h_p(s)$ is the hydraulic head at the given location s (along the principal axis), $S_{sp}=\rho g\beta$ is the specific storage, Q_p is the rate of water consumption at the location s_c, k is the dimensional unit conversion factor ($0.849m^{0.37}/s$), C_{HW} is the Hazen-Williams roughness coefficient, and R_H is the hydraulic radius defined as the ratio of the area of flow and the wetted perimeter ($R_H\equiv A_f/P_f$). The hydraulic radius for a full-pipe flow is defined as:

$$R_H=\frac{\pi r_w^2}{2\pi r_w}=\frac{r_w}{2} \quad (2.57)$$

Because water supply systems carry pressurized water through pipe networks, they lose a certain portion of water throughout the networks. The leakage of water can be assumed to follow a first-order leakance relationship and is incorporated into Equation 2.56 as:

$$\Gamma_{p\to pm}=-2\pi r_p K_{exch(pm,p)}\frac{h_p-h}{l_{exch(pm,p)}} \quad (2.58)$$

$$\frac{\partial}{\partial s}\left(k\cdot C_{HW}\cdot A_f\cdot(R_H)^{0.63}\cdot\left[\frac{\partial h_p}{\partial s}\right]^{0.54}\right)+Q_p\delta(s-s_c)+\Gamma_{p\to pm}=\pi r_p^2 S_{sp}\frac{\partial h_p}{\partial t} \quad (2.59)$$

Note that the head in water supply pipes, h_p, is supposed to be significantly greater than the surrounding head, h, and thus water should always leak from the water supply pipe into the subsurface or $\Gamma_{p\to pm}$.

2.3.2.4 Open Channel Flow

Open channel flow along rivers and streams in the surface or for gravity flow in sewer systems is best described with Manning's empirical formula:

$$Q_{1D} = -\frac{1}{n_s} \cdot A_f \cdot (R_H)^{2/3} \cdot \left[\frac{\partial h_c}{\partial s}\right]^{1/2} \tag{2.60}$$

$$\frac{\partial}{\partial s}\left(-\frac{1}{n_s} \cdot A_f \cdot (R_H)^{2/3} \cdot \left[\frac{\partial h_c}{\partial s}\right]^{1/2}\right) = \frac{\partial A_f}{\partial t} \tag{2.61}$$

where n_s is the Manning roughness coefficient, h_c is the hydraulic head [L] in the channel, and A_f and R_H are functions of h_c. Surface rivers and streams may interact with both the overland domain (river banks) and also the porous medium (stream beds), for example, see Figure 2.3. Sewer systems, typically buried underground, only interact directly with the

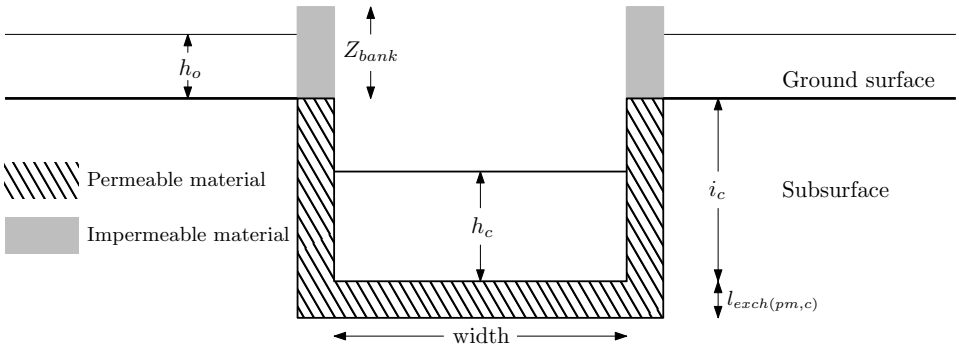

Figure 2.3: Rectangular 1-D channel cross section showing the stream bank height Z_{bank}, incision depth i_c, streambed thickness $l_{exch(pm,c)}$, overland head h_o, and channel head h_c.

porous medium domain. Exchange between the 1-D channel domain and overland domain, $\Gamma_{\text{olf}\to c}$, is given by

$$\Gamma_{\text{olf}\to c} = \begin{cases} 0, & \text{if } h_c - i_c < Z_{bank} \text{ and } h_o < Z_{bank} \\ \frac{(4C_d/3)(h_{up}-Z_{bank})\sqrt{2g(h_{up}-h_{dn})}}{\text{sgn}(h_o-h_c+i_c)}, & \text{if } h_c - i_c \geq Z_{bank} \text{ and } h_o \geq Z_{bank} \\ \frac{(4C_d/3)(h_{up}-Z_{bank})\sqrt{2g(h_{up}-Z_{bank})}}{\text{sgn}(h_o-h_c+i_c)}, & \text{otherwise} \end{cases} \tag{2.62}$$

where i_c is the channel incision depth [L], h_{up} and h_{dn} are the upstream and downstream heads [L], respectively, among h_o and $h_c - i_c$, Z_{bank} is the stream bank elevation [L], and C_d is the weir discharge coefficient [-]. Exchange between the 1-D channel domain and subsurface, $\Gamma_{pm\to c}$, is given by

$$\Gamma_{pm\to c} = -P_f \cdot (k_r)_{exch(pm,c)} \cdot K_{exch(pm,c)} \frac{h_c - i_c - h}{l_{exch(pm,c)}} \tag{2.63}$$

where P_f is wetted perimeter [L], $l_{exch(pm,c)}$ is the streambed thickness [L], $K_{exch(pm,c)}$ is the streambed hydraulic conductivity, and the upstream relative permeability is defined as

$$(k_r)_{exch(pm,c)} = \begin{cases} (k_r)_{pm}, & \text{if } h > h_c - i_c \\ (k_r)_c, & \text{if } h \leq h_c - i_c \end{cases} \tag{2.64}$$

Incorporating the exchange terms into Equation (2.61) yields the final equation for 1-D channel flow

$$\frac{\partial}{\partial s}\left(\frac{1}{n_s} \cdot A_f \cdot (R_H)^{2/3} \cdot \left[\frac{\partial h_c}{\partial s}\right]^{1/2}\right) + \Gamma_{pm\to c} + \Gamma_{\text{olf}\to c} = \frac{\partial A_f}{\partial t} \tag{2.65}$$

2.4 Flow Coupling

Two different approaches are used to define the water exchange terms Γ_{ex} between two different domains. The first approach is based on superposition (see Therrien and Sudicky (1996)), where continuity of hydraulic head is assumed between the two domains concerned, which corresponds to instantaneous equilibrium between the two domains. In that case, the Γ_{ex} term does not need to be evaluated implicitly in the model and we do not present its definition. However, the fluid exchange can be computed after the numerical solution of the discrete equations as a post-processing step. This approach corresponds to the common node scheme mentioned later in the manual.

The second method is more general because it does not assume continuity of hydraulic head between two domains but uses a Darcy flux relation to transfer water from one domain to the other. The Darcy flux is computed from the hydraulic head difference between two domains and assumes that they are separated by a (possibly) thin layer of porous material across which water exchange occurs. This second approach corresponds to the dual node scheme mentioned later in the manual.

Table 2.1 summarizes the types of fluid flow coupling currently available in **HydroGeoSphere**. Both common node and dual node approaches are currently available in the model to simulate the exchange between the subsurface porous medium and fractures, between the porous medium and wells, and between the porous medium and the tile drains. On the other hand, fluid exchange between the subsurface porous medium and a dual continuum can only be simulated with the dual node approach. We present here the definition of the exchange term for the dual node approach.

2.4.1 Dual Continuum Subsurface Coupling

When the dual node approach is chosen to represent simultaneous flow in the subsurface porous medium and a second continuum (representing fractures or macropores), the exchange term can be defined as (Gerke and van Genuchten, 1993):

$$\Gamma_d = \alpha^*_{wd} K_a k_{ra} (\psi_d - \psi), \tag{2.66}$$

Table 2.1: Types of Coupling and Dimensionality for Fluid Flow.

	Coupling	
Domains	Common	Dual
Porous medium - Discrete fractures (2-D)	√	√
Porous medium - Second continuum (3-D)		√
Porous medium - Wells (1-D)	√	√
Porous medium - Tile drains (1-D)	√	√
Porous medium - Surface (2-D)	√	√
Porous medium - Channel (1-D)	√	√

where

$$\alpha_{wd}^{*} = \frac{\beta_d}{a} \cdot \frac{\gamma_w}{a}, \tag{2.67}$$

β_d/a is the macropore surface area per unit total volume of the medium [L^{-1}], β_d is a dimensionless geometrical shape factor, a is the fracture-matrix skin thickness [L] over which the flow exchange occurs, and γ_w is a dimensionless empirical coefficient. The hydraulic conductivity of the interface between the two domains is given by K_a [$L\ T^{-1}$] and its relative permeability is k_{ra} [-]. For dual-porosity systems, the geometry factor β_d has been shown to be equal to 3 for rectangular slabs and 15 for spheres. Gerke and van Genuchten (1993) provide more detail on the evaluation of the exchange term.

2.4.2 Surface - Subsurface Coupling

When the dual node approach is chosen to represent simultaneous flow in the subsurface and the surface domain, the exchange term is given by:

$$d_o\Gamma_o = w_m \frac{k_r K_{zz}}{l_{exch}}(h - h_o) + w_d \frac{k_{dr} K_{dzz}}{l_{exch}}(h_d - h_o) \tag{2.68}$$

where a positive Γ_o represents flow from the subsurface system to the surface system as determined by Equation 2.32, h_o is the surface water head, h and h_d are the subsurface porous medium and dual medium heads, respectively, k_r and k_{dr} are the relative permeabilities for the exchange flux, K_{zz} and K_{dzz} are the vertical saturated hydraulic conductivities of the underlying porous and dual media, respectively, and l_{exch} is the coupling length. The relative permeability term is same as the subsurface relative permeability when water flows from subsurface to surface, while, when water flows from surface to subsurface it is determined by the ratio of the water depth in the surface to the total obstruction height (H_s) such that

$$k_r = \begin{cases} S_{exch}^{2(1-S_{exch})} & \text{when } d_o < H_s \\ 1 & \text{when } d_o > H_s \end{cases} \tag{2.69}$$

where $S_{exch} = d_o/H_s$.

2.5 Flow Boundary Conditions

2.5.1 Subsurface flow

Boundary conditions for subsurface flow include the following: first-type (Dirichlet) boundaries of prescribed hydraulic or pressure head, areal infiltration or recharge, source/sinks, evaporation, seepage faces, free-drainage and drain nodes, and third-type boundary conditions. The boundary conditions can also be allowed to vary in time. Details of the implementation of these boundary conditions in the model are given in the next chapter.

When **HydroGeoSphere** is used to solve fully coupled subsurface and surface flow, the areal recharge boundary for subsurface flow is not required since the solution to the interacting system determines the subsurface recharge.

2.5.2 Surface Flow

Boundary conditions to the surface flow system include the following: first-type (Dirichlet) boundaries of prescribed water elevation, direct rainfall inputs, source/sinks, evaporation, zero-depth gradient and nonlinear critical-depth conditions, as discussed in the next chapter.

2.5.3 Interception and Evapotranspiration

Interception and actual evapotranspiration are simulated as mechanistic processes governed by plant and climatic conditions. The formulation used here is similar to that proposed by Kristensen and Jensen (1975) and Allen et al. (1998), which is used in the model presented by (Panday and Huyakorn, 2004). Actual evapotranspiration is calculated by reducing potential evapotranspiration according to vegetation characteristics, subsurface saturation, and rainfall distribution.

2.5.3.1 Interception and Canopy Evaporation

Interception is the retention, or storage, of a certain amount of precipitation on the leaves, branches, and stems of vegetation. The interception storage varies between zero and the interception storage capacity S_{int}^{max} [L], which depends on the vegetation type and its stage of development. It is calculated from (Kristensen and Jensen, 1975)

$$S_{int}^{max} = c_{int} \cdot LAI \tag{2.70}$$

where LAI is the dimensionless leaf area index, which is the cover of leaves over a unit area of ground surface, and c_{int} is the canopy storage parameter [L].

The interception storage is filled by rainfall and depleted by evaporation from interception, which is equivalent to canopy evaporation. When the canopy evaporation interval is zero,

filling and emptying are done within a single time step of size Δt according to the following equations:

$$E_{can} = \min\left(E_p,\ P_p + S^0_{int}/\Delta t\right) \tag{2.71}$$

$$S_{int} = \min\left(S^{max}_{int},\ \max(0,\ S^0_{int} + (P_p - E_{can})\Delta t)\right) \tag{2.72}$$

where E_p is potential evapotranspiration [L T^{-1}], P_p is the precipitation rate [L T^{-1}], and S^0_{int} [L] is the value of S_{int} [L] at the previous time.

If the canopy evaporation interval Δt_{can} [T] is positive, then canopy storage is allowed first to fill and then empty once per interval, which typically comprises a number of simulation timesteps. When filling

$$E_{can} = 0 \tag{2.73}$$

$$S_{int} = \min\left(S^{max}_{int},\ S^0_{int} + P_p \cdot \Delta t\right) \tag{2.74}$$

and when emptying

$$E_{can} = \min\left(E_p, S^0_{int}/\max(\Delta t, \Delta t_{can} + t^0_{can} - t)\right) \tag{2.75}$$

$$S_{int} = \max\left(0,\ S^0_{int} - E_{can} \cdot \Delta t\right) \tag{2.76}$$

where t is the current simulation time and $t^0_{can} \leq t$ is the starting time of the current filling/emptying cycle.

Potential evapotranspiration E_p is an input to the model and it may be derived from pan measurements or computed from vegetation and climatic factors (radiation, wind, humidity, and temperature) using the Penman–Monteith equation (Monteith, 1981) for vegetated surfaces or a bare-ground evaporation formula (Senarath et al., 2000) for non-vegetated surfaces, as a function of temperature, wind, and humidity conditions.

The interception process is simulated by a bucket model where precipitation in excess of interception storage and canopy evaporation reaches ground surface. The effective rainfall rate, or reduced rainfall rate, P^E_p [L T^{-1}] that reaches ground surface after interception and canopy evaporation is given by:

$$P^E_p = \max\left(0, P_p - \frac{S_{int} - S^0_{int}}{\Delta t} - E_{can}\right) \tag{2.77}$$

2.5.3.2 Evapotranspiration

Evapotranspiration affects both surface and subsurface flow domains and it is rigorously modeled as a combination of transpiration from vegetation and evaporation.

Transpiration from vegetation occurs within the root zone of the subsurface, which may be above or below the water table. The rate of transpiration T_p [L T^{-1}] is estimated using

the following relationship that distributes the net capacity for transpiration among various factors (Kristensen and Jensen, 1975)

$$T_p = f_1(LAI)\, f_2(\theta)\, RDF\, (E_p - E_{can})\,, \tag{2.78}$$

where $f_1(LAI)$ is a dimensionless vegetation term that is a function of the leaf area index, $f_2(\theta)$ is a function of the soil water content [-] and RDF is the time-varying root distribution function [-]. The vegetation term $f_1(LAI)$ is expressed as

$$f_1(LAI) = \max\{0,\, \min\{1,\, C_2 + C_1 \cdot LAI\}\}\,, \tag{2.79}$$

where C_1 and C_2 are dimensionless fitting parameters. The root distribution function RDF is defined as

$$RDF = \frac{\displaystyle\int_{z_1'}^{z_2'} r_F(z')dz'}{\displaystyle\int_0^{L_r} r_F(z')dz'}\,, \tag{2.80}$$

where L_r is the effective root length [L], z' is the depth with respect to ground surface [L], and $r_F(z')$ is the root extraction function [$\mathrm{L}^3\ \mathrm{T}^{-1}$], which typically varies logarithmically with depth. The soil water content function $f_2(\theta)$ is expressed as

$$f_2(\theta) = \begin{cases} 0 & \text{for } 0 \le \theta \le \theta_{wp} \\ f_3 & \text{for } \theta_{wp} \le \theta \le \theta_{fc} \\ 1 & \text{for } \theta_{fc} \le \theta \le \theta_o \\ f_4 & \text{for } \theta_o \le \theta \le \theta_{an} \\ 0 & \text{for } \theta_{an} \le \theta \end{cases}\,, \tag{2.81}$$

$$f_3(\theta) = 1 - \left[\frac{\theta_{fc} - \theta}{\theta_{fc} - \theta_{wp}}\right]^{C_3}\,, \tag{2.82}$$

$$f_4(\theta) = \left[\frac{\theta_{an} - \theta}{\theta_{an} - \theta_o}\right]^{C_3}\,, \tag{2.83}$$

where C_3 is a dimensionless fitting parameter, θ_{fc} is the water content at field capacity, θ_{wp} is the water content at the wilting point, θ_o is the water content at the oxic limit, and θ_{an} is the water content at the anoxic limit.

The function $f_1(LAI)$ linearly correlates transpiration (T_p) with the leaf area index (LAI). The function $f_2(\theta)$ correlates T_p with the water state of the roots and is an extension of the function of Kristensen and Jensen (1975) to account for root processes in greater detail. Below the wilting-point water content, transpiration is zero; transpiration then increases to a maximum at the field-capacity water content. This maximum is maintained up to the oxic water content, beyond which the transpiration decreases to zero at the anoxic water content. When the available water is greater than the anoxic water content, the roots become inactive due to lack of aeration (Feddes et al., 1978). In general, $f_2(\theta)$ is a nonlinear function of θ, although the ramping function is linear when $C_3 = 1$.

To incorporate root growth or time-varying root depths ($L_r(t)$), the equation to calculate the transpiration rate needs to be modified as

$$T_p = f_1(LAI) f_2(\theta) RDF(t)(E_p - E_{can}) \tag{2.84}$$

The time-varying root density function $RDF(t)$ is defined as

$$RDF(t) = L_m f_r(t) = \frac{L_m L_0}{L_0 + (L_m - L_0)e^{-rt}} \tag{2.85}$$

where L_m is the maximum root depth [L], $f_r(t)$ is the root growth coefficient, L_0 is the initial root depth [L], and r is the classical Verhulst–Pearl logistic growth rate [T^{-1}].

The model used for evaporation assumes that it occurs along with transpiration, resulting from energy that penetrates the vegetation cover, and is expressed as

$$E_{OLF} = \alpha^*_{OLF}(E_p - E_{can})\,(1 - f_1(LAI)) \tag{2.86}$$

$$E_s = \alpha^*(E_p - E_{can} - E_{OLF})\,(1 - f_1(LAI))\,EDF\,, \tag{2.87}$$

where EDF is the evaporation distribution function (EDF) that includes the overland and subsurface flow domains, and α^*_{OLF} and α^* are the wetness factors for surface and subsurface given by

$$\alpha^*_{OLF} = \begin{cases} (\frac{d_o}{H_s})^{2(1-d_o/H_s)} & \text{for } 0 \le d_o \le H_s \\ 1 & \text{for } d_o > H_s \end{cases} \tag{2.88}$$

$$\alpha^* = \begin{cases} \frac{\theta - \theta_{e2}}{\theta_{e1} - \theta_{e2}} & \text{for } \theta_{e2} \le \theta \le \theta_{e1} \\ 1 & \text{for } \theta > \theta_{e1} \\ 0 & \text{for } \theta < \theta_{e2} \end{cases} \tag{2.89}$$

The parameter θ_{e1} is the water content at the end of the energy-limiting stage (above which full evaporation can occur) and θ_{e2} is the limiting water content below which evaporation is zero (Allen et al., 1998).

Equation 2.89 expresses the water availability term for the subsurface domain. For the overland flow domain, α^*_{OLF} is calculated as varying between unity when the elevation of flow is at or above depression storage plus obstruction storage $z_o + H_s$ and zero for a flow elevation at the land surface (z_o), thus representing the reduced evaporative area of available water in the overland flow domain within the depressions and with obstructions.

For the evaporation distribution function EDF used in Equation 2.87, it is assumed that evaporation decreases with depth below the surface (subject to available water) due to the reduction of energy penetration in the soil. Therefore, an appropriate EDF may be prescribed as a function of its depth from land surface and includes constant, linear (default), quadratic, and cubic decay functions.

2.5.3.3 Actual Evapotranspiration

Actual evapotranspiration is the sum of canopy evaporation (E_{can}), surface evaporation (E_{OLF}), subsurface evaporation (E_s), and subsurface transpiration (T_p), which are defined in the previous sections.

2.6 Winter Hydrological Processes

2.6.1 Surface Water Flow with Snowmelt

Depth integrated surface water flow equation describes only the mass balance of the liquid water in the overland flow domain. In order to consider both solid and liquid phases of water in the surface flow domain, the governing equation needs to be expanded to include both water and snow mass ($\rho_w d_{wv}$ and $\rho_{snow} d_{snow}$). If the solid phase snow is assumed to be immobile, the mass balance of the total water can be formulated as the following:

$$\begin{aligned}\frac{\partial\left(\rho_w d_{wv}+\rho_{snow} d_{snow}\right)}{\partial t} = \\ \frac{\partial}{\partial x}\left(\rho_w d_f K_{ox}\frac{\partial h_o}{\partial x}\right)+\frac{\partial}{\partial y}\left(\rho_w d_f K_{oy}\frac{\partial h_o}{\partial y}\right)-\rho_w\Gamma_{\text{ex}}+\rho_w Q_o+\rho_{snow}\left(Q_{snow}-\mu\right)\end{aligned} \tag{2.90}$$

where Q_{snow} and μ_{snow} represent the rates of snow precipitation and sublimation per unit surface area [$\mathrm{L}^3\ \mathrm{T}^{-1}\ \mathrm{L}^{-2}$]. The depth of snow is determined by the rates of snow precipitation, sublimation, and melting (always sink) which is caused by temperature change.

$$\frac{\partial}{\partial t}\left(\rho_{snow} d_{snow}\right)=\rho_{snow}\left(Q_{snow}-\mu\right)-\rho_{snow} Q_{melt} \tag{2.91}$$

where the depth of snow is always positive and the rate of melting is assumed to be proportional to a constant (η) and the difference between air temperature (T_{air}) and threshold temperature ($T_{threshold}$) when $T_{air} > T_{threshold}$ or $\eta = 0$ when $T_{air} \leq T_{threshold}$.

$$\rho_{snow} Q_{melt}=\eta\left(T_{air}-T_{threshold}\right) \tag{2.92}$$

By combining the total water mass balance equation with the snow balance equation, the balance equation for the liquid phase water is derived as

$$\begin{aligned}\frac{\partial\left(\rho_w d_{wv}\right)}{\partial t} = \frac{\partial}{\partial x}\left(\rho_w d_f K_{ox}\frac{\partial h_o}{\partial x}\right)+\frac{\partial}{\partial y}\left(\rho_w d_f K_{oy}\frac{\partial h_o}{\partial y}\right) \\ -\rho_w\Gamma_{\text{ex}}+\rho_w Q_o+\rho_{snow} Q_{melt}\end{aligned} \tag{2.93}$$

The above equation indicates that the snowmelt always acts as a source for the liquid water balance in the surface flow domain.

2.6.2 Groundwater Flow with Freezing and Thawing of Pore Water

In the subsurface flow system, a conventional groundwater flow equation describes the mass balance of only the liquid water in a three-dimensional porous medium. When the liquid phase of water can be transformed into the solid phase ice (i.e., freezing) or vice versa (i.e., melting), the total mass of water in the system is $\rho_w\theta_s S_w + \rho_{ice}\theta_s S_{ice}$ where the subscripts *ice* represents the solid phase ice. If the ice is assumed to be immobile, then the balance of the total water mass can be described by the following equation:

$$\frac{\partial}{\partial t}(\rho_w\theta_s S_w+\rho_{ice}\theta_s S_{ice})=-\nabla\cdot\rho_w\mathbf{q}+(\rho_w Q_w) \tag{2.94}$$

where ρ_{ice} and S_{ice} are the density and saturation of solid phase ice in the porous medium.

The partitioning of water between solid and liquid phases is assumed to be determined only by the temperature (which is a function of time at a given point) such that

$$p(T) = \frac{\rho_{ice} S_{ice}}{\rho_w S_w + \rho_{ice} S_{ice}} = \begin{cases} 0 & \text{if } T \geq T_f \\ \left(\dfrac{T_f - T}{T_f - T_m}\right)^{\beta} & \text{if } T_m \leq T < T_f \\ 1 & \text{if } T < T_m \end{cases}, \tag{2.95}$$

where T_f and T_m are the freezing and melting temperatures, respectively. Based on experimental data, Rempel (2008) showed that the fitting parameter β [-] ranges between 0.19 and 1.15, with a mean of 0.42. If the density difference between solid and liquid phases of water is assumed to be negligible and the total water saturation remains constant at a given time at a given location,

$$\frac{\partial}{\partial t}(\rho_{ice}\theta_s S_{ice}) = \frac{\partial p(T)}{\partial t}\theta_s \left[S_w \rho_w + S_{ice}\rho_{ice}\right] \tag{2.96}$$

By subtracting the balance equation of ice mass from the balance equation of the total water mass, mass balance for the liquid phase water is derived as the following:

$$\frac{\partial}{\partial t}(\rho_w \theta_s S_w) = -\nabla \cdot \rho_w \mathbf{q} + (\rho_w Q_w) - \frac{\partial p(T)}{\partial t}\theta_s \left[S_w \rho_w + S_{ice}\rho_{ice}\right] \tag{2.97}$$

where the last term for the freezing or melting shows that the freezing of water (with decreasing temperature) plays a role of sink for the liquid phase water while the melting with increasing temperature being a source for the liquid phase.

A simple one-dimensional analytical model is employed to determine the vertical distribution of the temperature of bulk porous medium.

$$\frac{\partial}{\partial t}(T_{pm} - T_b) = \frac{\partial}{\partial z}\left(\frac{k_{pm}}{c_{pm}}\frac{\partial (T_{pm} - T_b)}{\partial z}\right) \tag{2.98}$$

where T_{pm} is the temperature of the bulk porous medium, k_{pm} and c_{pm} are the bulk thermal conductivity and heat capacity, respectively, and it is assumed that the temperature at depth is given as T_b and the surface temperature is same as the atmospheric temperature (T_{atm}) such that

$$T_{pm}(z = 0, t) = T_{atm}(t) \tag{2.99}$$

$$T_{pm}(z \gg 0, t) = T_b \tag{2.100}$$

The analytical solution of the equation is given as follows:

$$\begin{aligned} T_{pm}(z,t) &= T_b + \frac{z}{\sqrt{4\pi\kappa}}\int_{\tau=0}^{t} \frac{\partial T_{atm}(\tau)}{\partial \tau}\,\mathrm{erfc}\left(\frac{z}{\sqrt{4\kappa(t-\tau)}}\right) d\tau \\ &= T_b + \frac{z}{\sqrt{4\pi\kappa}}\int_{\tau=0}^{t} T_{atm}(\tau)\frac{e^{-z^2/4\kappa(t-\tau)}}{(t-\tau)^{3/2}} d\tau \end{aligned} \tag{2.101}$$

where the thermal diffusivity κ is defined as k_{pm}/c_{pm}.

2.6.3 Dual Continuum Freezing and Thawing of Pore Water

Groundwater flow and with freezing and thawing in the three-dimensional porous medium domain (Equation 2.94) is extended to include a dual continuum linked by a fluid exchange term:

$$w_d \frac{\partial}{\partial t}(\rho_w \theta_s S_{w,d} + \rho_w \theta_s S_{ice,d}) = -\nabla \cdot (w_d \rho_w \mathbf{q}_d) + \rho_w Q_d + \rho_w \Gamma_d \tag{2.102}$$

The fluid exchange term is proportional to the head difference between the two domains, the relative hydraulic conductivity of the interface, and the ice content of the porous medium domain:

$$\Gamma_d = \alpha^*_{wd} K_a (1 - S_{ice}) k_r (\psi_d - \psi) \tag{2.103}$$

Partitioning of water between solid and liquid phases in the porous medium domain is assumed to be determined only by the temperature (which is a function of time at a given point), as given previously in Equation 2.95. Within the dual continuum domain, two options for freezing and thawing exist. The first option uses the same formulation as used in the porous medium domain (default). The second option gives the rate of ice-formation after Mohammed et al. (2020) and is controlled by the soil matrix temperature (T), and a specified thermal transfer coefficient (α^*) according to

$$\frac{\partial \theta_{ice,d}}{\partial t} = -\alpha^* T \tag{2.104}$$

The thermal transfer coefficient α^* [T^{-1} $^\circ\mathrm{C}^{-1}$] may be calculated by

$$\alpha^* = \frac{\alpha^*_{wd} \lambda_m}{\rho_{ice} L_i w_d}, \tag{2.105}$$

where L_i (= 335,000 J kg^{-1}) is the enthalpy of fusion for water, λ_m [W m^{-1} $^\circ\mathrm{C}^{-1}$] is the thermal conductivity of the domain interface, which is assumed equal to the thermal conductivity of the matrix domain, and α^*_{wd} is the exchange coefficient that is defined based on the geometry of heat transfer between domains (Equation 2.67).

2.7 Solute Transport

2.7.1 Governing Equations

We present here the basic subsurface transport equation solved by **HydroGeoSphere** which is expanded in its use to incorporate, among other features, discrete fractures, a second porous continuum, wells, tile drains, and the surface flow domain.

2.7.1.1 Porous Medium

Three-dimensional transport of solutes in a variably-saturated porous matrix is described by the following equation:

$$-\nabla \cdot w_m \left(\mathbf{q}C - \theta_s S_w \mathbf{D} \nabla C\right) + \left[w_m \theta_s S_w R \lambda C\right]_{par} + \sum \Omega_{\text{ex}} + Q'_{bc} C_{bc}$$

$$= w_m \left[\frac{\partial(\theta_s S_w R C)}{\partial t} + \theta_s S_w R \, \lambda \, C\right] \tag{2.106}$$

where C is the solute concentration [M L^{-3}] of the current species amongst possibly multiple species and λ is a first-order decay constant [L^{-1}]. The subscript *par* designates parent species for the case of a decay chain. For the case of a straight decay chain, there is only one parent species, as might be the case for a radioactive decay chain; however, for degrading organic species, a particular species may have several parent sources through a complex degradation process.

The terms Q'_{bc} and C_{bc} are the volumetric fluid (water) flow rate per unit volume [L^3 T^{-1} L^{-3}] and the solute concentration [M L^{-3}] at a boundary or at a fluid injection or withdrawal location, respectively. The volumetric flow rate Q'_{bc} is positive for an inflow boundary or an injection location and it is negative for an outflow boundary or a withdrawal location. Furthermore, for an outflow boundary or a withdrawal location, the boundary concentration C_{bc} is equal to the solute concentration C.

The assumption of fluid incompressibility is made in Equation 2.106. The dimensionless retardation factor, R, is given by (Freeze and Cherry, 1979):

$$R = 1 + \frac{\rho_b}{\theta_s S_w} K' \tag{2.107}$$

where ρ_b is the bulk density of the porous medium [M L^{-3}] and K' is the equilibrium distribution coefficient describing a linear Freundlich adsorption isotherm [M^{-1} L^3]. Note that for variably-saturated conditions, the water saturation appears in the definition of R.

The hydrodynamic dispersion tensor $\mathbf{D}$ [L^2 T^{-1}] is given by (Bear, 1972):

$$\theta_s S_w \mathbf{D} = (\alpha_l - \alpha_t) \frac{\mathbf{qq}}{|\mathbf{q}|} + \alpha_t |\mathbf{q}| \mathbf{I} + \theta_s \, S_w \, \tau D_{free} \, \mathbf{I} \tag{2.108}$$

where α_l and α_t are the longitudinal and transverse dispersivities [L], respectively, $|\mathbf{q}|$ is the magnitude of the Darcy flux, τ is the matrix tortuosity [-], D_{free} is the free-solution diffusion coefficient [L^2 T^{-1}] and $\mathbf{I}$ is the identity tensor. The product τD_{free} represents an effective diffusion coefficient for the matrix. In the unsaturated zone, the tortuosity is allowed to vary with the water saturation, S_w, according to the Millington-Quirk relationship (Millington and Quirk, 1961), given by:

$$\tau = (S_w \theta_s)^{7/3} / \theta_s^2 \tag{2.109}$$

In Equation 2.106, Ω_{ex} represents the mass exchange rate of solutes per unit volume [M L^{-3} T^{-1}] between the subsurface domain and all other types of domains supported by the model. Currently, these additional domains are surface, wells, tile drains, channels, discrete fractures, immobile second continuum and mobile dual continuum. The definition of Ω_{ex} depends on the conceptualization of solute exchange between the domains and will be defined later. In the equations shown for the other domains, we will use the notation ex=f, ex=im, ex=d, ex=w, ex=t, ex=c ex=o, for the fracture, immobile continuum, dual continuum, well, tile drain, channel and surface domains, respectively.

2.7.1.2 Discrete Fractures

The equation for two-dimensional solute transport in a variably-saturated fracture follows from the equation describing solute transport in a fully-saturated fracture (Tang et al., 1981; Sudicky and McLaren, 1992; Therrien and Sudicky, 1996). Its form is:

$$-\nabla \cdot (w_f \mathbf{q_f} C_f - w_f S_{wf} \mathbf{D_f} \nabla C_f) + w_f \left[R_f \lambda_f C_f\right]_{par} - w_f \Omega_f + w_f Q'_{bc} C_{bc} =$$

$$w_f \left[\frac{\partial (S_{wf} R_f C_f)}{\partial t} + S_{wf} R_f \lambda_f C_f\right] \tag{2.110}$$

where C_f is the concentration in a fracture [M L^{-3}], λ_f is a first-order decay constant [L^{-1}] and $\mathbf{D_f}$ is the hydrodynamic dispersion tensor of the fracture [L^2 T^{-1}]. An expression similar to Equation 2.108 can be used to represent $\mathbf{D_f}$, where dispersivities and fluxes correspond to those of the fracture and the fracture porosity is assumed to be unity. The definition of the boundary terms Q'_{bc} and C_{bc} is similar to that presented above for the porous medium.

The dimensionless retardation factor R_f is defined according to (Freeze and Cherry, 1979):

$$R_f = 1 + \frac{2K'_f}{w_f} \tag{2.111}$$

where K'_f is a fracture-surface distribution coefficient [L], which is defined as the ratio between the mass of solute on the solid phase per unit area of an assumed planar fracture surface over the concentration of a solute in solution.

2.7.1.3 Double Porosity

The model can simulate double-porosity transport with the classical first-order theory (see Sudicky (1990)), which divides the subsurface domain into a mobile and an immobile region. The formulation used here for double-porosity is restricted to steady-state flow conditions. It is assumed that the porous medium represents the mobile domain, where flow is described by Equation 2.1 and solute transport is described by Equation 2.106. It is also assumed that there is no flow in the immobile domain, therefore no equation is required for immobile flow, and solute mass balance is given by:

$$\frac{\partial (\theta_{\text{Imm}} C_{\text{Imm}})}{\partial t} - \Omega_{\text{Imm}} = 0 \tag{2.112}$$

where C_{Imm} is the solute concentration in the immobile region [M L^{-3}], θ_{Imm} is the porosity of the immobile region [-] and Ω_{Imm} represents the solute exchange flux between the mobile and immobile zones [M L^{-3} T^{-1}].

2.7.1.4 Isotopic Fractionation

The model can simulate isotope fractionation, using a first-order kinetic formulation that is mathematically similar to double-porosity transport. In analogy to double-porosity, we assume here that the mobile domain represents the water phase and the immobile domain is associated with the solid, or rock, phase.

Similarly to double-porosity transport, the formulation used here for isotope fractionation is restricted to steady-state flow conditions. Fractionation from the water phase is also restricted to a single solid (or rock) phase. It is assumed that the porous medium represents the water domain, where flow is described by Equation (2.1) and isotope transport is described by Equation (2.106). It is also assumed that there is no isotope flow in the solid phase, therefore no equation is required for flow in the solid phase.

Mass balance for the isotope in the solid phase is given by:

$$\frac{\partial C_{\text{Imm}}}{\partial t} - \frac{\Omega_{\text{Imm}}}{x_r} = 0 \tag{2.113}$$

where C_{Imm} is the isotope concentration in the solid, or immobile region [M L^{-3}], Ω_{Imm} represents here the isotope exchange flux between the mobile (water) and immobile (solid) zones [M L^{-3} T^{-1}], and x_r is the dimensionless mass ratio of the isotope in the solid phase to that in the water phase, for a unit volume of water-saturated rock of constant porosity.

2.7.1.5 Dual Continuum

When the dual continuum option is used, advective-dispersive solute transport can be simulated in a second continuum based on the formulation presented by Gerke and van Genuchten (1993). Note that, as opposed to the double-porosity option, the dual continuum option is not restricted to steady-state flow conditions because it allows transient fluid exchange between the two interacting continua. Also, fluid flow and advective-dispersive solute transport can be simultaneously solved in the porous medium and the second continuum. Three-dimensional transport of solutes in a variably-saturated dual continuum is described by:

$$-\nabla \cdot w_d \left(\mathbf{q_d} C_d - \theta_{sd} S_{wd} \mathbf{D_d} \nabla C_d\right) + \left[R_d \lambda_d C_d\right]_{par} - w_d \Omega_d \pm Q_{cd} + Q'_{bc} C_{bc} =$$

$$w_d \left[\frac{\partial(\theta_{sd} S_{wd} R_d C_d)}{\partial t} + \theta_{sd} S_{wd} R_d \lambda_d C_d\right] \tag{2.114}$$

where C_d is the solute concentration in the dual continuum [M L^{-3}] and λ_d is a first-order decay constant [L^{-1}]. Solute exchange with the outside of the simulation domain, as specified

from boundary conditions, is represented by Q_{cd} [M L^{-3} T^{-1}] which represents a source (positive) or a sink (negative) to the dual continuum. The definition of the boundary terms Q'_{bc} and C_{bc} is similar to that presented above for the porous medium.

The dimensionless retardation factor, R_d, is given by (Freeze and Cherry, 1979):

$$R_d = 1 + \frac{\rho_{bd}}{\theta_{sd} S_{wd}} K'_d \tag{2.115}$$

where ρ_{bd} is the bulk density of the dual continuum [M L^{-3}] and K'_d is the equilibrium distribution coefficient describing a linear Freundlich adsorption isotherm [M^{-1} L^3]. Note that for variably-saturated conditions, the water saturation appears in the definition of R_d.

The hydrodynamic dispersion tensor $\mathbf{D_d}$ [L^2 T^{-1}] is given by (Bear, 1972):

$$\theta_{sd} S_{wd} \mathbf{D_d} = (\alpha_{ld} - \alpha_{td}) \frac{\mathbf{q_d q_d}}{|\mathbf{q_d}|} + \alpha_{td} |\mathbf{q_d}| \mathbf{I} + \theta_{sd}\, S_{wd}\, \tau_d D_{free}\, \mathbf{I} \tag{2.116}$$

where α_{ld} and α_{td} are the longitudinal and transverse dispersivities [L], respectively, $|\mathbf{q_d}|$ is the magnitude of the Darcy flux, τ_d is the dual continuum tortuosity [-], D_{free} is the free-solution diffusion coefficient [L^2 T^{-1}] and $\mathbf{I}$ is the identity tensor. The product $\tau_d D_{free}$ represents an effective diffusion coefficient for the dual continuum. Recall from the previous discussion on flow in the unsaturated zone that the tortuosity is a function of the degree of saturation according to Equation 2.109.

2.7.1.6 Wells

One-dimensional solute transport along the axis of a well is described by:

$$-\overline{\nabla} \cdot \pi r_s^2 \left(\mathbf{q_w} C_w - S_{ww} D_w \overline{\nabla} C_w \right) + \pi r_s^2 \left[\lambda C_w \right]_{par} + \pi r_s^2 Q'_{bc} C_{bc} \delta(l - l') - \pi r_s^2 \Omega_w =$$

$$\pi r_s^2 \frac{\partial C_w}{\partial t} + \pi r_s^2 \lambda C_w \tag{2.117}$$

where C_w is the solute concentration in the well [M L^{-3}], $\mathbf{q_w}$ is the fluid flux along the well axis [L T^{-1}]. The term Q'_{bc} represents the injection or withdrawal flow rate [L^3 T^{-1}], C_{bc} is the concentration of injection or withdrawal water [M L^{-3}] and l' is the injection or withdrawal location along the well. For the case of a withdrawal well, C_{bc} is equal to the concentration in the well C_w at the withdrawal location.

The dispersion coefficient for the well, D_w [L^2 T^{-1}] is equal to (Lacombe et al., 1995):

$$D_w = \frac{r_s^2 \mathbf{q_w}^2}{48 D_{free}} + D_{free} \tag{2.118}$$

2.7.1.7 Tile Drains

One-dimensional solute transport along the axis of a tile drain is described by:

$$-\overline{\nabla} \cdot A \left(\mathbf{q_t} C_t - S_{wt} D_t \overline{\nabla} C_t \right) + A \left[\lambda C_t \right]_{par} - A \Omega_t + A Q'_{bc} C_{bc} \delta(l - l') =$$

$$\frac{\partial AC_t}{\partial t} + A\lambda C_t \tag{2.119}$$

where C_t is the solute concentration in the tile drain [M L^{-3}] and $\mathbf{q_t}$ is the fluid flux along the drain axis [L T^{-1}]. The term Q'_{bc} represents the withdrawal flow rate [L^3 T^{-1}], C_{bc} is the concentration of withdrawal water [M L^{-3}], which is equal to the concentration in the tile drain C_t at the withdrawal location, and l' is the withdrawal location along the tile drain. Contrary to a well, water can only be withdrawn from a tile drain and cannot be injected.

The dispersion coefficient for the tile drain, D_t [L^2 T^{-1}] has a form similar to that for a one-dimensional well and is equal to:

$$D_t = \frac{r_t^2 {\mathbf{q_t}}^2}{48 D_{free}} + D_{free} \tag{2.120}$$

where r_t is an equivalent radius for a tile drain of cross-section A.

2.7.1.8 Surface Domain

The equation for two-dimensional transport of solutes along the surface domain is written as

$$-\overline{\overline{\nabla}}(q_o C_o - \mathbf{D_o}\phi_o h_o \overline{\nabla} C_o) + [\phi_o h_o R_o \lambda C_o]_{par} - d_o \Omega_o + d_o Q'_{bc} C_{bc}$$

$$= \frac{\partial}{\partial t}(\phi_o h_o R_o C_o) + \phi_o h_o R_o \lambda C_o \tag{2.121}$$

where C_o is the concentration in water on the surface domain [M L^{-3}], $\mathbf{D_o}$ is the hydrodynamic dispersion tensor of the surface flow domain [L^2 T^{-1}] and $\overline{\overline{\nabla}}$ is the vertically integrated two-dimensional gradient operator. An expression similar to Equation 2.108 is used to represent the dispersion coefficient D_o and the retardation factor R_o is represented by an expression similar to Equation 2.111. The definition of the boundary terms Q'_{bc} and C_{bc} is similar to that presented above for the porous medium.

2.7.1.9 Channels

One-dimensional solute transport along the axis of a channel is described by:

$$-\overline{\nabla} \cdot A\left(\mathbf{q_c} C_c - D_c \overline{\nabla} C_c\right) + A\left[\lambda C_c\right]_{par} - A\Omega_c + A Q'_{bc} C_{bc}$$

$$= \frac{\partial AC_c}{\partial t} + A\lambda C_c \tag{2.122}$$

where C_c is the solute concentration in the channel [M L^{-3}] and $\mathbf{q_c}$ is the fluid flux along the channel axis [L T^{-1}]. The definition of the boundary terms Q'_{bc} and C_{bc} is similar to that presented above for the porous medium.

The dispersion coefficient for the channel, D_c [L^2 T^{-1}] has a form similar to that for a one-dimensional well and is equal to:

$$D_c = \frac{r_c^2 \mathbf{q_c}^2}{48 D_{free}} + D_{free} \tag{2.123}$$

where r_c is an equivalent radius for a channel of cross-section A.

2.8 Solute Transport Coupling

Similarly to fluid flow, two different approaches are used to define the solute exchange terms Ω_{ex} between two different domains. The first approach is based on a numerical superposition principle (see Therrien and Sudicky (1996)), where continuity of solute concentration is assumed between the two domains concerned, which corresponds to instantaneous equilibrium between the two domains. In that case, the Ω_{ex} term does not need to be evaluated explicitly in the model and we do not present its definition. However, the solute exchange flux between domains can be computed after the numerical solution at a given time step. This approach corresponds to the common node scheme.

The second method is more general because it does not assume continuity of concentration between two domains, but uses a first-order expression to approximate Fickian transport to transfer solute from one domain to the other. This second approach corresponds to the dual-node scheme mentioned later in the manual.

Table 2.2 summarizes the types of solute transport coupling currently available in **HydroGeoSphere**. Solute exchange between the subsurface porous medium and the immobile region (double-porosity option), and between the subsurface porous medium and a dual continuum is only simulated by the dual-node approach. For solute exchange between the domains, both the common-node approach as well as the dual-node approach are available options for coupling. We present here the definition of the exchange term for the dual-node approach.

Table 2.2: Types of Coupling and Dimensionality Solute Transport.

	Coupling	
Domains	Common	Dual
Porous medium - Discrete fractures (2-D)	√	√
Porous medium - Second continuum (3-D)		√
Porous medium - Double porosity (3-D)		√
Porous medium - Wells (1-D)	√	√
Porous medium - Tile drains (1-D)	√	√
Porous medium - Surface (2-D)	√	√
Porous medium - Channel (1-D)	√	√

2.8.1 Mobile - Immobile Region Coupling

Solute exchange between the mobile and immobile region of a porous medium (double-porosity approach) is given by:

$$\Omega_{\text{Imm}} = \alpha_{\text{Imm}}(C - C_{\text{Imm}}) \tag{2.124}$$

where α_{Imm} is a first-order mass transfer coefficient between the mobile and immobile regions [T^{-1}].

For fractured porous media, Sudicky (1990) presents relationships for the mass transfer coefficient as a function of fracture geometry. For example, if a porous medium is highly fractured and the shape of the porous medium block delineated by the fracture network can be approximated as spheres, the mass transfer coefficient can be approximated by:

$$\alpha_{\text{Imm}} = \frac{15\theta_{\text{Imm}} D^*_{\text{Imm}}}{r_0^2} \tag{2.125}$$

where D^*_{Imm} is the effective diffusion coefficient in the immobile region and r_0 is the radius of a representative sphere [L]. Another expression can be given for the case of a system of parallel fractures, with a uniform fracture spacing equal to B_f and where the porous matrix blocks are prismatic slabs:

$$\alpha_{\text{Imm}} = \frac{3\theta_{\text{Imm}} D^*_{\text{Imm}}}{(B_f/2)^2} \tag{2.126}$$

2.8.2 Isotopic Fractionation Coupling

Isotopic exchange between the mobile (water) and immobile (solid) region of a porous medium is similar to the double-porosity approach and is given by:

$$\Omega_{\text{Imm}} = x_r k_r(\alpha_r C - C_{\text{Imm}}) \tag{2.127}$$

where k_r is a reverse fractionation rate [L^{-1}] and $k_r\alpha_r$ is the forward reaction rate with α_r being the isotope fractionation factor between water and the solid phase. Concentration C_{Imm} describes here the isotopic concentration in the solid phase.

2.8.3 Dual Continuum Subsurface Coupling

When the dual-node approach is chosen to represent simultaneous transport in the subsurface porous medium and a dual continuum (representing fractures), the solute exchange term can be defined as (Gerke and van Genuchten, 1993):

$$\Omega_d = -u_m C - u_d C_d \tag{2.128}$$

where:

$$u_m = d^* \Gamma_d \phi - \alpha_s w_m \theta_s S_w \tag{2.129}$$

and:

$$u_d = (1 - d^*) \Gamma_d \phi^* + \alpha_s w_m \theta_s S_w \tag{2.130}$$

In Equation 2.129 and 2.130, α_s is a mass transfer coefficient [T^{-1}] resembling that defined for the double porosity option. We further define the following variables:

$$d^* = 0.5 \left(1 - \frac{\Gamma_d}{|\Gamma_d|} \right) \tag{2.131}$$

and

$$\phi = w_m \frac{\theta_s S_w}{\theta_{tot}}; \quad \phi^* = (1 - w_m) \frac{\theta_{sd} S_{wd}}{\theta_{tot}}; \quad \theta_{tot} = w_m \theta_s S_w + (1 - w_m) \theta_{sd} S_{wd} \tag{2.132}$$

For the case where the hydraulic heads of the porous medium and the second continuum are equivalent, then, according to Equation 2.66, the term Γ_d above becomes equal to 0 and the solute exchange given by term Ω_d reduces to a diffusion-type exchange between the two domains, similar to that for the double porosity medium (see Equation 2.124).

2.8.4 Surface Subsurface Coupling

When the dual node approach is chosen to represent simultaneous transport in the subsurface and the surface domain, the solute exchange term Ω_o [M L^{-3} T^{-1}] is defined as follows

$$d_o \Omega_o = d_o \Gamma_o C_{ups} + \left(\frac{|d_o \Gamma_o| \alpha_c + \theta_s S_w \tau D_{free}}{l_{exch}} \right) (C - C_o) \,. \tag{2.133}$$

The term α_c [L] is the coupling dispersivity between the subsurface and surface and the upstream concentration C_{ups} [M L^{-3}] is defined as

$$C_{ups} = \begin{cases} C & \text{when flow is from the subsurface to the surface (exfiltration)} \\ C_o & \text{when flow is from the surface to the subsurface (infiltration)} \end{cases} \tag{2.134}$$

where C is the subsurface concentration and C_o is the surface concentration.

2.9 Solute Transport Boundary Conditions

2.9.1 Subsurface

Boundary conditions for subsurface transport include the following: first-type (Dirichlet) boundaries of prescribed concentration, prescribed mass flux or third-type (Cauchy) boundary conditions. For chain-decay of solutes, Bateman's equation is used to prescribe the concentrations for the daughter products. The boundary conditions can also be allowed to vary in time. Details of the implementation of these boundary conditions in the model are given in the next chapter.

2.9.2 Surface

Boundary conditions to the surface flow system include at the moment first-type (Dirichlet) boundaries of prescribed concentration.

2.10 Colloid Transport

2.10.1 Subsurface - Porous Medium and Dual Continuum

HGS can simulate colloid transport, for example bacteria or viruses, based on (Bradford et al., 2009) who presented a conceptual model and governing equations to simulate colloid transport in a dual-permeability system. The dual-permeability system contains two regions and, in each region, colloids can be present in the liquid phase and also attached to the solid phase. Colloid transfer from the liquid to the solid phase (attachment or retention) and from the solid to the liquid phase (detachment) is represented by kinetic terms in the governing equation for transport.

Colloid attachment to a solid phase and detachment from a solid phase can only be simulated for the porous medium domain and for the dual continuum domain, if a dual continuum domain is activated. For other domains, colloids can be present in the liquid phase but they do not undergo attachment nor detachment. For these other domains, the relevant governing equation presented previously (see Section 2.7) applies for the colloid in the liquid phase.

The following equation, which is a modified form of transport Equation (2.106), describes colloid transport in the fluid phase of the porous medium:

$$w_m \left[\frac{\partial \left(\theta_s S_w C \right)}{\partial t} + \lambda_c \theta_s S_w C \right] =$$

$$w_m \left[\frac{\partial}{\partial x_i} \left(\theta D_{ij} \frac{\partial C}{\partial x_j} \right) - \frac{\left(\partial q_i C \right)}{\partial x_i} - \theta_s S_w k_{ret} C + \rho_b k_{det} S \right] + \Omega_d \tag{2.135}$$

where C [$\mathrm{N}_c\ \mathrm{L}^{-3}$], with N_c being the number of colloids, is the liquid phase concentration of colloids in the porous medium expressed per unit volume of liquid, λ_c [T^{-1}] is a first-order colloid decay rate in the fluid phase, k_{ret} [T^{-1}] is a first-order colloid retention rate coefficient on the solid phase, k_{det} [T^{-1}] is a first-order colloid detachment coefficient from the solid phase.

The mass balance equation for colloid on the solid phase of the porous medium is

$$w_m \left[\frac{\partial \left(\rho_b S \right)}{\partial t} + \lambda_s \rho_b S \right] = w_m \theta_s S_w k_{ret} C - w_m \rho_b k_{det} S - \rho_b k_t S \tag{2.136}$$

where S [$\mathrm{N}_c\ \mathrm{M}^{-1}$] is the solid phase concentration of colloids in the porous medium, expressed per unit mass of solids, λ_s [T^{-1}] is a first-order colloid decay rate in the solid phase, and k_t [T^{-1}] is a coefficient for transfer of colloids from the solid phase of the porous medium

domain to the solid phase of the dual domain. That transfer is only applicable when a dual domain is present.

Similarly to the porous medium, the transport equation 2.114 for the dual continuum is modified for colloid transport

$$w_d \left[\frac{\partial \left(\theta_{sd} S_{wd} C_d \right)}{\partial t} + \lambda_{cd} \theta_{sd} S_{wd} C_d \right] =$$

$$w_d \left[\frac{\partial}{\partial x_i} \left(\theta_d D_{ijd} \frac{\partial C_d}{\partial x_j} \right) - \frac{\left(\partial q_{id} C_d \right)}{\partial x_i} - \theta_{sd} S_{wd} k_{retd} C_d + \rho_{bd} k_{detd} S_d \right] - \Omega_d \tag{2.137}$$

where C_d [N_c L^{-3}] is the liquid phase concentration of colloids in the dual continuum expressed per unit volume of liquid, λ_{cd} [T^{-1}] is a dual continuum first-order colloid decay rate in the fluid phase, k_{retd} [T^{-1}] is a dual continuum first-order colloid retention rate coefficient on the solid phase, k_{detd} [T^{-1}] is a dual continuum first-order colloid detachment coefficient from the solid phase.

The dual continuum mass balance equation for colloid on the solid phase is

$$w_d \left[\frac{\partial \left(\rho_{bd} S_d \right)}{\partial t} + \lambda_{sd} \rho_{bd} S_d \right] = w_d \theta_{sd} S_{wd} k_{retd} C_d - w_d \rho_{bd} k_{detd} S_d + \rho_b k_t S \tag{2.138}$$

where λ_{sd} [T^{-1}] is a dual continuum first-order colloid decay rate in the solid phase.

The Ω_d [N_c L^{-3} T^{-1}] term describing the liquid phase mass exchange of colloids between porous medium and dual domains is defined as

$$\Omega_d = \omega_{ex} w_m \theta_s S_w \left(C_d - C \right) \tag{2.139}$$

where ω_{ex} [T^{-1}] is a coefficient for liquid phase colloid exchange between the porous medium and dual domains.

2.11 Thermal Energy Transport

2.11.1 Porous Medium

The general equation for variably-saturated subsurface thermal energy transport is given by:

$$-\nabla \cdot w_m \left[\rho_w c_w \mathbf{q} T - \left(k_b + \rho_w c_w \theta_s S_w \mathbf{D} \right) \nabla T \right] + \sum \rho_w c_w \Omega_{\mathrm{ex}} + Q'_{bc} T_{bc} \rho_w c_w =$$

$$w_m \frac{\partial}{\partial t} \left[\theta_s \rho_a c_a (1 - S_w) T_a + \theta_s \rho_w c_w S_w T + (1 - \theta_s) \rho_s c_s T_s \right] \tag{2.140}$$

where c is specific heat [L^2 T^{-2} Θ^{-1}], T is the fluid temperature [Θ], k_b is the bulk thermal conductivity [M L T^{-3} Θ^{-1}], and Ω is the thermal surface/subsurface interaction term

[M L^{-1} T^{-3}] that is discussed in Section 2.11.9. Subscript s denotes the solid phase, subscript w represents the aqueous phase and subscript a represents the air phase.

The terms Q'_{bc} and T_{bc} are, respectively, the volumetric fluid (water) flow rate per unit volume [L^3 T^{-1} L^{-3}] and the temperature [Θ] at a boundary or at a fluid injection or withdrawal location. The volumetric flow rate Q'_{bc} is positive for an inflow boundary or an injection location and negative for an outflow boundary or a withdrawal location. Furthermore, for an outflow boundary or a withdrawal location, the boundary temperature T_{bc} is equal to the fluid temperature T.

On the right-hand side of the equation, T_a and T_s are the air and solids temperature, respectively. Assuming that a representative elementary volume is small enough such that $T_a = T = T_s$, the equation becomes

$$-\nabla \cdot w_m \left[\rho_w c_w \mathbf{q} T - \left(k_b + \rho_w c_w \theta_s S_w \mathbf{D}\right) \nabla T\right] + \sum \rho_w c_w \Omega_{\text{ex}} + Q'_{bc} T_{bc} \rho_w c_w =$$

$$w_m \frac{\partial}{\partial t} \left[\left\{\theta_s \rho_a c_a (1 - S_w) + \theta_s \rho_w c_w S_w + (1 - \theta_s) \rho_s c_s\right\} T\right] \tag{2.141}$$

When needed, bulk parameters, with the exception of thermal conductivity, are calculated by a volumetric average approximation. For example, bulk density ρ_b is defined as:

$$\rho_b = (1 - \theta_s)\rho_s + S_w \theta_s \rho_w + (1 - S_w)\theta_s \rho_a \tag{2.142}$$

The bulk thermal conductivity term (k_b) can either be specified, or calculated. It represents the thermal conductivity of the entire subsurface, which can include the matrix solids, the aqueous phase and air. Specifying a bulk thermal conductivity may be appropriate for saturated flow conditions, when the phase composition of the subsurface does not vary with space or time; however under variably-saturated flow conditions, the saturations of air and water in the subsurface may change with time, and thus the thermal conductivity may also change. Calculating a three-phase thermal conductivity is not straightforward; several approaches have been presented, and no one method has proven to consistently provide more representative solutions than others (Chaudhary and Bhandari, 1968; Markle et al., 2006).

Three methods of calculating the bulk thermal conductivity are available in **HydroGeoSphere**. The first method, which is the default, uses a volumetric average approximation similar to that employed in SUTRA (Voss, 1984):

$$k_b = (1 - \theta_s)k_s + S_w \theta_s k_w + (1 - S_w)\theta_s k_a \tag{2.143}$$

The second approximation extends the accepted two-phase thermal conductivity calculation provided by Sass et al. (1971) by calculating both a dry and saturated thermal conductivity (k_{dry} and k_{sat}, respectively), and then determining the bulk thermal conductivity using a geometric interpolation between the dry and saturated thermal conductivities based on the degree of water saturation:

$$k_{dry} = k_s^{(1-\theta_s)} {k_a}^{\theta_s} \tag{2.144}$$

$$k_{sat} = k_s^{(1-\theta_s)} {k_w}^{\theta_s} \tag{2.145}$$

$$k_b = S_w k_{sat} + (1 - S_w) k_{dry} \tag{2.146}$$

The third method uses the following non linear relationship developed by Côté and Konrad (2005):

$$k_b = k_{dry} + (k_{sat} - k_{dry})\, k_{br} \tag{2.147}$$

where k_{br} is a relative thermal conductivity given by

$$k_{br} = \frac{k_C S_w}{1 + (k_C - 1)\, S_w} \tag{2.148}$$

and where k_C is a fitting parameter. Typical values of k_C are 3.55 for a medium to fine sand, and 1.9 for silty and clayey soils (Côté and Konrad, 2005).

2.11.2 Discrete Fractures

The equation for two-dimensional thermal energy transport in a discrete fracture is:

$$-\nabla \cdot \left[w_f \rho_w c_w \mathbf{q_f} T_f - \left(S_{wf} k_w + (1 - S_{wf}) k_a + \rho_w c_w S_{wf} \mathbf{D_f} \right) \nabla T_f \right] + w_f \rho_w c_w \Omega_f$$

$$+ w_f Q'_{bc} T_{bc} \rho_w c_w = \frac{\partial}{\partial t} \left[w_f \left\{ \rho_a c_a (1 - S_{wf}) + \rho_w c_w S_{wf} \right\} T_f \right] \tag{2.149}$$

where T_f is the fluid temperature in the discrete fracture [Θ]. The definition of the boundary terms Q'_{bc} and T_{bc} is similar to that presented above for the porous medium.

2.11.3 Dual Continuum

The general equation for variably-saturated subsurface thermal energy transport in a dual continnum is given by:

$$-\nabla \cdot w_d \left[\rho_w c_w \mathbf{q} \right) \mathbf{d} T_d - \left(k_b + \rho_w c_w \theta_{sd} S_{wd} \mathbf{D_d} \right) \nabla T_d \right] + \rho_w c_w \Omega_{\mathrm{d}} + Q'_{bc} T_{bc} \rho_w c_w =$$

$$w_d \frac{\partial}{\partial t} \left[\theta_{sd} \rho_a c_a (1 - S_{wd}) T_a + \theta_{sd} \rho_w c_w S_{wd} T_d + (1 - \theta_{sd}) \rho_s c_s T_s \right] \tag{2.150}$$

where T_d is the fluid temperature in the dual continuum [Θ]. The definition of the boundary terms Q'_{bc} and T_{bc} is similar to that presented above for the porous medium.

2.11.4 Wells

The equation for one-dimensional thermal energy transport along the axis of a well is:

$$-\nabla \cdot \pi r_s^2 \left[\rho_w c_w \mathbf{q_w} T_w - \left(S_{ww} k_w + (1 - S_{ww}) k_a + \rho_w c_w S_{ww} \mathbf{D_w}\right) \nabla T_w\right] + \pi r_s^2 \rho_w c_w \Omega_w$$

$$+\pi r_s^2 Q'_{bc} T_{bc} \rho_w c_w = \frac{\partial}{\partial t} \left[\pi r_s^2 \left\{\rho_a c_a (1 - S_{ww}) + \rho_w c_w S_{ww}\right\} T_w\right] \tag{2.151}$$

where T_w is the fluid temperature in the well [Θ]. The definition of the boundary terms Q'_{bc} and T_{bc} is similar to that presented above for the porous medium. Note that k_w is here the thermal conductivity of water.

2.11.5 Tile Drain

The equation for one-dimensional thermal energy transport along the axis of a tile drain is:

$$-\nabla \cdot A \left[\rho_w c_w \mathbf{q_t} T_t - \left(S_{wt} k_w + (1 - S_{wt}) k_a + \rho_w c_w S_{wt} \mathbf{D_t}\right) \nabla T_t\right] + A \rho_w c_w \Omega_t$$

$$+A Q'_{bc} T_{bc} \rho_w c_w = \frac{\partial}{\partial t} \left[A \left\{\rho_a c_a (1 - S_{wt}) + \rho_w c_w S_{wtw}\right\} T_t\right] \tag{2.152}$$

where T_t is the fluid temperature in the tile drain [Θ]. The definition of the boundary terms Q'_{bc} and T_{bc} is similar to that presented above for the porous medium.

2.11.6 Channel

The equation for one-dimensional thermal energy transport along the axis of a channel is:

$$-\nabla \cdot A \left[\rho_w c_w \mathbf{q_c} T_c - \left(k_w + \rho_w c_w \mathbf{D_c}\right) \nabla T_c\right] + A \rho_w c_w \Omega_c$$

$$+A Q'_{bc} T_{bc} \rho_w c_w = A \frac{\partial \rho_w c_w T_c}{\partial t} \tag{2.153}$$

where T_t is the fluid temperature in the channel [Θ]. The definition of the boundary terms Q'_{bc} and T_{bc} is similar to that presented above for the porous medium.

2.11.7 Surface Water

The depth-averaged equation describing thermal energy transport in surface water is similar to that for solute transport in the surface water and is given by:

$$\nabla[\mathbf{q}_o \rho_w c_w d_o T_o - (k_w + \mathbf{D}_o \rho_w c_w) d_o \nabla T_o] + E_{atm} + d_o Q'_{bc} T_{bc} \rho_w c_w$$

$$+d_o\rho_w c_w \Omega_o = \frac{\partial \rho_w c_w d_o T_o}{\partial t} \tag{2.154}$$

where T_o is the temperature of the surface water [Θ] and E_{atm} [M T^{-3}] represents the atmospheric inputs to the surface thermal energy system. The definition of the boundary terms Q'_{bc} and T_{bc} is similar to that presented above for the porous medium.

In Equation 2.154, the overland water flux ($\mathbf{q}_o$) is calculated from the numerical solution of the Diffusion-wave equation. These derivations for thermal energy transport are hydrodynamically, and not thermodynamically based, and are not applicable to high temperature, high pressure hydrothermal conditions, but are valid for most shallow groundwater/surface water systems. In addition, the surface thermal regime is depth-averaged and cannot represent thermal stratification in surface water bodies.

2.11.7.1 Atmospheric Inputs

This section describes the atmospheric input source term (E_{atm} in Equation 2.154) that can be assigned to the surface water flow domain for thermal energy transport simulations. The atmospheric inputs from CLASS (Verseghy, 1991; Verseghy et al., 1993) are used to determine the surface heat fluxes in **HydroGeoSphere**. CLASS is a well established land surface scheme, and the atmospheric inputs incorporated into CLASS have been demonstrated to be representative (Verseghy, 1991; Verseghy et al., 1993). In addition to the reliability of the CLASS approach, the equations used for atmospheric inputs are also computationally inexpensive, relative to other atmospheric models, and thus are appropriate for implementing into **HydroGeoSphere**. The total atmospheric input to the surface thermal energy system can be expressed as:

$$E_{atm} = K_* + L_* + Q_H + Q_E \tag{2.155}$$

where K_* is the net shortwave radiation, L_* is the net longwave radiation, Q_H is the sensible heat flux and Q_E is the latent heat flux . All of the equations used here are taken from CLASS (Verseghy, 1991; Verseghy et al., 1993) with the exception of the incoming longwave radiation calculation, which is adapted from Fassnacht et al. (2001). All of the atmospheric thermal inputs are calculated explicitly, and are treated as a source/sink term in the thermal energy transport equation for the surface regime. A limitation to this approach is that the model does not provide feedback to the atmosphere; however, given the scale of the atmospheric regime, it is assumed that the feedback from the smaller hydrologic domains is negligible.

Shortwave radiation is the radiant energy in the visible, near-ultraviolet and near-infrared wavelengths from the atmosphere to the Earth's surface, broadly defined as between 0.1 and 5.0 micrometers. The equation used to calculate the thermal energy input to the surface from net shortwave radiation follows Verseghy (1991); Verseghy et al. (1993) and is:

$$K_* = (1 - \alpha_g)K^{\downarrow} \tag{2.156}$$

where α_g is the ground surface albedo, and $K^{\downarrow}$ is the incoming shortwave radiation. Ground surface albedo is dependent on the water content of the surficial soil, as formulated by Idso

et al. (1975), and is given by:

$$\begin{array}{lll} \alpha_g = & \frac{S_w(1-\theta)(\alpha_{sat}-\alpha_{dry})}{0.20} + \alpha_{dry} & \text{for} \quad S_w(1-\theta) < 0.20 \\ \alpha_g = & \alpha_{sat} & \text{for} \quad S_w(1-\theta) \geq 0.20 \end{array} \tag{2.157}$$

where α_{sat} and α_{dry} are the limiting wet and dry soil albedoes.

A variation of this equation is also available in **HydroGeoSphere** to account for cloud and canopy cover (given by C_c):

$$K_* = (1 - C_c)(1 - \alpha_g)K^{\downarrow} \tag{2.158}$$

The cloud and canopy cover term (C_c) varies between 0 and 1 and represents the fraction of the sky that is blocked by either clouds or vegetation from the ground surface. Net Longwave Radiation (L_*) Longwave radiation is the infrared energy emitted by the earth and atmosphere at wavelengths between about 5 and 25 micrometers. The equation for net longwave radiation to the surface following (Verseghy, 1991; Verseghy et al., 1993) is:

$$L_* = L^{\downarrow} - \sigma T_g^4 \tag{2.159}$$

where $L^{\downarrow}$ is the incoming longwave radiation, σ is the Steffan-Boltzmann constant, and T_g is the ground surface temperature (temperature of the surface regime). In the original CLASS formulation, the incoming radiation term is specified as an input parameter. However, due to the lack of longwave radiation data (incoming longwave radiation is not routinely measured), incoming longwave radiation can also be calculated in **HydroGeoSphere** using the formulation given by Fassnacht et al. (2001):

$$L^{\downarrow} = \varepsilon_{at}\sigma T_a^4 \tag{2.160}$$

where T_a is the air temperature, ε_{at} is the integrated emissivity of the atmosphere and canopy, calculated by:

$$\varepsilon_{at} = (0.53 + 0.2055\sqrt{e_a})(1 + 0.40C_c) \tag{2.161}$$

where e_a is the near surface vapour pressure. Emissivity is limited so that it cannot exceed 1.0, ensuring that the incoming longwave radiation is not overestimated.

Sensible heat flux represents the movement of energy from the Earth to the air above typically via conduction. The equation used for sensible heat flux follows Verseghy (1991); Verseghy et al. (1993) and is given by:

$$Q_H = \rho_a c_a V_a c_D [T_a - T_g] \tag{2.162}$$

where ρ_a is the density of the air, c_a is the specific heat of the air, V_a is the wind speed and c_D is the drag coefficient.

Latent heat flux represents the energy transfer during the evaporation/condensation process. There are three methods of accounting for evaporation in the flow solution. The quantity of water evaporated/condensed in the flow solution provides the basis for the amount of

energy transferred between the atmospheric and hydrologic regimes for latent heat flux. As such, the evaporation rate used in the flow solution must be linked to the latent heat flux term used to calculate the atmospheric thermal energy inputs. The first, and most simplistic method of accounting for evaporation, is to simply reduce the precipitation rate applied to the surface of the domain by the evaporation rate. By not explicitly specifying or calculating the evaporation rate in **HydroGeoSphere**, the latent heat flux must be determined independently. In this case the equation used by CLASS (Verseghy, 1991; Verseghy et al., 1993) is used, given by:

$$Q_E = L_V \rho_a V_a c_D [SH_a - SH_g] \tag{2.163}$$

Where L_V is the latent heat of vaporization, SH_a is the specific humidity of the air, and SH_g is the specific humidity of the ground surface. Specific humidity of the ground surface is calculated using the same formulation given by Verseghy (1991); Verseghy et al. (1993):

$$SH_g = h \cdot SH_{sat}[T_g] \tag{2.164}$$

Where h is the relative humidity of the air in the surface soils, calculated by:

$$h = \exp\left[\frac{-g\psi_g}{R_w T_g}\right] \tag{2.165}$$

and $SH_{sat}[T_g]$ is the saturation specific humidity at T_g, given by:

$$SH_{sat}[T_g] = \frac{0.622 e_{sat}[T_g]}{p_a - 0.378 e_{sat}[T_g]} \tag{2.166}$$

In these equations, g represents the acceleration due to gravity, ψ_g is the soil-water suction at the surface, R_w is the gas constant for water vapour, $e_{sat}[T_g]$ is the saturation vapour pressure at the ground surface and p_a is the air pressure. Evaporation can also be specified or calculated in **HydroGeoSphere**. When evaporation is specified, the evaporation rate is input to **HydroGeoSphere** and is subtracted from the incoming precipitation throughout the simulation. Internally calculating the evaporation rate is a more complex approach, based on the empirical Hargreaves equation for determining the potential evapotranspiration, and then calculating the actual evapotranspiration as a combination of plant transpiration and evaporation from the surface and the subsurface domains. The equations for this approach are given in detail by Li et al. (2008). Whether the evaporation is specified or calculated, the latent heat flux is then determined from the evaporation rate used in the flow solution, ensuring continuity between the flow and thermal transport simulations. The latent heat flux equation for a specified or calculated evaporation rates is:

$$Q_E = L_V E_{flux} \rho_w \tag{2.167}$$

where E_{flux} is the specified or calculated evaporation rate.

2.11.8 Thermal Energy Transport Boundary Conditions

Boundary conditions for thermal energy transport include the following: first-type (Dirichlet) boundaries of prescribed concentration, prescribed energy flux or third-type (Cauchy)

boundary conditions. The boundary conditions can also be allowed to vary in time. Details of the implementation of these boundary conditions in the model are given in the next chapter.

2.11.9 Thermal Energy Coupling

The coupling of the surface and subsurface thermal continua is similar to that used for advective-dispersive contaminant transport in **HydroGeoSphere**. There are two methods of coupling the surface and subsurface continua, the common node and the dual node approaches. The common node approach is based on the assumption of continuity of temperature at the surface/subsurface interface. The dual node approach on the other hand uses a first-order flux relation to transfer heat from one domain to the other. The equation for the dual-node coupling of the surface and subsurface thermal equations follows Brookfield et al. (2009) and is given by:

$$\Omega_o = \rho_w c_w T_{ups} \Gamma_o + \alpha_o \rho_{dwn} c_{dwn} (T - T_o) \tag{2.168}$$

where Γ_o [T^{-1}] represents the aqueous exchange flux between the surface and subsurface (the amount of water flowing between the two regimes; see Equation 2.68) and α_o [T^{-1}] is an energy transfer coefficient determined by the thermal dispersivity over the depth of the surface/subsurface exchange zone. The subscript *ups* represents the "upstream" direction and the subscript *dwn* represents the "downstream" direction, that is,

$$T_{ups} = \begin{cases} T, & \Gamma_o > 0 \\ T_o, & \Gamma_o < 0 \end{cases} \quad \text{and} \quad \rho_{dwn} c_{dwn} = \begin{cases} \rho_w c_w, & \Gamma_o > 0 \\ \rho_b c_b, & \Gamma_o < 0 \end{cases}$$

The most significant difference between the solute and the thermal transport coupling equations is the treatment of mass/energy transfer between the surface and subsurface. The downstream parameters are used to differentiate between the amount of thermal energy required to change the temperature of the surface and the subsurface domains, respectively. When the diffusive gradient is transferring thermal energy to the subsurface, the bulk heat capacity and density parameters regulate how much the temperature of the bulk subsurface changes given the amount of thermal energy added. Conversely, when the diffusive gradient is transporting thermal energy to the surface, the aqueous heat capacity and density terms regulate how much the surface water temperature increases given the thermal energy inputs. As the bulk and aqueous heat capacity and density terms can be significantly different, the amount of energy required to change the temperature of the surface and subsurface regimes can also be different. For this formulation, the downstream location (where the energy is diffusing to) determines how much thermal energy is required to reduce the thermal gradient between regimes. The movement of a solute between the two regimes is different from heat because a non-sorbing solute has a tendency to remain in the aqueous phase, whereas thermal energy tends to preferentially transfer into the solid phase of the porous medium, thus affecting the bulk temperature.

2.12 Travel Time Probability

2.12.1 Definitions

Groundwater age is usually defined as a relative quantity with respect to a starting location where age is assumed to be zero. For a given spatial position in the reservoir, the age (A) relates to the time elapsed since the water particles entered the system at the recharge limits, where age is zero. For the same spatial position, the life expectancy (E) is defined as the time required for the water particles to reach an outlet limit of the system. Life expectancy is therefore zero at an outlet. The total transit time (T) finally refers to the total time required by the same water particles to migrate from an inlet zone ($T = E$) to an outlet zone ($T = A$). The three variables A, E and T are random variables, characterized by probability density functions (PDFs) $g_{U=A,E,T}$, that can be regarded as the statistical occurrence of water particles with respect to time, which could be observed in a groundwater sample if any analytical procedure would allow such measurements.

The travel time probability $g_t(t, \boldsymbol{x} \mid t_0, \boldsymbol{x}_i)$ characterizes the probability density for the amount of time (t is a random variable) required by the water particles to travel from a given position $\boldsymbol{x}_i$ (at time $t = t_0$) to the position $\boldsymbol{x}$. The location probability $g_{\boldsymbol{x}}(\boldsymbol{x}, t \mid \boldsymbol{x}_i, t_0)$ characterizes the probability density of finding water particles at the position $\boldsymbol{x}$ ($\boldsymbol{x}$ is a random variable) at a given time t after their release at the position $\boldsymbol{x}_i$. If the input zone corresponds to the entire inlet Γ_-, then travel time corresponds to age A. Similarly, if the input zone corresponds to the entire outlet Γ_+, then travel time corresponds to life expectancy E.

The age (and/or forward travel time) and life expectancy (and/or backward travel time) PDFs can be obtained as solutions of advection-dispersion equations (ADE), by making use of specific boundary conditions.

2.12.2 Basic equations

2.12.2.1 Forward model

The age PDF at a position $\boldsymbol{x}$ in an aquifer Ω can be evaluated by solving the ADE when a unit pulse of conservative tracer is uniformly applied on the recharge area Γ_- (see Fig. 2.4). The resulting breakthrough curve is the probabilistic age distribution (Danckwerts, 1953; Jury and Roth, 1990). The pre-solution of a velocity field is performed by solving the groundwater flow equation. The age PDF is then obtained by solving the following forward boundary value problem:

$$\frac{\partial \theta g}{\partial t} = -\nabla \cdot \mathbf{q} g + \nabla \cdot \theta \mathbf{D} \nabla g + q_{\mathrm{I}} \delta(t) - q_{\mathrm{O}} g \qquad \text{in} \quad \Omega \tag{2.169a}$$

$$g(\boldsymbol{x}, 0) = g(\boldsymbol{x}, \infty) = 0 \qquad \text{in} \quad \Omega \tag{2.169b}$$

$$\mathbf{J}(\boldsymbol{x},t)\cdot\boldsymbol{n}=(\mathbf{q}\cdot\boldsymbol{n})\delta(t) \qquad \text{on} \quad \Gamma_- \tag{2.169c}$$

$$\mathbf{J}(\boldsymbol{x},t)\cdot\boldsymbol{n}=0 \qquad \text{on} \quad \Gamma_0 \tag{2.169d}$$

where $g(\boldsymbol{x},t)=g_A(\boldsymbol{x},t)$ denotes the transported age PDF [T^{-1}], $\mathbf{q}$ is the water flux vector [LT^{-1}], q_I and q_O are fluid source and sink terms, respectively [T^{-1}], $\mathbf{J}(\boldsymbol{x},t)$ is the total age mass flux vector [LT^{-2}], $\mathbf{D}$ is the tensor of macro-dispersion [$\mathrm{L}^2\mathrm{T}^{-1}$], $\boldsymbol{x}=(x,y,z)$ is the vector of Cartesian coordinates [L], t is time [T], $\theta=\theta(\boldsymbol{x})$ is porosity or mobile water content [−], $\boldsymbol{n}$ is a normal outward unit vector, and $\delta(t)$ is the time-Dirac delta function [T^{-1}], which ensures a pure impulse on Γ_-. The total age mass flux vector $\mathbf{J}(\boldsymbol{x},t)$ is classically defined by the sum of the convective and dispersive fluxes:

$$\mathbf{J}(\boldsymbol{x},t)=\mathbf{q}g(\boldsymbol{x},t)-\mathbf{D}\nabla g(\boldsymbol{x},t) \tag{2.170}$$

The third-type (Cauchy) boundary condition (2.169c) is the most meaningful condition to simulate the age problem since it prevents backward losses by dispersion (homogeneity of the condition at $t=0^+$).

2.12.2.2 Backward model

The life expectancy PDF satisfies the adjoint backward model of Eq. (2.169a):

$$\frac{\partial\theta g}{\partial t}=\nabla\cdot\mathbf{q}g+\nabla\cdot\theta\mathbf{D}\nabla g-q_\mathrm{I}g \qquad \text{in} \quad \Omega \tag{2.171a}$$

$$g(\boldsymbol{x},0)=g(\boldsymbol{x},\infty)=0 \qquad \text{in} \quad \Omega \tag{2.171b}$$

$$\mathbf{J}(\boldsymbol{x},t)\cdot\boldsymbol{n}=-(\mathbf{q}\cdot\boldsymbol{n})\delta(t) \qquad \text{on} \quad \Gamma_+ \tag{2.171c}$$

$$-\mathbf{D}\nabla g(\boldsymbol{x},t)\cdot\boldsymbol{n}=0 \qquad \text{on} \quad \Gamma_0 \tag{2.171d}$$

where $g(\boldsymbol{x},t)=g_E(\boldsymbol{x},t)$ denotes the transported life expectancy PDF, and where the total life expectancy mass flux vector $\mathbf{J}(\boldsymbol{x},t)$ is

$$\mathbf{J}(\boldsymbol{x},t)=-\mathbf{q}g(\boldsymbol{x},t)-\mathbf{D}\nabla g(\boldsymbol{x},t) \tag{2.172}$$

Eq. (2.171a) is the formal adjoint of Eq. (2.169a) (Garabedian, 1964; Arnold, 1974), known as the "backward-in-time" equation (Uffink, 1989; Wilson and Liu, 1997) or the backward Kolmogorov equation (Kolmogorov, 1931). Given the forward equation, the backward equation is technically obtained by reversing the sign of the flow field, and by adapting the boundary conditions (Neupauer and Wilson, 1999, 2001). On the impermeable boundary Γ_0, a third-type condition (Cauchy) in the forward equation becomes a second-type condition (Neumann) in the backward equation, and vice-versa. A second-type condition in the forward

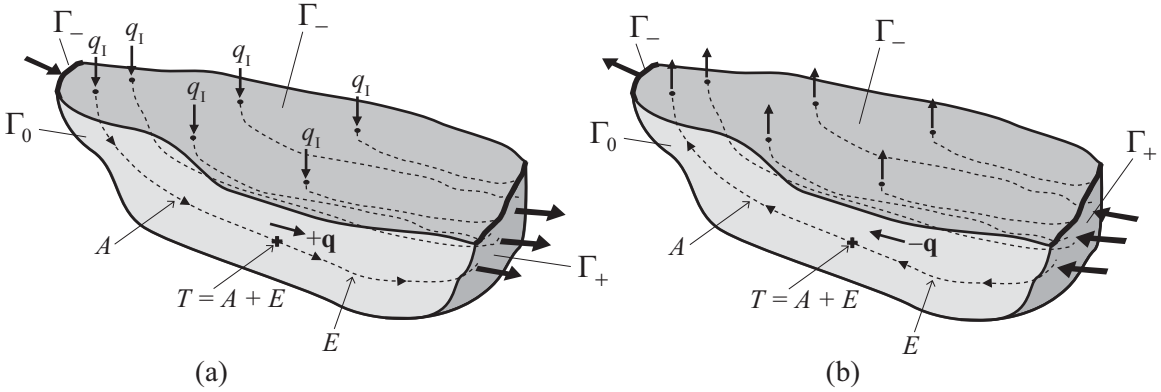

Figure 2.4: Schematic illustration of a groundwater reservoir Ω, with inlet (Γ_-) and outlet (Γ_+) boundaries: (a) Age problem with normal flow field; (b) Life expectancy problem with reversed flow field. The cross stands for a small water sample, to illustrate the random variable total transit time (T) as the sum of the two random variables age (A) and life expectancy (E).

model will also become a third-type condition in the backward model (Gardiner, 1983, p. 146). The advection term is known to be not self-adjoint (it should be written in the form $\mathbf{q} \cdot \nabla g$ in Eq. (2.171a)) unless flow is non-divergent. However, the backward equation can still handle divergent flow fields by means of the important sink term $-q_I g$ appearing in Eq. (2.171a). This sink term has been derived in Cornaton (2003) from the vertical averaging process of the general 3D backward ADE, and is consistent with the analysis of Neupauer and Wilson (2001, 2002) and Wilson and Liu (1997). Recharge by internal sources (3D or 2D vertical) or by areal fluxes (fluid source for 2D horizontal) is introduced by the first-order decay type term $-q_I g$, which is a consequence of the reversed flow field. Internal sources produce a sink of life expectancy probability, while internal sinks (term $q_O g$ in Eq. (2.169a)) do not appear in the backward model since a fluid sink may not influence the life expectancy PDF.

The life expectancy to a specific outlet $\Gamma_n \subset \Gamma_+$ can be calculated by modifying the boundary value problem (2.171) in such a way that the function g will characterize the probability density for the water particles to reach Γ_n, exclusively. This can be done by assuming a maximum intensity of probability of exit at Γ_n ($\mathbf{J}(\boldsymbol{x}, t) \cdot \boldsymbol{n} = -(\mathbf{q} \cdot \boldsymbol{n})\delta(t)$) and a minimum intensity of probability of exit at each other outlet ($\mathbf{J}(\boldsymbol{x}, t) \cdot \boldsymbol{n} = 0$).

2.12.2.3 Total transit time

Since $T = A + E$, and since A and E are independent variables, the total transit time PDF g_T is obtained by the following convolution product:

$$g_T(\boldsymbol{x}, t) = \int_0^t g_A(\boldsymbol{x}, \tau) g_E(\boldsymbol{x}, t - \tau) d\tau \tag{2.173}$$

The field of g_T characterizes the evolution of groundwater particles throughout the aquifer domain by specifying the amount of time from recharge to discharge. At a given position in the reservoir, the temporal evolution of the groundwater particles can be characterized by the three PDF's g_A, g_E and g_T. Each function contains specific information on a time of residence, the nature of which is a function of the spatial references that are chosen for evaluation. For instance, g_A is conditioned by the inlet limit Γ_-, where the variable A is nil, while g_E is conditioned by the outlet limit Γ_+, where the variable E is nil. For the variable T, the PDF g_T is conditioned by the fact that $T = A$ at outlet, and that $T = E$ at inlet.

2.12.2.4 Outlet/Inlet Transit Time PDF

The representative transit time distribution $\varphi(t)$ of the reservoir outlet zone can be defined as a flux averaged concentration (Rubin, 2003), i.e., $\varphi(t)$ is evaluated as the flow rate-normalized sum on Γ_+ of the total age mass flux response function $\mathbf{J}$ resulting from a unit flux impulse on Γ_-:

$$\varphi(t) = \frac{1}{F_0} \int_{\Gamma_+} \mathbf{J} \cdot \boldsymbol{n} \, d\Gamma \tag{2.174}$$

where F_0 denotes the total flow rate through Γ_+. Similarly, the inlet transit time PDF $\varphi(t)$ is derived by enforcing Eq. (2.174) on the inlet boundary Γ_-, given that the function $\mathbf{J}$ represents the life expectancy mass flux.

2.12.2.5 Travel Time Probabilities

The forward and backward travel time probabilities are calculated as solutions of the following forward and backward initial value problems:

$$\frac{\partial \theta g}{\partial t} = -\nabla \cdot \mathbf{q} g + \nabla \cdot \theta \mathbf{D} \nabla g - q_O g \qquad \text{in} \quad \Omega \tag{2.175a}$$

$$g(\boldsymbol{x}, 0) = \frac{\delta(\boldsymbol{x} - \boldsymbol{x}_i)}{\theta} \qquad \text{in} \quad \Omega \tag{2.175b}$$

$$[\mathbf{q} g(\boldsymbol{x}, t) - \mathbf{D} \nabla g(\boldsymbol{x}, t)] \cdot \boldsymbol{n} = 0 \qquad \text{on} \quad \Gamma_- \cup \Gamma_0 \tag{2.175c}$$

for the forward problem, and

$$\frac{\partial \theta g}{\partial t} = \nabla \cdot \mathbf{q} g + \nabla \cdot \theta \mathbf{D} \nabla g - q_I g \qquad \text{in} \quad \Omega \tag{2.176a}$$

$$g(\boldsymbol{x}, 0) = \frac{\delta(\boldsymbol{x} - \boldsymbol{x}_i)}{\theta} \qquad \text{in} \quad \Omega \tag{2.176b}$$

$$[-\mathbf{q}g(\boldsymbol{x},t) - \mathbf{D}\nabla g(\boldsymbol{x},t)] \cdot \boldsymbol{n} = 0 \qquad \text{on} \quad \Gamma_+ \tag{2.176c}$$

$$-\mathbf{D}\nabla g(\boldsymbol{x},t) \cdot \boldsymbol{n} = 0 \qquad \text{on} \quad \Gamma_0 \tag{2.176d}$$

for the backward problem. The variable $\boldsymbol{x}_i$ denotes the location for the release of a unit mass.

The forward and backward *location* probabilities [L^{-3}] are then defined by:

$$g_{\boldsymbol{x}}(\boldsymbol{x},t) = \theta(\boldsymbol{x})g(\boldsymbol{x},t) \tag{2.177}$$

The forward and backward *travel time* probabilities [T^{-1}] are defined by:

$$g_t(t,\boldsymbol{x}) = \|\mathbf{q}(\boldsymbol{x},t)\|A(\boldsymbol{x})g(t,\boldsymbol{x}) \tag{2.178}$$

where $A(\boldsymbol{x})$ denotes the area of a control plane orthogonal to velocity, through which the travel time probability is evaluated.

2.12.2.6 Age, Life Expectancy and Travel Time Statistics

Given an age/life expectancy/travel time PDF solution $g_t(t,\boldsymbol{x})$, the following descriptive statistics can be post-processed (see Fig. 2.5)):

1. Mean age/life expectancy/travel time μ:

$$\mu(\boldsymbol{x}) = \int_0^{+\infty} t g_t(t,\boldsymbol{x}) dt \tag{2.179}$$

2. Standard deviation σ:

$$\sigma(\boldsymbol{x}) = \sqrt{\int_0^{+\infty} t^2 g_t(t,\boldsymbol{x}) dt - \mu^2} \tag{2.180}$$

3. Mode $M(\boldsymbol{x})$.

2.12.2.7 Mean Age and Mean Life Expectancy Direct Solutions

Temporal moment equations can be derived from Eqs. (2.169) and (2.171). For instance, the *mean age equation* is obtained by taking the first moment form of Eq. (2.169):

$$-\nabla \cdot \mathbf{q}\langle A \rangle + \nabla \cdot \theta \mathbf{D} \nabla \langle A \rangle - q_{\mathrm{O}}\langle A \rangle + \theta = 0 \qquad \text{in} \quad \Omega \tag{2.181}$$

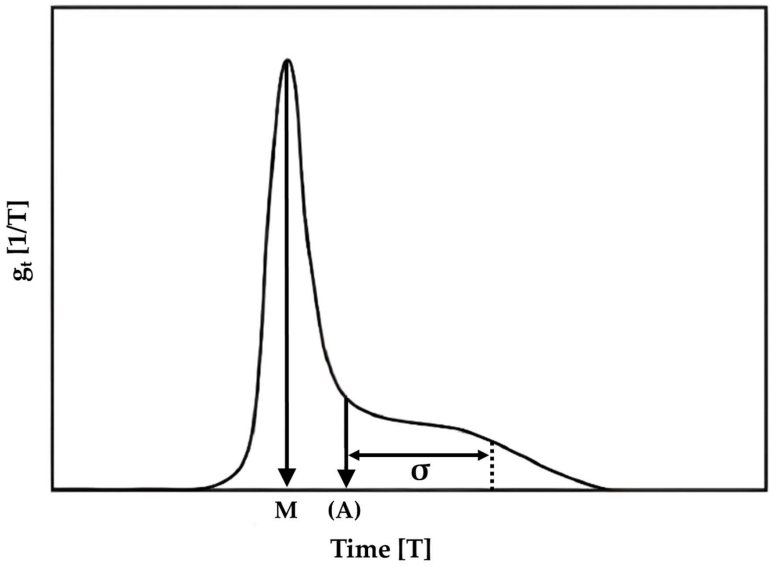

Figure 2.5: Descriptive statistics on the travel time PDF.

where $\langle A \rangle$ denotes mean age. It requires the following boundary conditions:

$$\langle A \rangle(\boldsymbol{x}) = 0 \qquad \text{on} \quad \Gamma_- \tag{2.182a}$$

$$\mathbf{J}(\boldsymbol{x}) \cdot \boldsymbol{n} = 0 \qquad \text{on} \quad \Gamma_0 \tag{2.182b}$$

The *mean life expectancy equation* is similarly obtained by taking the first moment form of Eq. (2.171):

$$\nabla \cdot \mathbf{q}\langle E \rangle + \nabla \cdot \theta \mathbf{D} \nabla \langle E \rangle - q_{\mathrm{I}} \langle E \rangle + \theta = 0 \qquad \text{in} \quad \Omega \tag{2.183}$$

where $\langle E \rangle$ denotes mean life expectancy. It requires the following boundary conditions:

$$\langle E \rangle(\boldsymbol{x}) = 0 \qquad \text{on} \quad \Gamma_+ \tag{2.184a}$$

$$-\mathbf{D} \nabla \langle E \rangle(\boldsymbol{x}) \cdot \boldsymbol{n} = 0 \qquad \text{on} \quad \Gamma_0 \tag{2.184b}$$

Mean age and mean life expectancy are continuously generated during groundwater flow, since porosity $\theta = \theta(\boldsymbol{x})$ acts as a source term in Eqs. (2.181) and (2.183). This source term indicates that groundwater is aging one unit per unit time, in average. Finally, mean total transit time (from inlet to outlet) can be obtained by taking the first moment form of Eq. (2.173), yielding to $\langle T \rangle = \langle A \rangle + \langle E \rangle$.

2.12.2.8 Evaluating the travel time PDF from the travel time CDF

An alternative technique for the evaluation of the travel time PDF is to solve for the CDF, which can be done by making use of the following forward and backward boundary value problems:

$$\frac{\partial \theta G}{\partial t} = -\nabla \cdot \mathbf{q} G + \nabla \cdot \theta \mathbf{D} \nabla G - q_{\mathrm{O}} G \qquad \text{in} \quad \Omega \tag{2.185a}$$

$$G(\boldsymbol{x}, 0) = 0 \qquad \text{in} \quad \Omega \tag{2.185b}$$

$$[\mathbf{q} G(\boldsymbol{x}, t) - \mathbf{D} \nabla G(\boldsymbol{x}, t)] \cdot \boldsymbol{n} = \mathbf{q} \cdot \boldsymbol{n} \qquad \text{on} \quad \Gamma_{-} \tag{2.185c}$$

$$[\mathbf{q} G(\boldsymbol{x}, t) - \mathbf{D} \nabla G(\boldsymbol{x}, t)] \cdot \boldsymbol{n} = 0 \qquad \text{on} \quad \Gamma_0 \tag{2.185d}$$

for the forward problem, and

$$\frac{\partial \theta G}{\partial t} = \nabla \cdot \mathbf{q} G + \nabla \cdot \theta \mathbf{D} \nabla G - q_{\mathrm{I}} G \qquad \text{in} \quad \Omega \tag{2.186a}$$

$$G(\boldsymbol{x}, 0) = 0 \qquad \text{in} \quad \Omega \tag{2.186b}$$

$$[-\mathbf{q} G(\boldsymbol{x}, t) - \mathbf{D} \nabla G(\boldsymbol{x}, t)] \cdot \boldsymbol{n} = -\mathbf{q} \cdot \boldsymbol{n} \qquad \text{on} \quad \Gamma_{+} \tag{2.186c}$$

$$-\mathbf{D} \nabla G(\boldsymbol{x}, t) \cdot \boldsymbol{n} = 0 \qquad \text{on} \quad \Gamma_0 \tag{2.186d}$$

for the backward problem. The function $G(\boldsymbol{x}, t)$ is the forward (or backward) travel time CDF, from which the travel time PDF $g(\boldsymbol{x}, t)$ can be deduced by enforcing:

$$g(\boldsymbol{x}, t) = \frac{\partial G(\boldsymbol{x}, t)}{\partial t} \tag{2.187}$$

This formulation is more appropriate to account for transient velocity fields. Note that the boundary conditions (2.185c) and (2.186c) may be replaced by the first-type condition $G(\boldsymbol{x}, t) = 1$. Note also that the n temporal moments μ_n of the travel time PDF can also be directly calculated from the CDF by means of the following formula:

$$\mu_n(\boldsymbol{x}) = \int_0^{+\infty} n\, t^{n-1} (1 - G(t, \boldsymbol{x})) dt \tag{2.188}$$

2.12.2.9 Capture zone probability

The capture zone probability of a specific outlet can easily be calculated by adapting Eq. (2.171) for the cdf of the life-expectancy-to-outlet Γ_n, $p_n(\boldsymbol{x},t) = \int_0^t g(\boldsymbol{x},u)du$:

$$\frac{\partial \phi p_n}{\partial t} = \nabla \cdot \mathbf{q} p_n + \nabla \cdot \theta \mathbf{D} \nabla p_n - q_I p_n \qquad \text{in} \quad \Omega \tag{2.189a}$$

$$p_n(\boldsymbol{x},0) = 0 \qquad \text{in} \quad \Omega \tag{2.189b}$$

$$[-\mathbf{q} p_n(\boldsymbol{x},t) - \mathbf{D} \nabla p_n(\boldsymbol{x},t)] \cdot \boldsymbol{n} = -\mathbf{q} \cdot \boldsymbol{n} \qquad \text{on} \quad \Gamma_n \tag{2.189c}$$

$$[-\mathbf{q} p_n(\boldsymbol{x},t) - \mathbf{D} \nabla p_n(\boldsymbol{x},t)] \cdot \boldsymbol{n} = 0 \qquad \text{on} \quad \Gamma_+ \tag{2.189d}$$

$$-\mathbf{D} \nabla p_n(\boldsymbol{x},t) \cdot \boldsymbol{n} = 0 \qquad \text{on} \quad \Gamma_0 \tag{2.189e}$$

The field of $p_n(\boldsymbol{x},t)$ defines the probabilistic drainage basin corresponding to the outlet Γ_n, or probabilistic capture zone relative to a particular transit time t. The ultimate, or steady-state probabilistic drainage basin is the field $p_n^\infty(\boldsymbol{x}) = p_n(\boldsymbol{x},\infty)$. Because in both 2D and 3D domains there is a non-zero probability that the water particles will *not* be intercepted by the outlet Γ_n (the only location where this probability is zero), $p_n^\infty(\boldsymbol{x})$ is less than one, $p_n^\infty(\boldsymbol{x}) = \int_0^\infty g(\boldsymbol{x},t)dt < 1 \ \forall \boldsymbol{x} \in \Omega$. An iso-probability value $p_n(\boldsymbol{x},\infty)$ includes the domain for which the fraction $1 - p_n(\boldsymbol{x},\infty)$ of its water amounts will reach the outlet Γ_n, sooner or later.

Chapter 3

Numerical Implementation

3.1 General

HydroGeoSphere uses the control volume finite element method to solve the flow equations for all domains considered in a simulation, and it uses either the standard Galerkin finite element method or the control volume finite element method to solve the transport equation. Elements available to solve the 3-D porous medium and dual continuum equations are rectangular prisms (8-node elements) and 3-D triangular prisms (6-node elements). The 2-D fracture and surface equations are solved for using either rectangular (4-node elements) or triangular elements (3-node elements) and the 1-D well, tile drain and channel equations are solved for 1-D linear elements (2-node elements). For the 3-D and 2-D elements, a finite difference approximation is also available, according to the method presented by Panday et al. (1993).

The model solves either linear equations (for fully-saturated flow or solute transport) or non-linear equations (for variably-saturated subsurface flow, surface flow, solute transport with a flux-limiter, including density-dependent flow and transport). To solve the non-linear equations, **HydroGeoSphere** uses the robust Newton-Raphson linearization method, except for the weakly nonlinear density-dependent problem, which is solved by the Picard method. Although the Newton-Raphson technique requires a larger amount of work for each solution step compared to other linearization methods such as Picard iteration, the robustness and higher order of convergence of the Newton method make it attractive.

The matrix equation arising from the discretization is solved by a preconditioned iterative solver, using either the ORTHOMIN, GMRES, or BiCGSTAB acceleration.

In this chapter, we present the discretized equations and provide details on the various solution schemes used by the model. We first present a general description of the control volume finite element method used to discretize the governing equations. We then present the discretized equations for subsurface and surface flow and for transport. We finally present the solution method for non-linear equations.

3.2 Control Volume Finite Element Method

The method of solution for the flow problem is based on the control volume finite element approach (Forsyth, 1991) which has been shown to be particularly well-suited for a fast and efficient implementation of the Newton–Raphson linearization technique (Forsyth and Simpson, 1991).

The basic idea of the control volume finite element approach is to obtain a discretized equation that mimics the governing mass conservation equation locally. A volume of influence, referred to as a control volume, is assigned to each node. Figure 3.1 illustrates nodal control volumes on the surface of a uniform triangular mesh. Each element that shares a node contributes a portion of its volume to that node's control volume. In general, an element defined on n nodes contributes $(1/n)$th of its volume to each node's control volume. The discretized equation for a given node then consists of a term describing the change in fluid mass storage for that volume which is balanced by the term representing the divergence of the fluid mass flux in the volume. The fluid mass flux will depend on the physical properties associated with the volume and the difference in the value of the primary variable between the node in question and its neighbors.

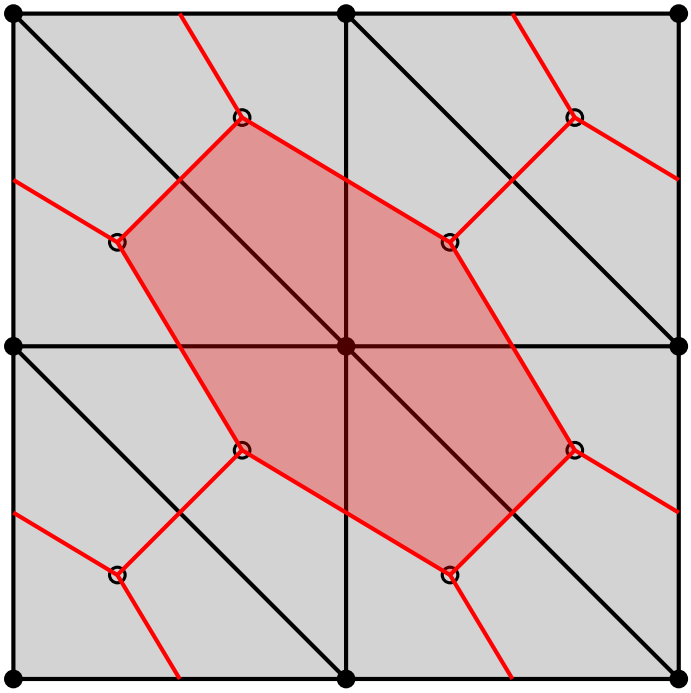

Figure 3.1: Nodal control volumes on the surface of a uniform triangular mesh with nine nodes (black disks) and eight elements. Black lines define element edges and red lines define nodal control volume edges, which intersect at the centroid (hollow disks) of each element.

Discretization of the subsurface and the surface flow equations is identical except for the difference in dimensionality. For the sake of clarity, we present here a detailed description

of the control volume finite element method applied to discretize a simplified prototype continuity equation. The final discretized equations for all subsurface domains and for surface flow are then presented without providing the details of the derivation.

Let us assume the following prototype flow equation:

$$\frac{\partial}{\partial t}(\theta_s S_w) - \nabla \cdot (\mathbf{K} \cdot k_r \nabla h) + Q = 0 \tag{3.1}$$

where h is the hydraulic head, equal to $\psi + z$.

Let N_i be the standard finite element basis functions such that:

$$\begin{aligned} N_i &= 1 \text{ at node } i \\ &= 0 \text{ at all other nodes} \\ \sum_j N_j &= 1 \text{ everywhere in the solution domain} \end{aligned} \tag{3.2}$$

Using the standard basis function, an approximating function is defined in the usual way for the spatially and temporally variable h and S_w:

$$h \simeq \hat{h} = \sum_j N_j h_j(t)$$

$$S_w \simeq \hat{S_w} = \sum_j N_j S_{wj}(t) \tag{3.3}$$

where j is a nodal index ranging from 1 to n, where n is the total number of nodes.

The standard Galerkin technique (see e.g., Huyakorn and Pinder (1983)) is used to discretize Equation 3.1 over the domain of interest, V, leading to:

$$\int_V \left[\frac{\partial}{\partial t}(\theta_s \hat{S_w}) - \nabla \cdot \left(\mathbf{K} \cdot k_r \nabla \hat{h} \right) + Q \right] N_i \, dV = 0 \tag{3.4}$$

where i is the nodal index ranging from 1 to total number of nodes. We now only consider the equation applying to node i. Upon approximating the time derivative by a finite difference representation and using a lumped mass approach to treat the storage terms in Equation 3.4, we can write:

$$\int_v \frac{\partial}{\partial t}(\theta_s \hat{S_w}) N_i dv = \theta_s \frac{\left(\hat{S}_w^{L+1} - \hat{S}_w^L \right)}{\Delta t} \int_v N_i \, dv \tag{3.5}$$

where v is the region or control volume associated with node i, L is the time level and Δt is the time-step size. Here, a fully implicit discretization in time is used. Likewise, for the region v associated with node i, the source/sink term in Equation 3.4 becomes:

$$Q_i = \int_v Q N_i \, dv \tag{3.6}$$

It is now desired to express the flux term in Equation 3.4 as a function of the total head difference between node i and each of its neighbors. By applying the divergence theorem to this term in Equation 3.4, one obtains:

$$\int_v -\nabla \cdot \left(\mathbf{K} \cdot k_r \nabla \hat{h}\right) N_i \, dv = \int_v \nabla N_i \cdot \mathbf{K} \cdot k_r \nabla \hat{h} \, dv - \int_B q^* N_i \, dB \tag{3.7}$$

The last term on the right-hand side is the integral of the fluid flux q^* normal to the boundary, B, of volume v. Let us assume for clarity that this fluid flux is zero. Use can be made of Equation 3.3 to get:

$$\nabla N_i \cdot \nabla \hat{h} = \nabla N_i \cdot \nabla \left(\sum_j h_j N_j \right) \tag{3.8}$$

where the summation is carried over all the nodes. Using the relation $\sum N_j = 1$. we have:

$$N_i = 1 - \sum_{j \neq i} N_j \tag{3.9}$$

such that:

$$\nabla N_i = -\nabla \sum_{j \neq i} N_j \tag{3.10}$$

Using Equations 3.9 and 3.10, the right-hand side of Equation 3.8 can now be rewritten in the following way:

$$\begin{aligned} \nabla N_i \cdot \nabla \left(\sum_j h_j N_j \right) &= \nabla N_i \cdot \nabla \left(\sum_{j \neq i} h_j N_j \right) + \nabla \left(h_j N_j \right) \\ &= \nabla N_i \cdot \nabla \left(\sum_{j \neq i} N_j \right) \left(h_j - h_i \right) \end{aligned} \tag{3.11}$$

The relationship in Equation 3.11 is used to obtain:

$$\int_v \nabla N_i \cdot \mathbf{K} \cdot k_r \nabla \hat{h} \; dv = \int_v \nabla N_i \cdot \mathbf{K} \cdot k_r \nabla \left(\sum_{j \neq i} N_j \right) \left(h_j - h_i \right) \, dv \tag{3.12}$$

Discretization of the domain into finite elements will create a nodal connectivity (*i.e.* a table of nodal incidences for the elements). Defining η_i as being the set of nodes connected to node i, it is obvious that the nodes not included in η_i will not contribute to the change in storage or fluid flow at node i. Using this result from discretization and the fact that the $h_j - h_i$ are nodal quantities and that the summation and integration operations are interchangeable, the right-hand side of Equation 3.12 becomes:

$$\int_v \nabla N_i \cdot \mathbf{K} \cdot k_r \nabla \left(\sum_{j \neq i} N_j \right) \left(h_j - h_i \right) \, dv = \sum_{j \in \eta_i} \int_v \nabla N_i \cdot \mathbf{K} \cdot k_r \nabla N_j \left(h_j - h_i \right) \, dv \tag{3.13}$$

Using the following relation:

$$\gamma_{ij} = \int_v \nabla N_i \cdot \mathbf{K} \cdot \nabla N_j \; dv \tag{3.14}$$

the right-hand side of Equation 3.13 becomes:

$$\sum_{j \in \eta_i} \int_v \nabla N_i \cdot \mathbf{K} \cdot k_r \nabla N_j \left(h_j - h_i\right) \; dv = \sum_{j \in \eta_i} \lambda_{ij+1/2} \gamma_{ij} \left(h_j - h_i\right) \tag{3.15}$$

where $\lambda_{ij+1/2}$ represent a weighted value of the relative permeabilities for nodes i and j, evaluated at the interface between nodal volumes i and j.

Combining Equations 3.5, 3.6 and 3.15, and using fully implicit time weighting, the final form of the discretized equation for node i becomes:

$$\left[(\theta_s S_w)_i^{L+1} - (\theta_s S_w)_i^L\right] \frac{v_i}{\Delta t} = \sum_{j \in \eta_i} (\lambda)_{(ij+1/2)}^{L+1} \gamma_{ij} (h_j^{L+1} - h_i^{L+1}) + Q_i^{L+1} \tag{3.16}$$

where superscript L denotes the time level and where the volume of influence for node i is given by:

$$v_i = \int_v N_i \, dv \tag{3.17}$$

The discretized equation presented above is independent of the choice of element type. Of the numerous types of three-dimensional elements that can be used to discretize the porous blocks, both 8-node rectangular block elements (Huyakorn et al., 1986) and 6-node prism elements are implemented here. The two-dimensional fracture planes and the surface flow are discretized using either rectangular or triangular elements (Huyakorn et al., 1984). This choice of simple elements allows use of the influence coefficient technique (Frind, 1982; Huyakorn et al., 1984) to analytically evaluate the integrals appearing in Equation 3.14 in an efficient manner.

3.3 Finite Difference Formulation

A finite difference representation in the numerical formulation of HGS is available using a methodology identical to that described by Panday et al. (1993) and Therrien and Sudicky (1996). The problem and boundary conditions are defined in terms of finite elements upon input and new nodal connectivities are established when a finite difference formulation is chosen for both 3-D block and prism elements. The influence coefficient matrices for the finite element method, presented by Huyakorn et al. (1986), are manipulated in order to mimic a finite difference discretization. The reader is referred to Panday et al. (1993) and Therrien and Sudicky (1996) for details on the implementation. The finite difference form of the needed influence coefficient matrices are provided in Huyakorn et al. (1986). Because of the different number of nodal connections (i.e., 7 for finite difference, 27 for finite element for block elements), the finite element method requires nearly four times as much memory

to store the coefficient matrix compared to that for the finite difference method. For block elements, the size of the assembled coefficient matrix is $n \times 27$ for finite elements and $n \times 7$ for finite differences, where n is the number of nodes in the domain. A variety of subsurface flow simulations that we have performed for fractured porous media under either fully- or variably-saturated conditions, have indicated that the finite difference and finite element representations yield similar results. Also, experience has indicated that the CPU time required when using the finite difference method is also nearly a factor of four less.

3.4 Discretized Subsurface Flow Equations

We now present the discretized flow equations for the porous medium, dual continuum, and fracture domains. The discretized equations are similar in form to the discretized prototype equation (3.16) and their derivation, not shown here, follows the steps highlighted in that section.

3.4.1 Porous Medium

Using the control volume finite element method, with fully implicit time weighting, the following discretized porous medium flow equation is obtained:

$$\left[(S_s S_w \psi + \theta_s S_w)_i^{L+1} - (S_s S_w \psi + \theta_s S_w)_i^{L}\right] \frac{w_m v_i}{\Delta t} =$$

$$\sum_{j \in \eta_i} (\lambda)_{(ij+1/2)}^{L+1} \gamma_{ij} (h_j^{L+1} - h_i^{L+1}) - \left(\sum \Gamma_{\text{ex}}^{L+1}\right) v_i + Q_i^{L+1} \tag{3.18}$$

where:

$$h_i = \psi_i + z_i \tag{3.19}$$

and:

$$\gamma_{ij} = \int_v \nabla N_i \cdot w_m \mathbf{K} \cdot \nabla N_j \; dv \tag{3.20}$$

for interpolation functions N defined for the 3-D porous medium elements and where the 3-D volume associated with a given node is given by:

$$v_i = \int_v N_i \, dv \tag{3.21}$$

For upstream weighting, the $\lambda_{ij+1/2}$ values are given by:

$$\begin{aligned} \lambda_{ij+1/2} &= k_{rj} \quad \text{if} \;\; \gamma_{ij} \, (h_j - h_i) > 0 \\ \lambda_{ij+1/2} &= k_{ri} \quad \text{if} \;\; \gamma_{ij} \, (h_j - h_i) < 0 \end{aligned} \tag{3.22}$$

Upstream weighting of the relative permeability is highly recommended in order to ensure monotonicity of the solution (Forsyth, 1991). A monotone solution will yield saturations that always remain in the physical range, (i.e., between 0.0 and 1.0). Forsyth and Kropinski (1997) provides a vivid illustration of the importance of the type of relative permeability weighting on the quality and stability of the solution of Richards' equation. They considered a two-dimensional unsaturated flow problem in which the air entry pressure was low which makes the governing equation more hyperbolic in nature. Results showed that the use of central weighting produced significant negative saturations as the wetting front advanced in a relatively dry soil; however, the solution was stable and remained in the physical range when upstream weighting was used. Although it is well-known that the use of upstream weighting for advection-dispersion problems can lead to excessive smearing of a concentration front, its use in conjunction with hyperbolic-type equations, such as the one for variably-saturated flow, does not smear as much because the solution is self-sharpening. It has also been shown that, for purely hyperbolic equations, the use of central weighting can cause complete failure of the solution (Sammon, 1988).

The reduction of area available for flow across a fracture-matrix interface can be easily incorporated in Equation 3.18 in a manner suggested by Wang and Narasimhan (1985). The area between nodes i and j, which are both located in the matrix, is imbedded in the γ_{ij} term, defined by Equation 3.20. For cases where i or j also coincide with a fracture node, this area between the two nodes is multiplied by a factor representing the new effective area, accounting for a matrix-matrix flow area reduction when the fracture desaturates.

It should also be noted that in the discretized Equation 3.18, the saturation term is represented exactly and no use is made of the water capacity term which is known to induce severe mass balance errors (Milly, 1985; Celia et al., 1990). Various schemes ranging in complexity have therefore been derived to resolve this problematic mass balance error, e.g., (Cooley, 1983; Milly, 1985; Celia et al., 1990). In this work, the use of the Newton-Raphson procedure allows a direct representation of the saturation term, thereby completely avoiding the difficulties arising from the use of the water capacity term.

3.4.2 Discrete Fractures

The discretized 2-D equation for flow in fractures is:

$$\left[(S_{wf})_i^{L+1} - (S_{wf})_i^{L}\right] \frac{w_f a_i}{\Delta t} = \sum_{j \in \eta_{f_i}} (\lambda_f)_{(ij+1/2)}^{L+1} \gamma_{f_{ij}} ({h_f}_j^{L+1} - {h_f}_i^{L+1}) + w_f \Gamma_f^{L+1} a_i \qquad (3.23)$$

where η_{f_i} is the set of fracture nodes connected to fracture node i through the 2-D fracture elements and where:

$$h_{f_i} = \psi_{f_i} + z_{f_i} \qquad (3.24)$$

and:

$$\gamma_{f_{ij}} = \int_a \nabla N_i \cdot w_f \mathbf{K_f} \cdot \nabla N_j \; da \qquad (3.25)$$

with interpolation functions N defined for the 2-D fracture elements.

The 2-D area associated with a given fracture node is given by:

$$a_i = \int_a N_i \, da \tag{3.26}$$

For upstream weighting of relative permeabilities, the $(\lambda_f)_{ij+1/2}$ values are given by:

$$\begin{aligned} (\lambda_f)_{ij+1/2} &= k_{rfj} \quad \text{if} \quad \gamma_{f_{ij}} \left(h_{f_j} - h_{f_i} \right) > 0 \\ (\lambda_f)_{ij+1/2} &= k_{rfi} \quad \text{if} \quad \gamma_{f_{ij}} \left(h_{f_j} - h_{f_i} \right) < 0 \end{aligned} \tag{3.27}$$

3.4.3 Dual Continuum

Using the control volume finite element method, the discretized equation for flow in a dual continuum is:

$$\left[(S_{sd} S_{wd} \psi_d + \theta_{sd} S_{wd})_i^{L+1} - (S_{sd} S_{wd} \psi_d + \theta_{sd} S_{wd})_i^{L} \right] \frac{w_d v_i}{\Delta t} =$$

$$\sum_{j \in \eta_{id}} (\lambda_d)_{(ij+1/2)}^{L+1} \gamma_{dij} ({h_{dj}}^{L+1} - {h_{di}}^{L+1}) - \left[\Gamma_d^{L+1} + {Q_{di}}^{L+1} \right] v_i \tag{3.28}$$

where volume v_i is defined for the dual continuum nodes, with an expression similar to Equation 3.21 and where:

$$h_{di} = \psi_{di} + z_{di} \tag{3.29}$$

and:

$$\gamma_{dij} = \int_v \nabla N_i \cdot w_d \mathbf{K_d} \cdot \nabla N_j \; dv \tag{3.30}$$

where the interpolation functions N are defined for the 3-D dual continuum elements.

For upstream weighting of relative permeabilities, the $\lambda_{dij+1/2}$ values are given by:

$$\begin{aligned} \lambda_{dij+1/2} &= k_{drj} \quad \text{if} \quad \gamma_{dij} \left(h_{dj} - h_{di} \right) > 0 \\ \lambda_{dij+1/2} &= k_{dri} \quad \text{if} \quad \gamma_{dij} \left(h_{dj} - h_{di} \right) < 0 \end{aligned} \tag{3.31}$$

3.5 Discretized Surface Flow Equation

The discretized 2-D surface flow equation is:

$$\left[(h_o)_i^{L+1} - (h_o)_i^{L} \right] \frac{a_i}{\Delta t} = \sum_{j \in \eta_{oi}} (\lambda_o)_{(ij+1/2)}^{L+1} \gamma_{oij} ({h_o}_j^{L+1} - {h_o}_i^{L+1}) + d_o \Gamma_o^{L+1} a_i \pm q_{oi} \tag{3.32}$$

where η_{oi} is the set of surface nodes connected to surface node i through the 2-D surface elements and where:

$$h_{oi} = d_{oi} + z_{oi} \tag{3.33}$$

and:

$$\gamma_{oij} = \int_a \nabla N_i \cdot \mathbf{K_o} \cdot \nabla N_j \; da \tag{3.34}$$

with interpolation functions N defined for the 2-D surface elements.

The 2-D area associated with a given surface node is given by:

$$a_i = \int_a \phi_o N_i \, da \tag{3.35}$$

For upstream weighting of surface pseudo relative permeabilities, the $(\lambda_o)_{ij+1/2}$ values are given by:

$$\begin{aligned} (\lambda_o)_{ij+1/2} &= k_{roj} \quad \text{if} \;\; \gamma_{oij}\,(h_{oj} - h_{oi}) > 0 \\ (\lambda_o)_{ij+1/2} &= k_{roi} \quad \text{if} \;\; \gamma_{oij}\,(h_{oj} - h_{oi}) < 0 \end{aligned} \tag{3.36}$$

Careful consideration should be taken to implement the conductances of the flow terms of Equation 3.34. The conductance tensor $\mathbf{K}_o$ has two components in two dimensions, K_{ox} and K_{oy} that are combinations of the properties of the two nodes involved in the respective flow connection. The constant part in Equations 2.39 and 2.40, constitutes the frictional resistance term ($1/n_x$ and $1/n_y$) and is an input parameter for each element. The gradient part of Equations 2.39 and 2.40, $[\partial h_o/\partial s]^{-1/2}$, is calculated from the average x- and y-direction gradients of the connecting cells, to determine the gradient in the direction of maximum slope. The remaining terms in Equations 2.39 and 2.40, along with the depth within the first gradient operator of Equation 2.41, combine to give $d_o^{5/3}$. Full upstream weighting of this term between the two connecting nodes ensures a monotonic solution, without unphysical oscillations. Further, upstream weighting ensures that flow from a dry node is zero, maintaining the physical reality to the set of governing equations.

3.6 One-Dimensional Hydraulic Features

One-dimensional hydraulic features in **HydroGeoSphere** are used to simulate streams, rivers, wells, water supply lines and gravity driven drains. Similar to surface/subsurface flow, the 1D equations were discretized with a control volume finite element approach combined with the Newton-Raphson successive linearization method to solve the discrete set of nonlinear equations.

The governing equation for general one-dimensional flow can be written as:

$$L(h_{1D}) = A_f C_s \frac{\partial h_{1D}}{\partial t} + \frac{\partial A_f}{\partial t} - \frac{\partial}{\partial s}\left(K_{1D}\frac{\partial h_{1D}}{\partial s}\right) - Q_w \delta(s - s_p) - \Gamma_{exch} \tag{3.37}$$

$$K_{1D}(h_{1D}) = C \cdot A_f \cdot (R_H)^p \cdot \left[\frac{\partial h_{1D}}{\partial s}\right]^{q-1} \tag{3.38}$$

where the change in water volume is expressed as a function of the compressibility coefficient (C_s) and the change in the flow area. The fluid exchange between the surrounding environment and hydraulic feature is represented by Γ_{exch}.

The finite element analysis utilizes a trial solution for head, defined using the standard interpolation functions and then a weighted residual at node i can be defined as the weighted integral of the equation over the solution domain such that:

$$\hat{h}_{1D} = \sum_j N_j (h_{1D})_j \tag{3.39}$$

$$\begin{aligned}
&\int_{R^1} N_i L(\hat{h}_{1D}) dR^1 \\
&= \int_{R^1} N_i \left[\hat{A}_f C_s \frac{\partial \hat{h}_{1D}}{\partial t} + \frac{\partial \hat{A}_f}{\partial t} - \frac{\partial}{\partial s}\left(\hat{K}_{1D}\frac{\partial \hat{h}_{1D}}{\partial s}\right) - Q_w \delta(s - s_p) - \hat{\Gamma}_{exch}\right] dR^1 \\
&= 0
\end{aligned} \tag{3.40}$$

Introducing the trial solution and using a lumped capacitance formulation:

$$\begin{aligned}
&L_i \left[A_{f,i} C_s \frac{\partial h_{1D,i}}{\partial t} + \frac{\partial A_{f,i}}{\partial t}\right] \\
&= \int_{R^1} N_i \left[\frac{\partial}{\partial s}\left(\hat{K}_{1D}\frac{\partial}{\partial s}\left(\sum_j N_j h_{1D,i}\right)\right) + Q_w \delta(s - s_p) + \hat{\Gamma}_{exch}\right] dR^1 \\
&= -\sum_j h_{1D,j}\left[\int_{R^1} \hat{K}_{1D}\frac{\partial N_i}{\partial s}\frac{\partial N_j}{\partial s} dR^1\right] - q_{\delta R^1,i} + Q_{w,i} + \hat{\Gamma}_{exch,i}
\end{aligned} \tag{3.41}$$

where:

$$L_i \left[A_{f,i} C_s \frac{\partial h_{1D,i}}{\partial t} + \frac{\partial A_{f,i}}{\partial t}\right] \approx \int_{R^1} N_i \left[\hat{A}_f C_s \frac{\partial \hat{h}_{1D}}{\partial t} + \frac{\partial \hat{A}_f}{\partial t}\right] dR^1 \tag{3.42}$$

$$q_{\delta R^1,i} = -\int_{\delta R^1} N_i \left(\hat{K}_{1D}\frac{\partial \hat{h}_{1D}}{\partial s}\right) d(\delta R^1) \tag{3.43}$$

$$Q_{w,i} = \int_{R^1} N_i Q_w \delta(s - s_p) dR^1 + \int_{R^1} N_i \hat{\Gamma}_{exch} dR^1 \tag{3.44}$$

$$\hat{\Gamma}_{exch,i} = \int_{R^1} N_i \hat{\Gamma}_{exch} dR^1 \tag{3.45}$$

Incorporating the properties of standard interpolation functions $\sum_i N_j = 1$ or $N_i = 1 - \sum_{j \neq i} N_j$, the discrete control volume one-dimensional flow equation is converted to the following form:

$$L_i \left[A_{f,i} C_s \frac{\partial h_{1D,i}}{\partial t} + \frac{\partial A_{f,i}}{\partial t}\right] = \sum_{j \neq i} C_{1D,ij} \left[h_{1D,j} - h_{1D,i}\right] - q_{\delta R^1,i} + Q_{w,i} + \hat{\Gamma}_{exch,i} \tag{3.46}$$

where:

$$C_{1D,ij} = \int_{R^1} K_{1D}(h_{up,ij}) \frac{\partial N_i}{\partial s} \frac{\partial N_j}{\partial s} dR^1 \tag{3.47}$$

where the hydraulic properties (K_{1D}) are determined by the upstream weighting method determined by $h_{up,ij} = \max(h_{1D,i}, h_{1D,j})$.

3.7 Flow Coupling

The porous medium (and the dual continuum if present) is discretized in three dimensions with either rectangular prisms or triangular prisms. Two-dimensional rectangular or triangular elements represent the discrete fracture and the surface domains, and one-dimensional line elements represent the wells and the tile drains. When discretizing the domain, nodes forming the fracture or surface elements or nodes forming the well and tile drain elements have to coincide with those on the adjacent porous medium finite volumes, similarly to Sudicky et al. (1995). Because the fracture elements are generated such that they correspond to planes that intersect three or 4 nodes in the three-dimensional rectangular blocks or prisms, the nodes comprising the fracture elements are therefore common to nodes comprising the porous matrix elements. The commonality of these nodes thus ensures the continuity of hydraulic head at the fracture matrix interface. Also, by superimposing the contributions at each node from both element types, there is no need to explicitly calculate the fluid leakage terms appearing in the discretized equations. For the surface flow nodes, a choice of common or dual nodes is offered, but the surface flow nodes nevertheless have to coincide with porous medium nodes. Additionally, nodes forming the 3-D dual continuum domain coincide with the porous medium nodes, but they form duplicate nodes since the dual node approach is used.

With the common node approach, the matrix contributions arising from the discretization of the discrete fracture or the surface nodes, as well as matrix contributions from the well nodes and tile drain nodes are superimposed onto those stemming from the discrete form of porous medium equation. Continuity in pressure head is therefore ensured between the different domains, which avoids the need for a direct evaluation of the exchange fluxes between the porous medium elements and the other domains.

As an example, we write below the final discretized matrix equation when discrete fractures are located in the porous domain. Using discretized Equation (3.23), we write the coupling term Γ_f as:

$$w_f \Gamma_f^{L+1} a_i = \left[(S_{wf})_i^{L+1} - (S_{wf})_i^L \right] \frac{w_f a_i}{\Delta t} - w_f \sum_{j \in \eta_{f_i}} (\lambda_f)_{(ij+1/2)}^{L+1} \gamma_{f_{ij}} (h_{f_j}^{L+1} - h_{f_i}^{L+1}) \tag{3.48}$$

Replacing the expression for the coupling term into porous medium Equation 3.18 gives the following global equation:

$$\left[(S_s S_w \psi + \theta_s S_w)_i^{L+1} - (S_s S_w \psi + \theta_s S_w)_i^L \right] \frac{w_m v_i}{\Delta t} + \left[(S_{wf})_i^{L+1} - (S_{wf})_i^L \right] \frac{w_f a_i}{\Delta t} =$$

$$\sum_{j\in\eta_i}(\lambda)^{L+1}_{(ij+1/2)}\gamma_{ij}(h_j^{L+1}-h_i^{L+1})-\left(\sum\Gamma_{\text{ex}}^{L+1}\right)v_i\pm Q_i^{L+1}+$$

$$w_f\sum_{j\in\eta_{f_i}}(\lambda_f)^{L+1}_{(ij+1/2)}\gamma_{f_{ij}}({h_f}_j^{L+1}-{h_f}_i^{L+1}) \tag{3.49}$$

In Equation 3.49, we assume that $h_i = h_{f_i}$ for node that are common to the porous medium and fracture domains, which ensures continuity. The exact value of the fluid exchange between the domains, Γ_f, is therefore not computed explicitly prior to solution, but the exchange can be back-calculated during post-processing of results by evaluating Equation 3.48 at the desired nodes.

Similarly to the approach shown here for superposition of 2 domains, the model allows superposition of all flow domains by adding the relevant discretized equations and assuming continuity of head.

In the next section, we present coupling for the dual node approach when subsurface and surface flow equations are fully coupled. It is the only approach currently available for coupling the porous medium and second subsurface continuum and it is one of the two options available for coupling the porous medium and surface flow.

3.7.1 Dual-Continuum Subsurface Coupling

As mentioned previously, the porous medium equation is discretized everywhere for the 3-D simulation grid. On the other hand, the dual continuum need not be present everywhere in the domain. When dual continuum is simulated, the discretized dual continuum Equation 3.28 is applied only to those grid nodes where dual continuum conditions exist. Because the dual node approach is used to link the porous medium and the second continuum, the dual continuum nodes have the same spatial coordinates than the porous medium nodes. However, at a dual node, there are two unknowns to solve for: the total hydraulic head in the porous medium ($\psi + z$) and that in the second continuum ($\psi_d + z_d$). Fluid exchange between the two domains is provided by the exchange term Ω_d.

After the subsurface flow equations have been assembled into an implicit system of matrix equations, the 3-D dual continuum flow equations are added to the matrix along with their porous medium interactions, and the fully-integrated flow system is solved at each time step.

3.7.2 Surface - Subsurface Coupling

The 2-D areal surface flow modules of **HydroGeoSphere** follow the same conventions for spatial and temporal discretizations as those used by the subsurface modules. The surface flow equation is solved on a 2-D finite-element mesh stacked upon a subsurface grid when solving for both domains (i.e. the x- and y-locations of nodes are the same for each layer of nodes), as shown in Figure 3.2. For superposition, the grid generated for the

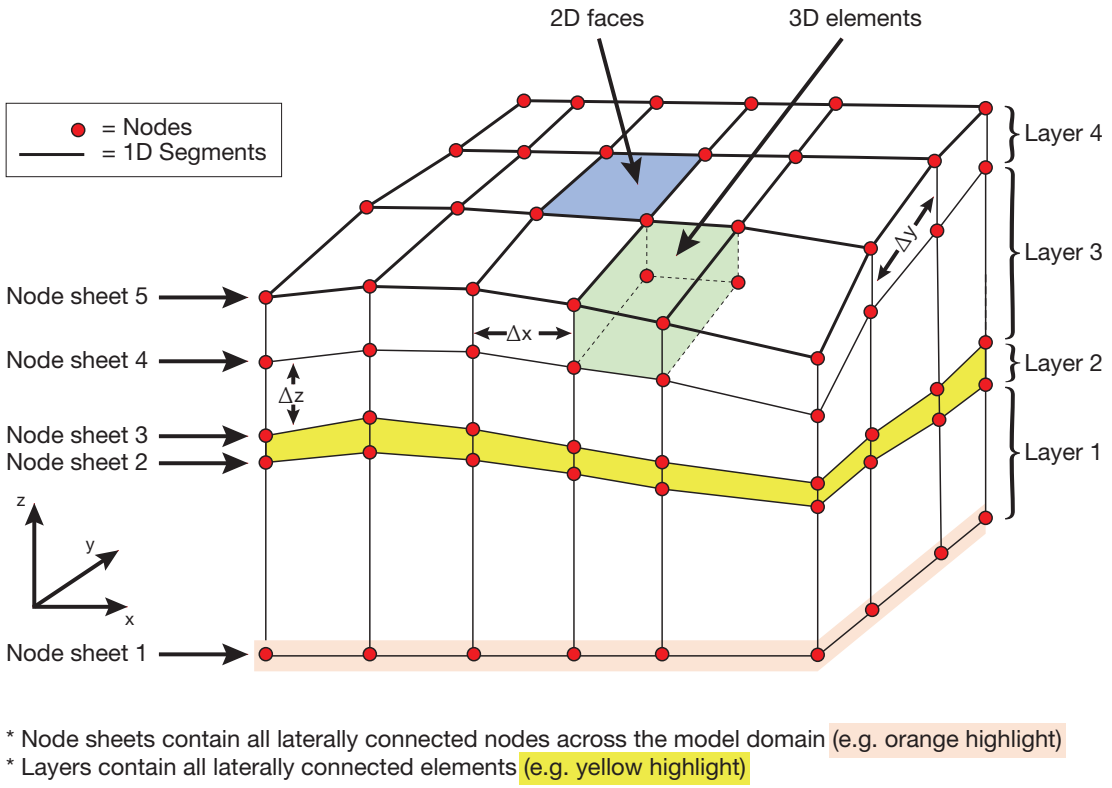

Figure 3.2: Spatial Discretization of the Surface Flow System and its Connection to the Subsurface (adapted from Panday and Huyakorn (2004, Figure 5)).

subsurface domain is mirrored areally for the surface flow nodes, with surface flow node elevations corresponding to the top elevation of the topmost active layer of the subsurface grid. Note that surface flow node elevations may vary substantially to conform with topography. However, the assumptions of small slope inherent in the diffusion-wave equation will not allow for modeling of inertial effects.

Although Figure 3.2 uses 2-D rectangular elements on the surface and 3-D hexahedral elements in the subsurface, **HydroGeoSphere** allows for the use of unstructured grids composed of, for example, 2-D triangles on the surface and 3-D 6 node prismatic elements in the subsurface.

The discretized surface Equation 3.32 is coupled with the 3-D subsurface flow Equation 3.18 via superposition (common node approach) or via leakage through a surficial skin layer (dual node approach). For both approaches, fully implicit coupling of the surface and subsurface flow regimes provides an integral view of the movement of water, as opposed to the traditional division of surface and subsurface regimes. Flux across the land surface is, therefore, a natural internal process allowing water to move between the surface and subsurface flow systems as governed by local flow hydrodynamics, instead of using physically

artificial boundary conditions at the interface.

When the subsurface connection is provided via superposition, **HydroGeoSphere** adds the surface flow equation terms for the 2-D surface mesh to those of the top layer of subsurface nodes in a manner similar to that described in Section 3.7 for the common node approach. In that case, the fluid exchange flux Γ_o, which contains leakance term K_{so} does not need to be explicitly defined.

For subsurface connection via skin leakance, the dual node approach is used and each surface flow node communicates with the first active subsurface flow node directly beneath it to form the subsurface connection. The subsurface flow connection term K_{so} must therefore be added to the left hand side of the respective row for corresponding subsurface flow nodes, in the column that connects them to the surface flow nodes. The interaction flux will also be added to the right hand side of the subsurface flow Equation 3.18. After the subsurface flow equations have been assembled into an implicit system of matrix equations, the 2-D areal surface flow equations are added to the matrix along with their subsurface interactions, and the fully-integrated flow system is solved at each time step. This provides significant robustness and accuracy over flux linkage techniques, often used when conjunctive modeling is required for the surface and subsurface regimes.

3.8 Flow Boundary Conditions

3.8.1 Subsurface Flow

Boundary conditions for subsurface flow include the following: first-type (Dirichlet) boundaries of prescribed hydraulic head, areal infiltration or recharge, source/sinks, evapotranspiration, and seepage faces.

The source/sink term in Equation 3.18 can be manipulated in order to impose prescribed head boundary conditions (Forsyth, 1988; Forsyth and Kropinski, 1997). To assign a prescribed pressure head, ψ_b, to a portion of the domain, the source/sink term becomes:

$$Q_i = K_{ij} k_{rw} W_i (\psi_b - \psi_i), \tag{3.50}$$

where W_i is a number large enough (e.g., 10^{20}) to ensure that $\psi_i = \psi_b$ when the assembled system of equations for all nodes is solved. This can be viewed as injecting or withdrawing sufficient fluid at node i to maintain the prescribed pressure head.

Seepage faces represent boundaries that require special treatment and a variety of methods have been suggested to implement such boundaries (Neuman, 1973; Cooley, 1983). The method used here is from Forsyth (1988) and requires that the approximate location of the seepage face be known a priori. The appropriate form of the source/sink term at the nodes forming the seepage face will be:

$$Q_i = \begin{cases} K^* k_{rw} W_i \left(\psi_{atm} - \psi_i\right), & \psi_i > \psi_{atm} \\ 0, & \psi_i \leq \psi_{atm}, \end{cases} \tag{3.51}$$

where K^* is the component of the hydraulic conductivity tensor normal to the seepage face. The above expression allows seepage only when the pressure in the medium is greater than the atmospheric pressure, ψ_{atm}.

A free drainage boundary is often used for unsaturated flow conditions. It assumes that a unit hydraulic gradient exists along the vertical direction, which results in the following volumetric flow rate out of the domain:

$$Q_i = -K_{zz} k_{rw} A_i, \tag{3.52}$$

where A_i is the outflow area associated with node i where free drainage occurs.

Drain nodes can be used to simulate fluid flow out of the domain, but without allowing inflow. For a given drain node i, the drain flow rate is given by

$$Q_i = \begin{cases} -C_{dr}(\psi_i - \psi_{dr}), & \psi_i > \psi_{dr} \\ 0, & \psi_i \leq \psi_{dr}, \end{cases} \tag{3.53}$$

where C_{dr} is an equivalent conductance [$\mathrm{L}^2\ \mathrm{T}^{-1}$] for the drain node and ψ_{dr} is the drain pressure head.

Makeup water nodes can be used to simulate fluid flow into the domain, but without allowing outflow. For a given makeup water node i, the makeup water flow rate is given by

$$Q_i = \begin{cases} -C_{mk}(\psi_i - \psi_{mk}), & \psi_i < \psi_{mk} \\ 0, & \psi_i \geq \psi_{mk}, \end{cases} \tag{3.54}$$

where C_{mk} is an equivalent conductance [$\mathrm{L}^2\ \mathrm{T}^{-1}$] for the makeup water node and ψ_{mk} is the makeup water pressure head.

River nodes can be used to simulate fluid flow into or out of the domain. For a given river node i, the flow rate is given by:

$$Q_i = -C_{riv}(h_i - h_{riv}), \tag{3.55}$$

where C_{riv} is an equivalent conductance [$\mathrm{L}^2\ \mathrm{T}^{-1}$] for the river node and h_{riv} is the river hydraulic head. Assuming the river bed acts as a semipervious layer, the equivalent conductance C_{riv} is given by:

$$C_{riv} = \frac{K_{bed}}{L_{bed}} W_{rch} L_{rch}, \tag{3.56}$$

where K_{bed} is the river bed conductivity [$\mathrm{L}\ \mathrm{T}^{-1}$], L_{bed} is the river bed thickness [L], W_{rch} is the width of the reach [L], and L_{rch} is the length of the reach [L].

3.8.2 Surface Flow

Boundary conditions to the surface flow system include the following: first-type (Dirichlet) boundaries of prescribed water elevation, rainfall rate, source/sinks, evaporation, zero-depth gradient and critical-depth conditions.

First-type boundary conditions are implemented in an identical manner to what is described for subsurface flow in Section 3.8.1 above. Areal rainfall (volumetric inflow over an area) is implemented as an input water flux multiplied by the contributing area. Sources/Sinks are applied as net fluxes to the surface flow nodes that receive them. Sinks are constrained by the physical property that water depth cannot be negative (i.e., water cannot be extracted when the water level is below bed elevation). If this condition occurs at any solution iteration, only as much water is withdrawn as to not violate this constraint. A further constraint is that injection should also be restricted at sink nodes. Thus, the sink strength should only reduce to zero under limited supply conditions and not become a negative sink (i.e., a source). Evaporation is applied as an areal sink to an surface flow node, subject to similar non-negative depth constraints as discussed for sinks, above.

Zero-depth gradient and critical depth boundary conditions are implemented to simulate conditions at the lower boundaries of a hill slope. The zero-depth gradient condition forces the slope of the water level to equal the bed slope, which is provided by the user at this boundary. The discharge, Q_o, at the zero-depth gradient boundary is given by

$$Q_o = \frac{1}{n_i} d_o^{5/3} \sqrt{S_o} \tag{3.57}$$

where Q_o is the flux per unit width, i is the direction of the zero-depth gradient discharge ($i = x$ in the x-direction and $i = y$ in the y-direction), n_i is the Manning roughness coefficient in the direction i, and S_o is the bed slope at the zero-depth gradient boundary.

Critical depth (CD) condition forces the depth at the boundary to be equal to the critical depth. The discharge Q_o per unit width at the critical depth boundary is given by:

$$Q_o = \sqrt{g d_o^3} \tag{3.58}$$

3.8.3 Interception and Evapotranspiration

3.8.3.1 Interception and Canopy Evaporation

For each time step Δt, the canopy evaporation E_{can}, actual interception storage S_{int} and effective rainfall rate P_p^E are calculated with Equations 2.71, 2.72 and 2.77, respectively. These parameters are calculated for surface elements for which a potential evapotranspiration boundary condition has been specified. The calculated values are then redistributed over the nodes that form these elements.

The effective rainfall rate for a given flux or rain boundary that also belongs to the evapotranspiration domain is computed with the precipitation rate specified by the user. For a given time step, the specified flux assigned to these boundaries is equal to the effective rainfall rate rather than the specified precipitation rate, to account for water intercepted by the canopy and canopy evaporation.

3.8.3.2 Surface and Subsurface Evapotranspiration

Evapotranspiration affects elements and nodes in both surface and subsurface flow domains and may involve several layers of nodes. For each time step, the transpiration (T_p) at a given areal location is the sum of transpiration rates for nodes distributed at depth over the effective root length

$$T_p = \sum_{i=1}^{n_r} T_{pi} \tag{3.59}$$

where n_r is the number of nodes that lie within the depth interval $0 \leq z \leq L_r$ at the areal location. The rate of transpiration T_{pi} for node i is calculated by substituting its nodal water content θ_i and nodal time-varying root distribution function RDF_i in Equations 2.78 to 2.83. The value of RDF at any areal location is typically equal to one but a smaller value can be specified to account for ineffective roots.

Similarly to transpiration, the rate of subsurface evaporation E_s at a given areal location is calculated as the sum of the nodal evaporation rates (E_{si}) at depth according to

$$E_s = \sum_{i=1}^{n_e} E_{si} \tag{3.60}$$

where n_e is the number of nodes that lie between ground surface and the evaporation depth. The nodal rate of evaporation E_{si} is calculated by substituting the nodal water content θ_i in Equation 2.89 and the nodal evaporation distribution function EDF_i in Equation 2.87.

An appropriate value of EDF_i for each nodal layer may be prescribed as a function of its depth from land surface.

3.9 Elemental Velocities

Elemental velocities or fluid fluxes can be computed after solving for fluid flow. The fluid flux is evaluated by combining its definition:

$$\mathbf{q} = -\mathbf{K} \cdot k_r \nabla(\hat{\psi} + z) \tag{3.61}$$

with the definition of the interpolation function for the unknown. For pressure head, the interpolation function is:

$$\hat{\psi} = \sum_j N_j \psi_j(t)$$

The evaluation of elemental velocities or fluid fluxes is done according to the simple formulas given by Huyakorn et al. (1986) for all types of 1-D, 2-D and 3-D elements available in the model.

3.10 Discretized Solute Transport Equations

3.10.1 Porous Medium

When the transport equation is linear, which is the case except when a flux limiter is used for the advective term in order to minimize adverse numerical dispersion, its solution is not as involved as that for the non-linear cases. We present here a discretization scheme for the transport equations based on the control volume finite element method presented in Section 3.2. The type of elements used for transport are identical to those used for the flow problem and the choice of superposition of several domains (common node approach) is also given, where elements representing one domain are superimposed onto the element representing a second domain, as performed for the flow equation. This ensures the continuity of concentration at the domain-to-domain interface and avoids the need to explicitly determine the solute mass exchange terms involving Ω_{ex} in the governing transport equations. When a dual continuum is simulated, the dual node approach is used to represent the interaction between the porous medium and the dual continuum.

We present here the standard discretized equation for the 3-D porous medium, obtained from the application of the control volume finite element method:

$$\left[(\theta_s S_w RC)_i^{L+1} - (\theta_s S_w RC)_i^{L}\right] \frac{w_m v_i}{\Delta t} = \sum_{j\in\eta_i} (C)_{(ij+1/2)}^{L+1} (\lambda)_{(ij+1/2)}^{L+1} \gamma_{ij} (h_j^{L+1} - h_i^{L+1}) +$$

$$\sum_{j\in\eta_i} \chi_{ij} (C_j^{L+1} - C_i^{L+1}) + (Q_i C_{ups})_i^{L+1} + \left[(R\lambda C_i)_{par} - (\theta_s S_w R\,\lambda\, C)_i + \sum \Omega_{\text{ex}}^{L+1}\right] v_i \quad (3.62)$$

where:

$$\begin{aligned} C_{ups} &= C_i \quad \text{if} \quad Q_i < 0 \\ &= C_{\text{inflow}} \quad \text{if} \quad Q_i > 0 \end{aligned} \quad (3.63)$$

and where C_{inflow} is the specified source inflow concentration (recall that Q_i is the source/sink term used to represent boundary conditions). Note that $\mathbf{q}_{(ij+1/2)}^{L+1} = (\lambda)_{(ij+1/2)}^{L+1} \gamma_{ij} (h_j^{L+1} - h_i^{L+1})$ is the fluid flux at the interface between nodes i and j and is back-calculated from the flow solution.

The term $C_{(ij+1/2)}$ in Equation 3.62 depends on the type of advective weighting used. For central weighting:

$$C_{(ij+1/2)} = \frac{C_i + C_j}{2} \quad (3.64)$$

Upstream weighting gives:

$$\begin{aligned} C_{(ij+1/2)} &= C_{ups} = C_j \quad \text{if} \quad \gamma_{ij}\,(h_j - h_i) > 0 \\ C_{(ij+1/2)} &= C_{ups} = C_i \quad \text{if} \quad \gamma_{ij}\,(h_j - h_i) < 0 \end{aligned} \quad (3.65)$$

A TVD type flux limiter is also available to evaluate $C_{(ij+1/2)}$ according to (van Leer, 1974; Unger et al., 1996):

$$C_{(ij+1/2)} = C_{ups} + \sigma(r_{ij}) \left(\frac{C_{dwn} - C_{ups}}{2} \right) \tag{3.66}$$

where C_{dwn} is the concentration of the downstream node between i and j. The smoothness sensor r_{ij} is given by:

$$r_{ij} = \left(\frac{C_{ups} - C_{i2ups}}{\|P_{ups} - P_{i2ups}\|} \right) \left(\frac{C_{dwn} - C_{ups}}{\|P_{dwn} - P_{ups}\|} \right)^{-1} \tag{3.67}$$

where C_{i2ups} is the second upstream node between i and j, and P_{ups}, P_{i2ups}, P_{dwn} are the position vectors of the upstream, second upstream and downstream nodes, respectively.

A van Leer flux limiter is used in Equation 3.66 such that:

$$\begin{aligned} \sigma(r) &= 0 \qquad \text{if} \quad r \leq 0 \\ \sigma(r) &= (2r)/(1+r) \quad \text{if} \quad r > 0 \end{aligned} \tag{3.68}$$

We further define:

$$\chi_{ij} = -\int_v \nabla N_i \cdot \theta_s S_w^{N+1} \mathbf{D} \cdot \nabla N_j \, dv \tag{3.69}$$

Other terms in Equation 3.62 are as defined for the discrete flow Equation 3.18.

3.10.2 Discrete Fractures

The discretized 2-D transport equation in fractures is:

$$\left[(S_{wf} R_f C_f)_i^{L+1} - (S_{wf} R_f C_f)_i^L \right] \frac{w_f a_i}{\Delta t} = w_f \sum_{j \in \eta_{f_i}} C_{f\,(ij+1/2)}^{L+1} \lambda_{f\,(ij+1/2)}^{L+1} \gamma_{f\,ij} (h_{f\,j}^{L+1} - h_{f\,i}^{L+1}) +$$

$$\sum_{j \in \eta_{f_i}} \chi_{fij} (C_{f\,j}^{L+1} - C_{f\,i}^{L+1}) + \left[(R_f \lambda C_{f\,i})_{par} - (S_{wf} R_f \, \lambda \, C_f)_i + \Omega_f^{L+1} \right] a_i \tag{3.70}$$

where:

$$\chi_{fij} = -\int_a \nabla N_i \cdot S_{wf}^{N+1} \mathbf{D_f} \cdot \nabla N_j \, da \tag{3.71}$$

and where the interface permeability can be either central or upstream weighted or given by a TVD flux limiter, as shown for the porous medium equation in Section 3.10.1. Other terms in Equation 3.70 are as defined for the discrete fracture flow Equation 3.23.

3.10.3 Double Porosity

The discrete equation for transport into the immobile region of a double-porosity domain is given by:

$$\left[(\theta_{\text{Imm}} C_{\text{Imm}})_i^{L+1} - (\theta_{\text{Imm}} C_{\text{Imm}})_i^{L}\right] \frac{v_i}{\Delta t} = \Omega_{\text{Imm}}^{L+1} v_i \tag{3.72}$$

3.10.4 Isotopic Fractionation

The discrete equation for isotopic fractionation into the immobile (solid) region is given by:

$$\left[(C_{\text{Imm}})_i^{L+1} - (C_{\text{Imm}})_i^{L}\right] \frac{v_i}{\Delta t} = \frac{\Omega_{\text{Imm}}^{L+1}}{x_r} v_i \tag{3.73}$$

3.10.5 Dual Continuum

For the dual continuum, the discretized 3-D transport obtained after using the control volume finite element method is:

$$\left[(\theta_{sd} S_{wd} R_d C_d)_i^{L+1} - (\theta_{sd} S_{wd} R_d C_d)_i^{L}\right] \frac{w_d v_i}{\Delta t} = \sum_{j \in \eta_{d_i}} (C_d)_{(ij+1/2)}^{L+1} (\lambda_d)_{(ij+1/2)}^{L+1} \gamma_{d_{ij}} (h_{d_j}^{L+1} - h_{d_i}^{L+1}) +$$

$$\sum_{j \in \eta_{d_i}} \chi_{d_{ij}} (C_{d_j}^{L+1} - C_{d_i}^{L+1}) + (Q_d C_{ups})_i^{L+1} + \left[(R_d \lambda_d C_{di})_{par} - (\theta_{sd} S_{wd} R_d \, \lambda_d \, C_d)_i + \Omega_d^{L+1}\right] v_i \tag{3.74}$$

All terms in Equation 3.74 are defined in a manner analogous to the discretized porous medium transport equation shown in Section 3.10.1.

3.10.6 Wells

One-dimensional transport along a well is described by the following discretized equation:

$$\left[(C_w)_i^{L+1} - (C_w)_i^{L}\right] \frac{\pi r_s^2 l_i}{\Delta t} = \sum_{j \in \eta_{w_i}} (C_w)_{(ij+1/2)}^{L+1} (\lambda_w)_{(ij+1/2)}^{L+1} \gamma_{w_{ij}} (h_{w_j}^{L+1} - h_{w_i}^{L+1}) +$$

$$\sum_{j \in \eta_{w_i}} \chi_{w_{ij}} (C_{w_j}^{L+1} - C_{w_i}^{L+1}) + (Q_w C_{ups})_i^{L+1} + \pi r_s^2 \left[(\lambda C_{wi})_{par} + \Omega_w^{L+1}\right] l_i \tag{3.75}$$

All terms in Equation 3.75 are defined in a manner analogous to the discretized porous medium transport equation shown in Section 3.10.1.

3.10.7 Tile Drains

One-dimensional transport in a tile drain is described by the following discretized equation:

$$\left[(C_t)_i^{L+1} - (C_t)_i^L\right] \frac{Al_i}{\Delta t} = \sum_{j \in \eta_{t_i}} (C_t)_{(ij+1/2)}^{L+1} (\lambda_t)_{(ij+1/2)}^{L+1} \gamma_{t_{ij}} (h_{t_j}^{L+1} - h_{t_i}^{L+1}) +$$

$$\sum_{j \in \eta_{t_i}} \chi_{t_{ij}} (C_{t_j}^{L+1} - C_{t_i}^{L+1}) + (Q_t C_{ups})_i^{L+1} + \left[A \left(\lambda C_{ti}\right)_{par} + A\Omega_t^{L+1}\right] l_i \tag{3.76}$$

All terms in Equation 3.76 are defined in a manner analogous to the discretized porous medium transport equation shown in Section 3.10.1.

3.10.8 Surface runoff

For the surface flow domain, the governing transport equation is discretized as:

$$\left[(\phi_o h_o R_o C_o)_i^{L+1} - (\phi_o h_o R_o C_o)_i^L\right] \frac{a_i}{\Delta t} = \sum_{j \in \eta_{o_i}} C_{o_{(ij+1/2)}}^{L+1} \cdot q_{o_{(ij+1/2)}}^{L+1}$$

$$+ \sum_{j \in \eta_{o_i}} \chi_{oij} (C_{oj}^{L+1} - C_{oi}^{L+1}) + \left[(\phi_o h_o R_o \lambda C_{oi})_{par} - (\phi_o h_o R_o \lambda C_o)_i + \Omega_o^{L+1}\right] a_i \tag{3.77}$$

where:

$$\chi_{oij} = -\int_a \nabla N_i \cdot (\phi_o h_o)^{N+1} D_o \cdot \nabla N_j da \tag{3.78}$$

and where the interface flux is obtained from the solution to the associated flow equation. The term $C_{o_{(ij+1/2)}}^{L+1}$ may be treated in a mid-point or upstream weighted manner, or by using the TVD flux limiter as discussed earlier in Section 3.10.1.

3.10.9 Channels

One-dimensional transport in a channel is described by the following discretized equation:

$$\left[(C_c)_i^{L+1} - (C_c)_i^L\right] \frac{Al_i}{\Delta t} = \sum_{j \in \eta_{c_i}} (C_c)_{(ij+1/2)}^{L+1} (\lambda_c)_{(ij+1/2)}^{L+1} \gamma_{c_{ij}} (h_{c_j}^{L+1} - h_{c_i}^{L+1}) +$$

$$\sum_{j \in \eta_{c_i}} \chi_{cij} (C_{c_j}^{L+1} - C_{c_i}^{L+1}) + (Q_c C_{ups})_i^{L+1} + \left[A \left(\lambda C_{ci}\right)_{par} + A\Omega_c^{L+1}\right] l_i \tag{3.79}$$

All terms in Equation 3.79 are defined in a manner analogous to the discretized porous medium transport equation shown in Section 3.10.1.

3.10.10 Thermal Energy

The numerical implementation of variably-saturated subsurface thermal energy transport is similar to that given by Graf (2005). The discrete form of equation 1 is given by:

$$\sum_{J=1}^{N_n} T_J^{L+1} \left\{ \sum_e \int_{V^e} \left(\frac{\rho_b c_b}{\Delta t} w_I w_J + (q_i \rho_w c_w) w_I \frac{\partial w_J}{\partial x_i} + (k_b + \rho_b c_b D_{ij}) \frac{\partial w_I}{\partial x_i} \frac{\partial w_J}{\partial x_j} \right) dV^e \right\}$$

$$= \sum_{J=1}^{N_n} T_J^L \left\{ \sum_e \int_{V^e} \frac{\rho_b c_b}{\Delta t} w_I w_J dV^e \right\} + \sum_{J=1}^{N_n} \left\{ \sum_e \oint_{\Gamma_e} \left((k_b + \rho_b c_b D_{ij}) w_I \frac{\partial T}{\partial n} \right) d\Gamma_e \right.$$

$$\left. + \sum_e \int_{V^e} (\pm Q_T) w_I dV^e + \sum_e \int_{\Gamma_b} \Omega_o w_I d\Gamma_b \right\} \quad i,j = 1,2,3 \tag{3.80}$$

where N_n represents the total number of subsurface nodes, L represents the time level at which a solution is known and $L+1$ represents the time level for which a solution is desired, $\sum_e$ represents the sum over all porous media elements connected to node J, V_e represents the elemental volume, w_I and w_J represent the linear basis functions following the Galerkin approach, Γ_e represents the elemental boundary with n as the unit vector normal to the boundary, and Γ_b represents the elemental boundary between the surface and subsurface domains.

The numerical implementation of the surface thermal energy transport equation is similar to that for the subsurface; however, the surface equation is depth-averaged and is thus evaluated over the elemental area (A_e), not volume. In addition, the surface thermal energy transport equation includes E_{atm} representing the atmospheric inputs to the surface thermal energy system. The discrete equation for the surface regime is given by:

$$\sum_{J=1}^{N_{on}} T_{oJ}^{L+1} \left\{ \sum_{e^o} \int_{A^e} \left(\frac{\rho_w c_w d_o}{\Delta t} w_I w_J + (q_{oi} \rho_w c_w) w_I \frac{\partial w_J}{\partial x_i} + (k_w + \rho_w c_w D_{oij}) d_o \frac{\partial w_I}{\partial x_i} \frac{\partial w_J}{\partial x_j} \right) dA^e \right\}$$

$$= \sum_{J=1}^{N_{on}} T_{oJ}^L \left\{ \sum_{e^o} \int_{A^e} \left(\frac{\rho_w c_w d_o}{\Delta t} w_I w_J \right) dA^e \right\} + \sum_{J=1}^{N_{on}} \left\{ \sum_{e^o} \oint_{\Gamma_e} \left((k_w + \rho_w c_w D_{oij}) d_o w_I \frac{\partial T}{\partial n} \right) d\Gamma_e \right.$$

$$\left. + \sum_{e^o} \int_{A^e} (E_{atm} \pm Q_T) w_I dA^e + \sum_{e^o} \int_{\Gamma_b} \Omega_o d_o w_I d\Gamma_b \right\} \quad i,j = 1,2 \tag{3.81}$$

where N_{on} represents the number of overland flow nodes, and e^o represents overland elements.

3.11 Travel Time Probability

Since the time-Dirac delta function $\delta(t)$ cannot properly be handled in the time domain, the PDF's are evaluated by solving initial value problems (cf Eqs. (2.175) and (2.176)). The following summarizes the main operations implemented in **FRAC3DVS**:

1. The age/life expectancy/travel time are taken as specific non-reactive species.

2. The input mass is controlled by nodal influence volumes (times mobile water content), according to Eq. (2.175b) or (2.176b). The injection point $\boldsymbol{x}_i$ corresponds to any point in the system for a travel time evaluation from $\boldsymbol{x}_i$ to $\boldsymbol{x}$, to any point on the recharge area Γ_- for the age problem, or to any point on the discharge area Γ_+ for the life expectancy problem.

3. The travel time probability can be calculated:

   - For each element: $\mathbf{q}(\boldsymbol{x}, t)$ and $g(\boldsymbol{x}, t)$ are evaluated at the element centroid, using element shape functions. The control plane section area $A(\boldsymbol{x})$ is evaluated by intersecting the plane normal to velocity with the corresponding element (see Fig. 3.3).
   - At each node: The **S**uper-**C**onvergent **P**atch **R**ecovery method (SCPR, see (Zienkiewicz and Zhu, 1992; Wiberg and Abdulwahab, 1997)) is used to evaluate the nodal velocity (see Fig. 3.4). The fundamental basis of the SCPR method is that there are specific locations in an element where the derivatives are more accurate for a given polynomial degree. These particular locations are referred to as element Super-Convergent points. The SCPR method can briefly be summarized by the following:
     - For a given node, a patch is made of neighboring elements (1D, 2D, 3D);
     - Velocity is evaluated at some sample points within the patch. These sample points correspond to a set of Gauss points;
     - A least-square fit is performed through these samples, and the local problem is solved with a Singular Value Decomposition Factorization solution method.

4. Travel time statistics are post-processed for each element (or node).

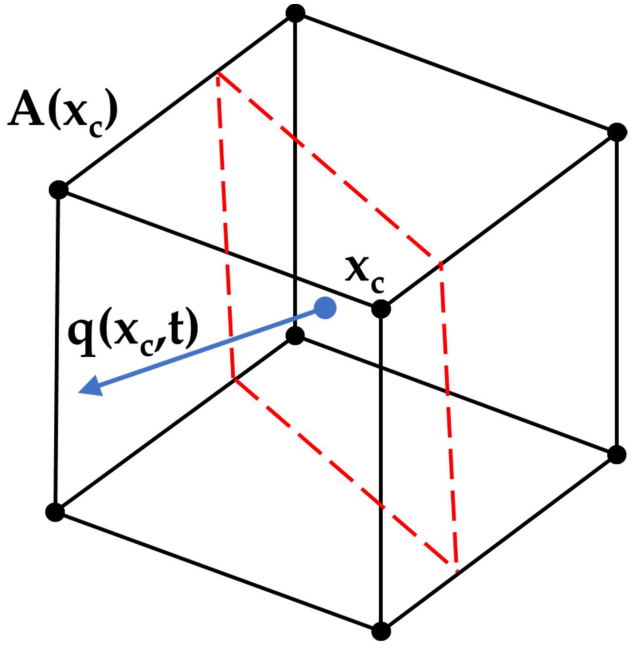

Figure 3.3: Procedure for the evaluation of the travel time PDF at the element centroid, for the case of a brick element.

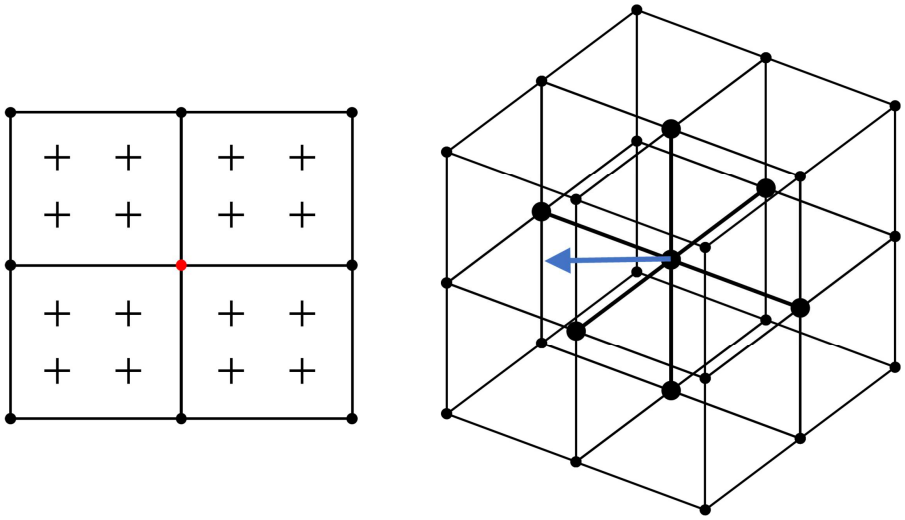

Figure 3.4: Schematic illustration of SCPR method. Left: Four quadrangles defining a patch of elements used to evaluate the velocity at a node (red circle), with indicated sample points (+); Right: Example of a patch made of 8 brick elements.

3.12 Solute Transport Coupling

Coupling of the various domains for solute transport is done in a manner similar to the coupling used for fluid flow. When the common node approach is used, the discretized equations for the coupled domains are added, and continuity of concentration is assumed at the nodes shared by the coupled domains. The exchange term Ω_{ex} does not need to be explicitly evaluated but can be back-calculated after solution.

For the dual node approach, currently available for coupling between the porous medium and dual continuum domains, the exchange term is explicitly evaluated and there is no assumption of equilibrium or continuity between the concentrations of the two domains. For the dual continuum approach, the coupling term is evaluated according to:

$$\Omega_d^{L+1} v_i = \left[-(u_m C)_i^{L+1} - (u_d C_d)_i^{L+1} \right] v_i \tag{3.82}$$

When the dual-node approach is used to couple the surface and subsurface domains, the coupling term may be expressed as:

$$\Omega_o^{L+1} = C_{ups}^{L+1} \Gamma_o \tag{3.83}$$

where $C_{ups}^{L+1} = C_o^{L+1}$ when the flux is from the surface to the subsurface system and $C_{ups}^{L+1} = C^{L+1}$ when the flux is from the subsurface to the surface system.

3.13 Solute Transport Boundary Conditions

3.13.1 Subsurface Transport

Boundary conditions for transport include the following: first-type (Dirichlet) boundaries, second type (mass flux), third type (total flux) and each can be input as time-dependent quantities.

Some input fluxes and boundary conditions for thermal energy transport were previously incorporated into **HydroGeoSphere** by Graf (2005), such as the prescribed temperature boundaries. Other thermal energy inputs were developed during this research; specifically the temperature flux input and atmospheric inputs.

The temperature input flux is incorporated into **HydroGeoSphere** to account for the thermal energy associated with incoming fluid flux. The temperature input flux can be used in both the surface and subsurface domains. The general equation is given as:

$$Q_{heat_i} = Q(\rho_{in} c_{in} T_{in} - \rho_i c_i T_i) \tag{3.84}$$

where Q_{heat_i} is the temperature flux into node i, Q is the volumetric flux of the carrier fluid, ρ is the density, c is the heat capacity, T is the temperature, in denotes the input term, and i denotes a nodal term. The density and heat capacity terms vary depending on the material

associated with the node or input flux (bulk or water). A temperature flux associated with surface water entering the surface domain (for example, a stream inlet) would use ρ and c terms for water for both the input condition (incoming surface water), and the surface node receiving the incoming fluid. However, the injection of heated water into the subsurface would use ρ and c terms for water for the injected fluid, but would use bulk values for the subsurface node.

The atmospheric temperature inputs implemented into **HydroGeoSphere** include prescribed values (i.e. incoming shortwave radiation, air temperature, cloud cover, etc.) or values determined by a sinusoidal input function. The addition of atmospheric inputs which can vary sinusoidally with time allows for the representation of diurnal fluxes for air temperature, shortwave radiation and wind speed.

3.14 Numerical Techniques

3.14.1 Matrix Solution

Discretized flow equations, such as Equations (3.18), (3.23), (3.28), (3.32), (3.46), or any combination of these equations, forms a matrix system of the form:

$$Ax = b \tag{3.85}$$

where x is the unknown, A is a matrix of coefficients and b is a force vector. When flow is fully-saturated, the discretized equations are linear and the matrix of coefficient A is also linear. A direct solution of the matrix equation is then possible. The resulting system of equations can be very large for a fully three-dimensional field-scale problem. A fast and efficient matrix solver is therefore critical in order to reduce core memory requirements and CPU time. The preconditioned Krylov subspace iterative solver has been shown to be very efficient and robust for solving large systems of equations (Behie and Forsyth, 1984) and it has therefore been implemented to solve the system of equations. The preconditioning chosen consists of performing an ILU decomposition of the assembled coefficient matrix without altering its original sparsity pattern (Behie and Forsyth, 1984). The solver has the capability, however, to perform a higher-order ILU decomposition of the coefficient matrix, where additional steps of a Gaussian elimination are performed, resulting in the addition of extra bands to the original matrix. Performing a higher-order decomposition results in a better-conditioned decomposed matrix, which can improve the convergence rate of the solver, but at the expense of increased storage requirements and additional computation time.

An option to use either a finite difference or finite element discretization, as described earlier, has also been implemented for the transport solution. Experience has indicated that for discretely-fractured porous media in which the matrix has low permeability such that mechanical dispersion in the matrix is weak relative to molecular diffusion, the finite element and finite difference representations give essentially identical results. This suggests that the cross-derivative terms in the transport equation are small compared to the terms that are retained in the finite difference approach.

As in the case of the flow problem, a mass balance is performed to assess the accuracy of the solution. A procedure similar to that described by Huyakorn and Pinder (1983) is used. The transport matrix equations are solved using the same ILU-preconditioned ORTHOMIN solver (Behie and Forsyth, 1984) as is used for the flow problem.

3.14.2 Newton-Raphson Method

The Newton-Raphson technique is used to linearize the non-linear equations arising from discretization of variably-saturated subsurface or surface flow equations. The method is described in Huyakorn and Pinder (1983) and is reproduced here to demonstrate the advantage of using the control volume finite element approach over a conventional Galerkin method. To illustrate the method, we apply it to Equation 3.16, which is rewritten in the following way:

$$f_i^r = \left\{[\theta_s S_w]_i^{L+1} - [\theta_s S_w]_i^L\right\} \frac{v_i}{\Delta t} - \sum_{j \in \eta_i} (\lambda)_{(ij+1/2)}^{L+1} \gamma_{ij} (h_j^{L+1} - h_i^{L+1}) - Q_i^{L+1} \tag{3.86}$$

where r represents the iteration level. Application of the Newton method to Equation 3.86 produces the following matrix equation:

$$F_{ij}^r \Delta\psi_j^{r+1} = -f_i^r \tag{3.87}$$

which can be solved with the same preconditioned iterative solver used for linear matrix equations, since the Jacobian matrix F_{ij} is linear.

In Equation 3.87, the Jacobian matrix, F_{ij}^r, is defined as:

$$F_{ij}^r = \frac{\partial f_i^r}{\partial \psi_j^r} \tag{3.88}$$

and vector f_i^r represents the residual of the discretized equation. The iteration process is carried out repeatedly until the change in the pressure head, $\Delta\psi_j^{r+1}$, or the residual of the equation, f_i^r, becomes less than a specified tolerance at all the nodes. It is important that the evolution of the residual, f_i^r, be monitored during iteration to ensure proper convergence.

Full Newton iteration can be computationally expensive mainly because of the need to evaluate the Jacobian matrix. It is therefore highly desirable to implement a scheme capable of evaluating it in an efficient manner. One option is to evaluate the Jacobian numerically (Forsyth and Simpson, 1991; Forsyth and Kropinski, 1997). Term by term evaluation of the Jacobian can be represented by (Forsyth and Kropinski, 1997):

$$\frac{\partial f_i^r}{\partial \psi_i^r} \approx \frac{f_i^r(\psi_i^r + \epsilon) - f_i^r(\psi_i^r)}{\epsilon} \tag{3.89}$$

where ϵ represents a small numerical shift in the pressure head value.

Obviously, from Equation 3.89, numerical differentiation requires more than one function evaluation for each term; however, it can be shown that not all terms in the Jacobian will

require two function evaluations. The form of the discretized Equation 3.86 also makes it intuitively easy to evaluate the Jacobian numerically. This is because the fluid flow terms appearing in the summation in Equation 3.86 depend only on nodes i and j. Forsyth and Simpson (1991) and Forsyth and Kropinski (1997) give a detailed procedure for the Jacobian evaluation and it is reproduced below for completeness.

The diagonal term of the Jacobian for node i can be determined from Equations 3.86 and 3.88 as:

$$\frac{\partial f_i^r}{\partial \psi_i^r} = \frac{\partial}{\partial \psi_i^r}\left\{[\theta_s S_w]_i^r - [\theta_s S_w]_i^L\right\}\frac{v_i}{\Delta t} - \sum_{J\in\eta_i}\frac{\partial}{\partial \psi_i^r}(\lambda)^r_{(ij+1/2)}\gamma_{ij}(h_j^r - h_i^r) - \frac{\partial Q_i^r}{\partial \psi_i^r} \tag{3.90}$$

The entries in column i of the Jacobian will be, excluding the diagonal:

$$F_{ji} = \frac{\partial f_j^r}{\partial \psi_i^r} \tag{3.91}$$

where $j \in \eta_i$. As stated previously, the only term in f_j^r depending on ψ_i^r will be the one representing flow from node i to node j. Therefore:

$$\frac{\partial f_j^r}{\partial \psi_i^r} = -\frac{\partial}{\partial \psi_i^r}(\lambda)^r_{(ji+1/2)}\gamma_{ji}(h_i^r - h_j^r) \tag{3.92}$$

Because of local conservation of mass, the fluid flow term between i and j appearing in the equation for node i will be similar to the one appearing in equation for node j. Therefore we have:

$$\begin{aligned}\lambda_{ij} &= \lambda_{ji}\\ \gamma_{ij} &= \gamma_{ji}\end{aligned} \tag{3.93}$$

Using Equation 3.93, 3.92 becomes:

$$\frac{\partial f_j^r}{\partial \psi_i^r} = \frac{\partial}{\partial \psi_i^r}(\lambda)^r_{(ij+1/2)}\gamma_{ij}(h_j^r - h_i^r) \tag{3.94}$$

The right hand side of Equation 3.94 is also found in the summation appearing in Equation 3.90. The expression for the diagonal term (Equation 3.90) can therefore be expressed as:

$$\frac{\partial f_i^r}{\partial \psi_i^r} = \frac{\partial}{\partial \psi_i^r}\left\{[\theta_s S_w]_i^r - [\theta_s S_w]_i^L\right\}\frac{v_i}{\Delta t} - \sum_{j\in\eta_i}\frac{\partial f_j^r}{\partial \psi_i^r} - \frac{\partial Q_i^r}{\partial \psi_i^r} \tag{3.95}$$

which shows that the evaluation of the diagonal term for node i incorporates all the terms appearing in column i of the Jacobian. The Jacobian can therefore be constructed by only evaluating the diagonal terms and subsequently filling in the off-diagonal terms in a column-wise fashion.

Forsyth and Simpson (1991) and Forsyth and Kropinski (1997) show that for n unknowns and with the summation in Equation 3.86 extending from unity to η_i, the building of the Jacobian requires $n(2+2\eta_i)$ function evaluations. The Picard iteration scheme, on the other hand, requires at least $n(1+\eta_i)$ function evaluations to compute the residual, which is seen to be only a factor of two less than the more robust Newton method. Numerical differentiation is also attractive because it allows easy use of tabular data to represent arbitrary constitutive relations should analytical expressions be unavailable.

3.14.3 Primary Variable Substitution

Forsyth et al. (1995) discuss the use of a saturation based form of Equation 2.1 which has good convergence properties in terms of nonlinear iterations when compared with a pressure based method. Because this method cannot be used in the saturated zone they define a new variable which is essentially the saturation in the unsaturated zone and the pressure head in the saturated zone.

They use full Newton iteration to solve the discrete equation everywhere and, in the case of a constant air phase pressure approximation, which applies here, they simply use a different primary variable in different regions. Note that primary variables are regarded as independent when constructing the Jacobian.

The primary variable at a given node may be switched after every Newton iteration using the following method:

$$\begin{array}{lll} \text{IF} & & \\ & S_i > tol_f & \text{Use } \psi_i \text{ as primary variable at node } i \\ \text{ELSE IF} & & \\ & S_i < tol_b & \text{Use } S_i \text{ as primary variable at node } i \\ \text{ELSE} & & \\ & & \text{Do not change primary variable at node } i \\ \text{ENDIF} & & \end{array} \tag{3.96}$$

with the requirements that:

$$tol_f < 1 \tag{3.97}$$

and:

$$tol_f \neq tol_b \tag{3.98}$$

3.14.4 Time Stepping

A variable time-stepping procedure similar to the one outlined by Forsyth and Sammon (1986) and Forsyth and Kropinski (1997) has been incorporated in the solution procedure. The time step is defined according to the rate of change of the solution unknown. For flow, the rate of change of hydraulic head, pressure head or saturation can be chosen. For transport, the rate of change of concentration or temperature is used for variable time-stepping.

Let's assume that X represent one of the unknowns mentioned above. After obtaining the solution at time level L, the next time-step is selected according to:

$$\Delta t^{L+1} = \frac{X_{max}}{\max \mid X_i^{L+1} - X_i^L \mid} \Delta t^L \tag{3.99}$$

where X_{max} is a desired maximum change in the unknown during a single time-step, defined by the user.

This implementation of variable time-stepping allows the use of increasingly larger time steps if the dependent variable does not experience drastic changes. It is also recognized that the number of Newton iterations taken to achieve convergence is a good indicator of the suitability of the current time-step size. If the number of iterations exceeds a specified maximum, IT_{max}, at time level $L+1$ in which the time step is currently Δt, the solution is restarted at time level L and the time-step is reduced, typically by a factor of two. Overall, the procedure can lead to a very significant reduction in computational effort, especially when the solution is desired only at a few widely-spaced target times (see Therrien and Sudicky (1996)).

3.14.5 Mass Balance

Mass balance calculation are done by **HydroGeoSphere** after solving for fluid flow and solute transport. The mass balance calculation gives information to the user on fluid flow and solute exchange through external boundaries. It also provides information on the accuracy of the numerical solution since the discretized flow and transport equations (for example, Equations 3.18 and 3.62 for the porous medium) are in a mass conservative form and are actually expressions for mass balance for the volume associated to a node in the grid. These equations are assembled into a global matrix whose solution is obtained by using iterative methods. Therefore, if the iterative process for solving the matrix converges within a prescribed tolerance, mass balance for each equation should be ensured to the level of precision of the convergence tolerance.

Mass balance for fluid flow and solute transport is performed by first computing the total mass change in the domain for a given time step (for steady-state simulations, there is no global mass change in the domain). The mass entering or leaving the domain through the boundaries or through internal sources and sinks is then computed and is compared to the total mass change, providing the mass balance check for the simulation. The procedure used to compute the mass entering or leaving the domain is similar to that described in Huyakorn and Pinder (1983) and involves reassembling the discretized equation for the first-type nodes.

3.14.6 Solution Procedures

The solution methodology for 2-D areal surface flow is embedded into the time looping of the solution methodology for the subsurface calculations of **HydroGeoSphere** (i.e., at each iteration, assembly of the matrix of flow equations for the subsurface is followed by assembly of its surface flow equations). The entire implicit system of matrix equations is then solved at each nonlinear iteration until convergence before proceeding to the next time step. Adaptive time-stepping, Newton-Raphson linearization, and under-relaxation formulas used for the solution are discussed in Chapter 3 among the sections that document solution to the subsurface equations.

References

Allen, R. G., Pereira, L. S., Raes, D., and Smith, M. (1998). Crop evapotranspiration: guidelines for computing crop water requirements. *FAO Irrigation and Drainage Paper*, 56.

Arnold, L. (1974). *Stochastic Differential Equations: Theory and Applications*. Wiley, New York, NY.

Bear, J. (1972). *Dynamics of Fluids in Porous Media*. Dover, New York, NY.

Behie, G. A. and Forsyth, P. A. (1984). Incomplete factorization methods for fully implicit simulation of enhanced oil recovery. *SIAM J. Sci. Comput.*, 5(3):543–561.

Berkowitz, B. J., Bear, J., and Braester, C. (1988). Continuum models for contaminant transport in fractured porous formations. *Water Resour. Res.*, 24(8):1225–1236.

Beven, K. J. (1985). Distributed models. In Anderson, M. G. and Burt, T. P., editors, *Hydrological Forecasting*, pages 425–435. Wiley, New York, NY.

Bradford, S. A., Torkzaban, S., Leij, F., Simunek, J., and van Genuchten, M. T. (2009). Modeling the coupled effects of pore space geometry and velocity on colloid transport and retention. *Water Resour. Res*, 45:W02414.

Brookfield, A. E., Sudicky, E. A., Park, Y.-J., and Conant, Jr., B. (2009). Thermal transport modelling in a fully integrated surface/subsurface framework. *Hydrol. Process.*, 23:2150–2164.

Brooks, R. J. and Corey, A. T. (1964). Hydraulic properties of porous media. Technical Report Hydrology Papers 3, Colorado State University, Fort Collins, CO.

Celia, M. A., Bouloutas, E. T., and Zarba, R. L. (1990). A general mass-conservative numerical solution for the unsaturated flow equation. *Water Resour. Res.*, 26(7):1483–1496.

Chaudhary, D. R. and Bhandari, R. C. (1968). Heat transfer through a three-phase porous medium. *J. Phys. D: Appl. Phys.*, 1(6):815–817.

Cooley, R. L. (1971). A finite difference method for unsteady flow in variably saturated porous media: Application to a single pumping well. *Water Resour. Res.*, 7(6):1607–1625.

Cooley, R. L. (1983). Some new procedures for numerical simulation of variably-saturated flow problems. *Water Resour. Res.*, 19(5):1271–1285.

Cornaton, F. (2003). *Deterministic models of groundwater age, life expectancy and transit time distributions in advective-dispersive systems*. PhD thesis, University of Neuchâtel, Neuchâtel, Switzerland.

Côté, J. and Konrad, J. M. (2005). A generalized thermal conductivity model for soils and construction materials. *Can. Geotech. J.*, 42:443–458.

Danckwerts, P. (1953). Continuous flow systems: Distribution of residence times. *Chem. Eng. Sci.*, 2(1):1–13.

Fassnacht, S. R., Snelgrove, K. R., and Soulis, E. D. (2001). Daytime long-wave radiation approximation for physical hydrological modelling of snowmelt: A case study of southwestern ontario. In *Soil-vegetation-atmosphere transfer Schemes and large-scale hydrological models. IAHS Publication No. 270*, pages 279–286.

Feddes, R. A., Kowalik, P. J., and Zaradny, H. (1978). *Simulation of field water use and crop yield*. Wiley, New York, NY.

Forsyth, P. A. (1988). Comparison of the single-phase and two-phase numerical formulation for saturated-unsaturated groundwater flow. *Comput. Methods Appl. Mech. Engrg.*, 69:243–259.

Forsyth, P. A. (1991). A control volume finite element approach to NAPL groundwater contamination. *SIAM J. Sci. Stat. Comput.*, 12(5):1029–1057.

Forsyth, P. A. and Kropinski, M. C. (1997). Monotonicity considerations for saturated-unsaturated subsurface flow. *SIAM J. Sci. Comput.*, 18:1328–1354.

Forsyth, P. A. and Sammon, P. H. (1986). Practical considerations for adaptive implicit methods in reservoir simulation. *J. Comput. Phys.*, 62:265–281.

Forsyth, P. A. and Simpson, R. B. (1991). A two phase, two component model for natural convection in a porous medium. *Int. J. Num. Meth. Fluids*, 12:655–682.

Forsyth, P. A., Wu, Y. S., and Pruess, K. (1995). Robust numerical methods for saturated-unsaturated flow with dry initial conditions in heterogeneous media. *Adv. Water Res.*, 18(1):25–38.

Freeze, R. A. and Cherry, J. A. (1979). *Groundwater*. Prentice-Hall, Inc., Englewood Cliffs, NJ.

Frind, E. O. (1982). Simulation of long-term transient density-dependent transport in groundwater. *Adv. Water Res.*, 5(2):73–88.

Garabedian, P. R. (1964). *Partial Differential Equations*. Wiley, New York, NY.

Gardiner, C. W. (1983). *Handbook of Stochastic Methods for Physics, Chemistry and Natural Sciences*. Springer-Verlag, Berlin, Germany.

Gerke, H. H. and van Genuchten, M. T. (1993). A dual-porosity model for simulating the preferential movement of water and solutes in structured porous media. *Water Resour. Res.*, 29(2):305–319.

Gottardi, G. and Venutelli, M. (1993). A control-volume finite-element model for two-dimensional overland flow. *Adv. Water Res.*, 16:277–284.

Graf, T. (2005). *Modeling coupled thermohaline flow and reactive solute transport in discretely-fractured porous media.* PhD thesis, University of Laval, Ste-Foy, PQ, Canada.

Guvanasen, V. and Chan, T. (2000). A three-dimensional numerical model for thermohydromechanical deformation with hysteresis in a fractured rock mass. *International Journal of Rock Mechanics and Mining Sciences*, 37(1–2):89–106.

Huyakorn, P. S. and Pinder, G. F. (1983). *Computational Methods in Subsurface Flow.* Academic Press, New York, NY.

Huyakorn, P. S., Springer, E. P., Guvanasen, V., and Wadsworth, T. D. (1986). A three-dimensional finite-element model for simulating water flow in variably saturated porous media. *Water Resour. Res.*, 22(13):1790–1808.

Huyakorn, P. S., Thomas, S. D., and Thompson, B. M. (1984). Testing and Validation of Models for Simulating Solute Transport in Groundwater: Development, Evaluation and Comparison of Benchmark Techniques. *Water Resour. Res.*, 20(8):1099–1115.

Idso, S. B., Jackson, R. D., Reginato, R. J., Kimball, B. A., and Nakayama, F. S. (1975). The dependence of bare soil albedo on soil water content. *J. Appl. Meteorol.*, 14:109–113.

Jury, W. A. and Roth, K. (1990). *Transfer Functions and Solute Movement Through Soil: Theory and Applications.* Birkhauser, Boston, Cambridge, MA.

Kolmogorov, A. N. (1931). Über die analytischen Methoden in der Wahrscheilichkeitsrechnung. *Math Ann.*, 104:415–458.

Kristensen, K. J. and Jensen, S. E. (1975). A model for estimating actual evapotranspiration from potential evapotranspiration. *Nordic Hydrol.*, 6(3):170–188.

Lacombe, S., Sudicky, E. A., Frape, S. K., and Unger, A. J. A. (1995). Influence of leaky boreholes on cross-formational groundwater flow and contaminant transport. *Water Resour. Res.*, 31(8):1871–1882.

Li, Q., Unger, A. J. A., Sudicky, E. A., Kassenaar, D., Wexler, E. J., and Shikaze, S. (2008). Simulating the multi-seasonal response of a large-scale watershed with a 3D phyiscally-based hydrologic model. *J. Hydrol.*, 357(3–4):317–336.

Markle, J. M., Schincariol, R. A., Sass, J. H., and Molson, J. W. (2006). Characterizing the two-dimensional thermal conductivity distribution in a sand and gravel aquifer. *Soil Sci. Soc. Am. J.*, 70(4):1281–1294.

Millington, R. J. and Quirk, J. P. (1961). Permeability of porous solids. *Trans. Faraday Society*, 15:1200–1207.

Milly, P. C. D. (1985). A mass-conservative procedure for time-stepping in models of unsaturated flow. *Adv. Water Resour.*, 8:32–36.

Mohammed, A., Cey, E., Hayashi, M., Callaghan, M., Park, Y.-J., Miller, K. L., and Frey, S. (2020). Dual-permeability modeling of preferential flow and snowmelt partitioning in frozen soils. *Vadose Zone J.*, 20(2):1–16.

Monteith, J. L. (1981). Evaporation and surface temperature. *Q. J. R. Meteorol. Soc.*, 107:1–27.

Mualem, Y. (1976). A new model to predict the hydraulic conductivity of unsaturated porous media. *Water Resour. Res.*, 12:513–522.

Neuman, S. P. (1973). Saturated-unsaturated seepage by finite elements. *Journal of the Hydraulics Division*, 99(HY12):2233–2251.

Neupauer, R. and Wilson, J. L. (1999). Adjoint method for obtaining backward-in-time location and travel time probabilities of a conservative groundwater contaminant. *Water Resour. Res.*, 35(11):3389–3398.

Neupauer, R. and Wilson, J. L. (2001). Adjoint-derived location and travel time probabilities for a multidimensional groundwater system. *Water Resour. Res.*, 37(6):1657–1668.

Neupauer, R. and Wilson, J. L. (2002). Backward probabilistic model of groundwater contamination in nonuniform and transient flow. *Adv. Water Res.*, 25:733–746.

Neuzil, C. E. (2003). Hydromechanical coupling in geological processes. *Hydrogeology Journal*, 11:41–83.

Panday, S. and Huyakorn, P. S. (2004). A fully coupled physically-based spatially-distributed model for evaluating surface/subsurface flow. *Adv. Water Resour.*, 27:361–382.

Panday, S., Huyakorn, P. S., Therrien, R., and Nichols, R. L. (1993). Improved three-dimensional finite element techniques for field simulation of variably saturated flow and transport. *J. Contam. Hydrol.*, 12:3–33.

Pruess, K. and Tsang, Y. W. (1990). On two-phase relative permeability and capillary pressure of rough-walled rock fractures. *Water Resour. Res.*, 26(9):1915–1926.

Rasmussen, T. C. and Evans, D. D. (1989). Fluid flow and solute transport modeling through three-dimensional networks of variably saturated discrete fractures. Technical Report NUREG/CR-5239, U. S. Nuclear Regulatory Commission.

Refsgaard, J. C. (1997). Parameterisation, calibration, and validation of distributed hydrological models. *J. Hydrol.*, 198(1–4):69–97.

Reitsma, S. and Kueper, B. H. (1994). Laboratory measurement of capillary pressure-saturation relationships in a rock fracture. *Water Resour. Res.*, 30(4):865–878.

Rempel, A. W. (2008). A theory for ice till interactions and sediment entrainment beneath glaciers. *J. Geophys. Res.*, 113(F01013):1–20.

Rubin, Y. (2003). *Applied Stochastic Hydrogeology.* Oxford University Press, New York, NY.

Sammon, P. H. (1988). An analysis of upstream differencing. *Soc. Pet. Engrg. Reserv. Engrg.*, 3:1053–1056.

Sass, J. H., Lachenbruch, A. H., and Munroe, R. J. (1971). Thermal conductivity of rocks from measurements on fragments and its application to heat-flow determination. *J. Geophys. Res.*, 76:3391–3401.

Senarath, S. U. S., Ogdon, F. L., Downer, C. W., and Sharif, H. O. (2000). On the calibration and verification of two-dimensional, distributed, Hortonian, continuous watershed models. *Water Resour. Res.*, 36(6):1495–1510.

Sudicky, E. A. (1990). The Laplace transform Galerkin technique for efficient time-continuous solution of solute transport in double-porosity media. *Geoderma*, 46:209–232.

Sudicky, E. A. and McLaren, R. G. (1992). The Laplace transform Galerkin technique for large-scale simulation of mass transport in discretely-fractured porous formations. *Water Resour. Res.*, 28(2):499–514.

Sudicky, E. A., Unger, A. J. A., and Lacombe, S. (1995). A noniterative technique for the direct implementation of well bore boundary conditions in three-dimensional heterogeneous formations. *Water Resour. Res.*, 31(2):411–415.

Tang, D. H., Frind, E. O., and Sudicky, E. A. (1981). Contaminant transport in fractured porous media: Analytical solution for a single fracture. *Water Resour. Res.*, 17(3):555–564.

Therrien, R. and Sudicky, E. A. (1996). Three-dimensional analysis of variably-saturated flow and solute transport in discretely-fractured porous media. *J. Contam. Hydrol.*, 23(1–2):1–44.

Therrien, R. and Sudicky, E. A. (2000). Well bore boundary conditions for variably-saturated flow modeling. *Adv. Water Resour.*, 24:195–201.

Uffink, G. J. M. (1989). Application of the Kolmogorov's backward equation in random walk simulation of groundwater contaminant transport. In Kobus, H. E. and Kinzelbach, W., editors, *Contaminant Transport in Groundwater*, pages 283–289, Rotterdam, Netherlands.

Unger, A. J. A., Forsyth, P. A., and Sudicky, E. A. (1996). Variable spatial and temporal weighting schemes for use in multi-phase compositional problems. *Adv. Water Resour.*, 19(1):1–27.

van Genuchten, M. T. (1980). A closed-form equation equation for predicting the hydraulic conductivity of unsaturated soils. *Soil Sci. Soc. Am. J.*, 44:892–898.

van Leer, B. (1974). Towards the ultimate conservative difference scheme. II. Monotonicity and conservation combined in a second order scheme. *J. Comp. Phys.*, 14:361–370.

Verseghy, D. L. (1991). CLASS—A Canadian land surface scheme for GCMs. I. Soil model. *Int. J. Climatol.*, 11:111–133.

Verseghy, D. L., McFarlane, N. A., and Lazare, M. (1993). CLASS—A Canadian land surface scheme for GCMs. II. Vegetation model and coupled runs. *Int. J. Climatol.*, 13:347–370.

Viessman Jr., W. and Lewis, G. L. (1996). *Introduction to Hydrology*. HarperCollins College, New York, NY, fourth edition.

Voss, C. (1984). A finite-element simulation model for saturated-unsaturated, fluid-density-dependent ground-water flow with energy transport or chemically-reactive single-species solute transport. Technical Report Water-Resources Investigations Report 84-4369, U. S. Geological Survey.

Wang, J. S. Y. and Narasimhan, T. N. (1985). Hydrologic mechanisms governing fluid flow in a partially saturated, fractured, porous medium. *Water Resour. Res.*, 21(12):1861–1874.

Wiberg, N. E. and Abdulwahab, F. (1997). Superconvergent path recovery in problems of mixed form. *Commun. Numer. Methods Eng.*, 13(2):207–217.

Wilson, J. L. and Liu, J. (1997). Field Validation of the Backward-in-Time Advection Dispersion Theory. In *Proceedings of the 1996 HSRC/WERC Joint Conference on the Environment*, Manhattan, KS. Great Plains/Rocky Mountain Hazardous Substance Research Center.

Woolhiser, D. A. (1996). Search for physically based runoff model—A hydrologic El Dorado? *J. Hydrol. Eng.*, 122(3):122–129.

Woolhiser, D. A., Smith, R. E., and Giraldez, J. V. (1997). Effects of spatial variability of saturated hydraulic conductivity on Hortonian overland flow. *Water Resour. Res.*, 32(3):671–678.

Zienkiewicz, O. C. and Zhu, J. Z. (1992). The superconvergent patch recovery and a posteriori error estimates. Part 1: The recovery technique. *Int. J. Numer. Methods Eng.*, 33(7):1331–1364.

Mathematical Notation

a	Subsurface-macropore coupling, distance from block centre to fracture [L].
A	Tile drain, cross-sectional area in the wetted portion [L^2].
A_f	Cross sectional flow area [L^2].
B	Boundary of finite-element volume v [L].
B_f	Uniform spacing for a set of parallel fractures [L].
B_T	Top width of 1-D channel flow [L].
C	Subsurface, solute concentration [M L^{-3}].
	Variants:
	C_d Dual continuum.
	C_{Imm} Double-porosity immobile region.
	C_f Fracture.
	C_o Surface (overland) flow.
	C_t Tile drain.
	$C_{t_{\text{Inj}}}$ Tile drain, injected water.
	C_w Well.
	$C_{w_{\text{Inj}}}$ Well, injected water.
	C_c Channel.
	$C_{c_{\text{Inj}}}$ Channel, injected water.
C_d	Weir discharge coefficient [-].
C_{dwn}	Concentration of downstream node between nodes i and j [M L^{-3}].
	Variants:
	C_{ups} Upstream node.
	C_{i2ups} Second upstream node.
C_L	A constant which depends on rainfall intensity r [-].
$\mathbf{D}$	Subsurface, hydrodynamic dispersion tensor [L^2 T^{-1}].
	Variants:
	$\mathbf{D_d}$ Dual continuum.
	$\mathbf{D_f}$ Fracture.
	$\mathbf{D_o}$ Surface (overland) flow.
D_{free}	Solute, free-solution diffusion coefficient [L^2 T^{-1}].
D^*_{Imm}	Double-porosity, effective diffusion coefficient in the immobile region [L^2 T^{-1}].
d_o	Surface (overland) flow, water depth [L].
D_t	Tile drain, dispersion coefficient [L^2 T^{-1}].
D_w	Well, dispersion coefficient [L^2 T^{-1}].

ET_S	Surface water, evapotranspiration [L^3 T^{-1}].
ET_G	Subsurface water, evapotranspiration [L^3 T^{-1}].
F	Jacobian matrix.
f_s	Fracture, spacing [L].
g	Gravitational acceleration [L T^{-2}].
h	Subsurface, hydraulic head [L].
	Variants:
	h_d Dual continuum.
	h_f Fracture.
	h_o Surface (overland) flow, water surface elevation.
	h_c Channel.
	h_t Tile drain.
	h_w Well.
H_d	Surface (overland) flow, depression storage height [L].
H_o	Surface (overland) flow, obstruction storage height [L].
H_s	Surface (overland) flow, maximum height over which area covered by surface water goes from 0 to unity [L].
i_c	Channel incision depth [L].
I	Net infiltration [L^3 T^{-1}].
IT_{max}	The maximum number of iterations allowed during a single time level.
$\mathbf{I}$	Identity tensor.
$\mathbf{k}$	Subsurface, permeability tensor [L^2].
$\mathbf{K}$	Subsurface, saturated hydraulic conductivity tensor [L T^{-1}].
K^*	Component of hydraulic conductivity tensor normal to a seepage face.
K'	Subsurface, equilibrium distribution coefficient [M^{-1} L^3].
	Variants:
	K'_d Dual continuum.
	K'_f Fracture.
K_a	Subsurface-macropore coupling, interface hydraulic conductivity [L T^{-1}].
$\mathbf{k_d}$	Dual continuum, permeability tensor [L^2].
$\mathbf{K_d}$	Dual continuum, saturated hydraulic conductivity tensor [L T^{-1}].
$\mathbf{K_f}$	Fracture, saturated hydraulic conductivity tensor[L T^{-1}].
$\mathbf{K_o}$	Surface (overland) flow, conductance tensor[L T^{-1}].
k_{det}	First-order colloid detachment coefficient from the solid phase [T^{-1}].
	Variants:
	k_{detd} Dual continuum.
k_r	Subsurface, relative permeability [-].
	Variants:
	k_{rd} Dual continuum.
	k_{rf} Fracture.
	k_{ro} Surface (overland) flow.
	k_{rt} Tile drain.
	k_{rw} Well.
k_{ra}	Subsurface-macropore coupling, interface relative permeability [-].

k_{ret}	First-order colloid retention coefficient on the solid phase [T^{-1}].
	Variants:
	k_{retd} Dual continuum.
k_{rso}	Subsurface-surface (overland) flow coupling, rill effect term [-].
k_t	Coefficient for the solid phase transfer of colloids from the porous medium domain to the dual domain [T^{-1}].
K	Bulk modulus of porous media [M T^{-2} L^{-1}].
K_f	Bulk modulus of fluid [M T^{-2} L^{-1}].
K_{ss}	Bulk modulus of solids [M T^{-2} L^{-1}].
K_s	Surface flow, conductance term reduction factor [-].
K_{so}	Subsurface-surface (overland) flow coupling, leakance term [T^{-1}].
K_t	Tile drain, hydraulic conductivity [L T^{-1}].
K_w	Well, saturated hydraulic conductivity [L T^{-1}].
K_{ox}	Surface (overland) flow, conductance in x-direction [L T^{-1}].
K_{oy}	Surface (overland) flow, conductance in y-direction [L T^{-1}].
l	Well or tile drain, length coordinate along the axis [L].
l'	Location at which specified well or tile discharge (or recharge) is applied [L].
l_p	Pore-connectivity parameter for unsaturated functions [-].
L_s	Well, screen length [L].
N	Finite element basis function [-].
N_c	Unit symbol for the number of colloids.
n^*	Brooks-Corey exponent equal to $2 + 3\lambda^*$ [-].
n	Manning roughness coefficient [$L^{-1/3}$ T].
n_x	Manning roughness coefficient in the x-direction [$L^{-1/3}$ T].
n_y	Manning roughness coefficient in the y-direction [$L^{-1/3}$ T].
P	Net precipitation [L^3 T^{-1}].
$\mathbf{q}$	Subsurface, fluid flux [L T^{-1}].
	Variants:
	$\mathbf{q_d}$ Dual continuum.
	$\mathbf{q_f}$ Fracture.
	$\mathbf{q_o}$ Surface (overland) flow.
	$\mathbf{q_t}$ Tile drain.
	$\mathbf{q_w}$ Well.
P_c	Capillary pressure head [L].
P_{dwn}	Position vector of downstream node between nodes i and j.
	Variants:
	P_{ups} Upstream node.
	P_{i2ups} Second upstream node.
P_f	Wetted perimeter of 1-D flow [L].
P_w	Well, wetted perimeter [L].
P_t	Tile drain wetted perimeter [L].
Q	Subsurface, fluid source or sink [T^{-1}].
Q_c	Channel, fluid source or sink [L^3 T^{-1}].
Q_{cd}	Dual continuum, solute source or sink [T^{-1}].
Q_d	Dual continuum, fluid source or sink [T^{-1}].

Q_G^W	Subsurface water, withdrawal [L^3 T^{-1}].
Q_{G1}	Subsurface water, inflow [L^3 T^{-1}].
Q_{G2}	Subsurface water, outflow [L^3 T^{-1}].
Q_{GS}	Surface/subsurface water interactive flow [L^3 T^{-1}].
Q_o	Surface (overland) flow, volumetric flow rate per unit area representing external source and sinks [L T^{-1}].
Q_S^W	Surface water, withdrawal [L^3 T^{-1}].
Q_{S1}	Surface water, inflow [L^3 T^{-1}].
Q_{S2}	Surface water, outflow [L^3 T^{-1}].
Q_t	Tile drain, specified fluid flow rate in or out [L^3 T^{-1}], applied at location l'.
Q_w	Well, discharge (or recharge) per unit length [L^2 T^{-1}] applied at location l'.
r	Rainfall intensity [L T^{-1}].
R	Subsurface, retardation factor [-]. Variants: R_d Dual continuum. R_f Fracture. R_o Overland flow. R_t Tile drain.
R_H	Hydraulic radius of 1-D flow [L].
r_0	Double porosity, radius of a representative sphere [L].
r_c	Well, casing radius [L].
r_s	Well, screen radius [L].
Re_i	Reynolds number in coordinate direction i.
s	Surface (overland) flow, coordinate along direction of maximum ground surface slope [L].
S_e	Effective saturation [-].
S_{fx}	Surface (overland) flow, friction slope in the x-direction [-].
S_{fy}	Surface (overland) flow, friction slope in the y-direction [-].
S_{ox}	Surface (overland) flow, bed slope in the x-direction [-].
S_{oy}	Surface (overland) flow, bed slope in the y-direction [-].
S_s	Subsurface, specific storage [L^{-1}].
S_{sf}	Fracture, specific storage [L^{-1}].
S_w	Subsurface, water saturation [-]. Variants: S_{wd} Dual continuum. S_{wf} Fracture. S_{wt} Tile drain. S_{ww} Well.
S_{wmax}	The maximum change in water saturation allowed during a single time-step.
S_{wr}	Residual water saturation [-].
t	Time [T].
tol_b, tol_f	Switching parameters for primary variable substitution [-].
v	Region or control volume associated with a node [L^3].
V	Volume of the finite-element domain [L^3].
$\overline{v}_{io}$	Surface (overland) flow, vertically averaged flow velocity in the coordinate

	direction i [L T^{-1}].
$\overline{v}_{xo}$	Surface (overland) flow, vertically averaged flow velocity in the x-direction [L T^{-1}].
$\overline{v}_{yo}$	Surface (overland) flow, vertically averaged flow velocity in the y-direction [L T^{-1}].
w_d	Dual continuum, volumetric fraction of the total porosity [-].
w_f	Fracture, aperture or width [L].
w_m	Subsurface, volumetric fraction of the total porosity [-].
W	A large number, e.g., 10^{20}.
x, y, z	Global Cartesian coordinates [L].
x_i	Component of the Cartesian coordinate system [L].
z	Subsurface, elevation head [L]. Variants: z_d Dual continuum. z_f Fracture. z_t Tile drain. z_w Well.
z'	Depth coordinate from the soil surface [L].
z_o	Overland flow, bed (land surface) elevation [L].
Z_{bank}	River bank elevation [L].
α	Van Genuchten parameter [L^{-1}].
α_c	Subsurface-surface coupling dispersivity [L].
α_{Imm}	Double-porosity, first-order mass transfer coefficient between the mobile and immobile regions [T^{-1}].
α_l	Subsurface, longitudinal dispersivity [L]. Variants: α_{ld} Dual continuum.
α_s	Subsurface-macropore coupling, first-order mass transfer [T^{-1}].
α_t	Subsurface, transverse dispersivity [L]. Variants: α_{td} Dual continuum.
α_w	Water, compressibility [L T^2 M^{-1}].
α_m	Matrix compressibility [L T^2 M^{-1}].
α_{ss}	Solids compressibility [L T^2 M^{-1}].
α_{wd}	Subsurface-macropore coupling, first-order fluid exchange coefficient [L^{-1} T^{-1}].
α^*_{wd}	Subsurface-macropore coupling, geometric factor [L^{-2}].
α'	$= 1 - K/K_s$ [-].
β	Van Genuchten parameter [-].
β_d	Subsurface-macropore coupling, geometrical factor [-].
β_{ske}	Skempton's coefficient [-].
γ	Water, kinematic viscosity [L^2 T^{-1}].
γ_{ij}	Term describing fluid flow between nodes i and j [L^2 T^{-1}].
Γ_{ex}	Subsurface, fluid exchange rate with all other domains [T^{-1}].
Γ_d	Dual continuum, fluid exchange rate with subsurface domain [T^{-1}]. Variants:

	Γ_f Fracture.
	Γ_o Surface (overland) flow.
	Γ_t Tile drain.
	Γ_w Well.
γ_w	Subsurface-macropore coupling, empirical constant [-].
δ	Dirac delta function.
ΔS_G	Subsurface, change in water storage [L^3].
ΔS_S	Surface flow, change in water storage [L^3].
Δt	Time step [T].
ϵ	A small numerical shift in the pressure head value used in the Newton–Raphson method.
η_i	Subsurface, a set of nodes connected to node i.
	Variants:
	η_{di} Dual continuum.
	η_{f_i} Fracture.
	η_{wi} Well.
	η_{t_i} Tile drain.
θ	Subsurface, water content [-].
θ_{Imm}	Double-porosity, porosity of the immobile region [-].
θ_s	Subsurface, saturated water content [-].
	Variants:
	θ_{sd} Dual continuum.
λ	Subsurface, solute first-order decay constant [L^{-1}].
	Variants:
	λ_d Dual continuum.
	λ_f Fracture.
	λ_o Surface (overland) flow.
	λ_t Tile drain.
	λ_w Well.
λ^*	Brooks-Corey pore-size index [-].
μ	Water, viscosity [M L^{-1} T^{-1}].
ν	Van Genuchten parameter equal to $1 - \frac{1}{\beta}$ [-].
ν^*	Poisson's ratio [-].
π	The constant 3.1415....
ψ	Subsurface, pressure head [L].
	Variants:
	ψ_d Dual continuum.
	ψ_f Fracture.
	ψ_t Tile drain.
	ψ_w Well.
ψ_{atm}	Atmospheric pressure [L].
ψ_b	An assigned pressure head [L].
ρ	Water, density [M L^{-3}].
ρ_b	Subsurface, bulk density [M L^{-3}].
	Variants:

	ρ_{bd} Dual continuum.
$\sigma(r)$	Van Leer flux limiter [-] with smoothness sensor r.
σ_{zz}	Surface vertical stress [M T^{-2} L^{-1}].
τ	Subsurface, matrix tortuosity [-].
	Variants:
	τ_d Dual continuum.
ϕ_o	Surface (overland) flow, surface porosity [-].
χ	Water, surface tension [M T^{-2}].
ω_{ex}	Coefficient for liquid phase colloid exchange between the porous medium and dual domains [T^{-1}].
Ω_{ex}	Subsurface, solute exchange rate with all other domains [T^{-1}].
Ω_d	Dual continuum, solute exchange rate with subsurface domain [T^{-1}].
	Variants:
	Ω_{Imm} Double-porosity immobile zone.
	Ω_f Fracture.
	Ω_o Surface (overland) flow.
	Ω_t Tile drain.
	Ω_w Well.
$\overline{\nabla}$	One-dimensional gradient operator.
$\overline{\overline{\nabla}}$	Two-dimensional gradient operator.
∇	Three-dimensional gradient operator.
ζ	Loading efficiency [-].

Index

Aquifer, *see* Porous medium
Aquitard, *see* Porous medium

Boundary conditions
  flow
    Evapotranspiration, 29, 76

Channels
  numerical techniques
    transport, 81
  theory
    transport, 40
Control volume finite-element method
  numerical techniques, 62

Decay, *see* Radioactive decay
Discrete fractures
  numerical techniques
    flow, 67
    transport, 79
  theory
    flow, 13
    transport, 37
Double porosity transport
  coupling, 42
  numerical techniques, 80
  theory, 37
Dual continuum
  numerical techniques
    flow, 68
    flow coupling , 72
    transport, 80
  theory
    flow, 14
    flow coupling , 27
    transport, 38
    transport coupling , 42

Elemental velocities, 77

Finite difference formulation
  numerical techniques, 65
Finite difference solution
  theory, 61
Fractures, *see* Discrete fractures

Hydromechanical coupling
  theory
    flow, 15

Isotopic fractionation
  transport coupling, 42
Isotopic fractionation transport
  numerical techniques, 80
  theory, 38

Mass balance
  numerical techniques, 90
Matrix solver
  numerical techniques, 86

Newton-Raphson method
  numerical techniques, 87

Porous medium
  numerical techniques
    flow, 66
    transport, 78
  theory
    flow, 10
    transport, 36

Primary variable substitution
numerical techniques, 89

Radioactive decay
theory, 36
Rill storage
theory, 19
Runoff
numerical techniques
flow, 68
transport, 81
theory
flow, 18
transport, 40

Solution procedures
numerical techniques, 90
Subsurface domain
numerical techniques
elemental velocities, 77
flow, 66
flow boundary conditions, 74
flow coupling, 71
transport boundary conditions, 85
transport coupling , 85
travel time probability , 82
theory
colloid transport, 44
flow boundary conditions, 29
transport boundary conditions, 43
transport coupling , 41–43
travel time probability, 53

Surface domain
boundary conditions
flow, 29, 75
transport, 44
numerical techniques
flow, 68
numerical techniques
flow coupling , 72
theory
rill storage, 19
transport coupling , 43
coupling, 28

Thermal energy
numerical techniques
transport, 82
transport coupling, 52
Tile drains
numerical techniques
transport, 81
theory
transport, 39
Time stepping, 2
Time stepping
adaptive
numerical techniques, 89

Wells
numerical techniques
transport, 80
theory
transport, 39